Dielectric Study on Dynamics and Conformation of Flexible Polymers

A Doctoral Thesis

by

Osamu Urakawa

Submitted to the Faculty
of Science, Osaka University

February 1994

Dielectric Study on Dynamics and Conformation of Flexible Polymers

A Doctoral Thesis

by

Osamu Urakawa

Submitted to the Faculty
of Science, Osaka University

February 1994

Approval

February, 1994

This thesis is approved as to
style and content by

小高忠男

Member-in-chief

小林雅通

Member

蒲池幹治

Member

則末尚志

Member

足立桂一郎

Member

Acknowledgments

This thesis is based on my research carried out from 1989 to 1994 at the Kotaka Laboratory of the Department of Macromolecular Science, Faculty of Science, Osaka University.

I would like to express my sincere gratitude to Professor Tadao Kotaka for his valuable advice, comments, and constructive criticisms. I am very grateful to Associate Professor Keiichiro Adachi for his advice and suggestions in the experiments, and helpful consultations throughout the course of this work. I also thank Dr. Hiroshi Watanabe for his strict guidance of the research for dielectric relaxation of dipole inverted PI chain (in Chapter VI). He suggested me the way of this work and discussed with me repeatedly. I am greatly indebted to Mr. Shinsaku Uemura and Dr. Toshiyuki Shikata for their useful advice and consultations.

I wish to express my thanks to Professor Akio Teramoto and Associate Professor Takashi Norisue for their admitting the usage of a light scattering photometer and their helpful discussions. In carrying out the measurements, I am indebted to Dr. Yo Nakamura for his helpful advice.

I also acknowledge Professor Hajime Yasuda, Faculty of Engineering, Hiroshima University for his supply of poly(ε-caprolactone) and poly(δ-varerolactone) samples.

For the molecular orbital calculation, I was very much obliged to Associate Professor Kazuyuki Tatsumi, Faculty of Engineering Science, Osaka University. I would like to express my thanks to him.

Thanks are also extended to all the member of Professor Kotaka's Laboratory for their advice and friendship. Finally I would like to thank my fiancee and parents for their constant encouragement.

February, 1994

浦川 理

Osamu Urakawa

Contents

I. General Introduction

I-1. Historical Survey of Dielectric Studies of Polymers

Dielectric spectroscopy has long been used as a powerful tool for studying stereochemical structure and dynamics of polar molecules.[1-3] Before various modern techniques of analyses such as nuclear magnetic resonance (NMR) were developed, the dipole moment was one of key information for determination of molecular structure of low molecular weight compounds. From the static dielectric constant the molecular polarization was determined with the Clausius-Mossoti equation and was compared with theoretical polarizations derived for possible chemical structures.[1] Frequency dependence of the complex dielectric constant provides another important information on the rotational diffusion of polar molecules. Debye[4] proposed a theory of dielectric relaxation in 1929, and since then the dielectric method has been one of the most reliable methods for determining the orientational relaxation time of polar molecules. At present, a variety of sophisticated techniques such as NMR,[5] electron spin resonance (ESR),[6] dynamic light scattering,[7] and fluorescence depolarization[8] are available for studying molecular dynamics. However, the dielectric spectroscopy is still a unique method in the sense that it provides us with direct information on the orientation of the molecules.

The dielectric spectroscopy also played an important role in studying the structure and dynamics of polymer molecules.[9-12] For understanding the dielectric properties of polymers, it is important to specify how and in what direction the monomer dipoles are attached to the chain backbone. Stockmayer classified polymer dipoles into three major types.[9] The component of monomer dipoles aligned in the same direction parallel to the chain contour are referred to as *type-A*, those perpendicular to the chain contour as *type-B*, and those on flexible side groups as *type-C*, as schematically depicted in Figure I-1. Although W.Kuhn[13]

already noted the features of type-A polymers in 1950, Stockmayer pointed out that the dipole moment $\boldsymbol{P}$ of a totally type-A chain is directly proportional to the end-to-end vector $\boldsymbol{r}$ of the chain:

$$\boldsymbol{P} = \mu \boldsymbol{r} \qquad \text{(I-1)}$$

where μ is the dipole moment per unit contour length of the chain. Thus the dielectric relaxation of type-A dipoles reflects fluctuation and orientation of the end-to-end vector and consequently the global motion of the chain prevailing in viscoelastic terminal relaxation.[9,10,14,15] In addition to the dynamical features, the dielectric relaxation of a type-A chain provides information on the mean square end-to-end distance $\langle r^2 \rangle$ of the chain, being proportional to the relaxation strength $\Delta\varepsilon$. Such a relaxation process was thus designated as *"dielectric normal mode process"*.[16] On the other hand, relaxation of type-B dipoles reflects local segmental motion relevant to the glass transition, while that of type-C dipoles reflects local motion within the side groups responsible to high frequency modes at sub-T_g temperature, if the polymer molecules considered possess such components. Usually these two types of dipole moments contribute to multiple-relaxation phenomena often designated as α, β, γ, *etc.* relaxation modes from the high temperature side.[11]

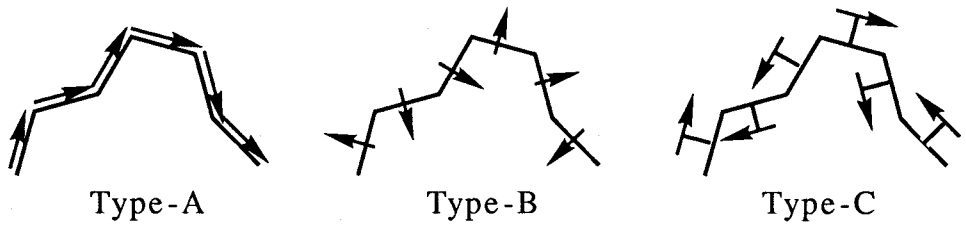

Figure I-1. Stockmayer's classification of polymer dipole moments.

Before Stockmayer's classification of the polymer dipoles, the dielectric relaxation of type-B dipoles was the main subject of concern of many scientists, among whom Kirkwood and Fuoss[17,18] were the pioneer. They recognized that the dielectric relaxation spectrum of a type-B polymer is much broader than those of simple polar molecules. They called such a relaxation the *anomalous relaxation*, which was often referred to as the primary α process or the segmental mode process and was empirically expressed by the Kohlraush-Williams-Watts equation[19,20] and/or the Haviriliak-Negami equation.[21] However, these empirical equations have not yet been explained theoretically in a satisfactory manner.

Although many studies on type-B and type-C polymers were reported by early 1960's, those on type-A polymers had not been explored until Stockmayer[9] pointed out their significance in 1967. A pioneering theoretical study of the dielectric relaxation of type-A chains was first reported by W. Kuhn[13] in as early as 1950, but the theoretical development of this normal mode relaxation had to wait the advent of a molecular model describing global motion of a flexible polymer chain. The bead-spring model proposed by Rouse[22] in 1953 provided a clear picture of the molecular motion related to the viscoelastic relaxation of an isolated and/or unentangled flexible polymer chain. On the basis of this bead-spring model, Zimm[23] presented a theory of viscoelastic and dielectric relaxations of a type-A chain with incorporating hydrodynamic interactions between beads. Van Beek and Hermans also developed a theory of the normal mode relaxation.[24] These theories were further developed by Stockmayer and Baur in 1964.[25]

Although the bead-spring model successfully explained viscoelastic and dielectric relaxation behavior of non-entangled chains, it failed to explain the behavior of entangled chains. The reptation model proposed by de Gennes[26,27] in 1971 and developed by Doi and Edwards[28,29] provided a clear picture on the dynamics of entangled chains, predicting the dielectric normal mode process as well.

Experimental studies on the dielectric relaxation of type-A polymers were also initiated by Stockmayer and coworkers.[30-32] Baur and Stockmayer[30] first reported an experimental study on bulk poly(propylene oxide) (PPO) which has both type-A and type-B dipoles. They observed a small side peak (due to the type-A dipoles) on the low frequency side of the main dielectric loss (ε'') peak due to the type-B dipoles. Because the type-A component of PPO was much smaller than the type-B component, their dielectric data were not clear enough to investigate detailed aspects of the normal mode relaxation, *e.g.*, the shape of the dielectric loss (ε'') curve reflecting the relaxation-mode distribution and/or the relaxation strength $\Delta\varepsilon$ reflecting the mean square end-to-distance $\langle r^2 \rangle$ of the chain.

Then Jones *et al.*[32] studied dielectric relaxations of benzene and dioxane solutions of high molecular weight poly(ε-caprolactone) (PCL) which also possesses both type-A and type-B dipoles. They found that dilute PCL solutions exhibited a clear ε'' peak due to the normal mode, and discussed the relaxation time determined as the reciprocal of the ε'' peak angular frequency. The relaxation time data were well explained by the Rouse-Zimm theory.[22,23]

Dielectric studies of *cis*-polyisoprene (PI), initiated by Adachi and Kotaka[33], gave a breakthrough in the study of entangled polymer systems. High *cis*-content PI also has both type-A and type-B dipoles. PI samples with narrow molecular weight distribution can be relatively easily prepared over a wide range of molecular weight *via* anionic living polymerization. Since this polymer is essentially nonpolar, it is easily freed from moisture and ionic contaminants which are always hazards in carrying out low-frequency dielectric measurements indispensable for the dielectric normal mode study of entangled systems. Because of these advantages of PI samples, Adachi and Kotaka were able to observe very clear ε'' curves due to the normal modes over wide ranges of concentration and molecular weight. Thus detailed investigation of the polymer chain conformation and dynamics of the global motion became possible.

I-2. Background: Overview of Studies on Dimensions and Dynamics of Flexible Chain Polymers

I-2-1. Polymer Chain Dimensions

In the previous section, we emphasized that dielectric studies on type-A chains will provide us with fruitful information on the chain conformation as well as the dynamics of the global motion of the chain. In this section, we briefly review the current status of studies on polymer chain conformation covering from dilute solution to the bulk state.

Since Staudinger established the concept of macromolecules in the 1930's, much work has been done on dilute solution properties of polymers to determine the molecular characteristics and conformation of the dissolved macromolecules.[34,35] However, studies on concentrated solutions and bulk polymers were started only about 20 years ago after the advent of powerful scattering techniques including small angle neutron scattering (SANS). The behavior of polymer chains in solution may be divided into three categories: the dilute, semidilute, and concentrated regimes, according to the change in polymer concentration C.[27] These three regimes are schematically illustrated in Figure I-2. The dilute solution regime is defined as the region of C where polymer coils do not overlap. With increasing C, the polymer chains begin to overlap as C reaches a critical concentration called *overlapping concentration* C^* expressed by

$$C^* \cong \frac{3M}{4\pi N_A \langle S^2 \rangle^{3/2}} \qquad \text{(I-2)}$$

where M is the molecular weight of the polymer; N_A, the Avogadro constant; $\langle S^2 \rangle$, the mean-square radius of gyration.[27] The semidilute region is defined as the region where the polymer chains overlap one another but C is still not high enough so that the segment density is *not uniform* throughout the solution. In this region the segment density fluctuation plays an important role in the thermodynamic and

dynamic behavior of the polymer chains. In the concentrated regime, on the other hand, the segment density fluctuation is negligible and a mean field theory may be applicable. Generally the concentration C^{**} representing the transition from the semidilute-to-concentrated region does not depend on the molecular weight but depends on the chemical nature of the polymer species involved.

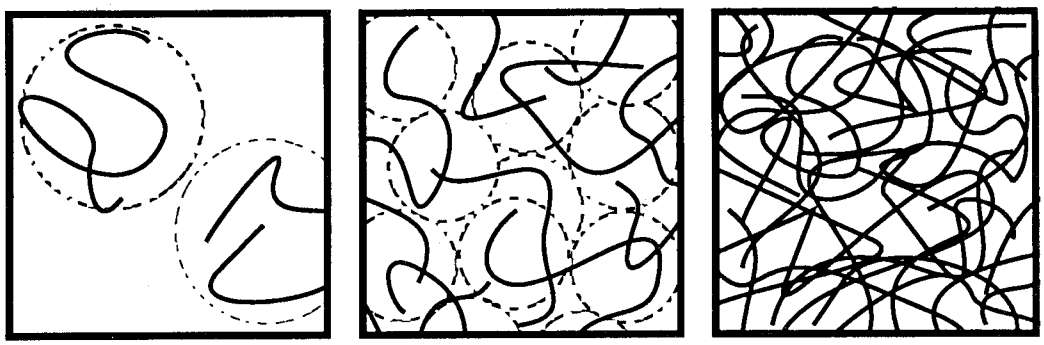

Figure I-2. Schematic representation of the classification of polymer solutions.

Numerous studies on chain dimensions in dilute solution have been made by several techniques: light scattering, small angle X ray scattering (SAXS), and intrinsic viscosity measurements. The dependence of the mean-square radius of gyration $\langle S^2 \rangle$ of a chain on the degree of polymerization N can be summarized as

$$\langle S^2 \rangle \propto N^{2\nu} \qquad \text{(I-3)}$$

where the excluded volume exponent ν varies with solvent quality from 0.5 in a theta solvent to 0.6 in an extremely good solvent. Monomer-monomer interactions in the latter solvent are predominantly repulsive, and due to this intra-chain excluded volume effect, the polymer coil is swollen to a dimension larger than the unperturbed Gaussian dimension with $\nu = 0.5$. Flory first treated the excluded-volume problem in a mean-field approximation and predicted $\nu = 0.6$ at the extremely good solvent limit.[34,36] A later renormalization group calculation gave $\nu = 0.588 \pm 0.001$,[37] supporting the Flory exponent.

In a semidilute solution of a good solvent, the intra-chain excluded volume effect is supposed to be partially screened by inter-chain interactions. Thus with increasing C the dimensions of a polymer chain may decrease. Such concentration dependence of chain dimensions in semidilute solution was investigated by Daoud *et at.*[38] and King *et al*[39] with SANS on deuterated polystyrene. Their results indicated that $\langle S^2 \rangle$ decreased in proportion to $C^{-1/4}$.

Daoud and Jannink developed a scaling theory[40] and calculated the mean square end-to-end distance $\langle r^2 \rangle$ using a model composed of freely jointed *blobs* in each of which the excluded volume effect is exerted but between which the excluded volume effect is screened. This scaling theory predicted the C dependence of $\langle r^2 \rangle$ as:

$$\langle r^2 \rangle \propto N C^{(2\nu - 1)/(1 - 3\nu)} \qquad \text{(I-4)}$$

For $\nu = 0.6$, the exponent to C becomes -1/4 in agreement with the experiments, if $\langle r^2 \rangle$ and $\langle S^2 \rangle$ possess the same scaling exponent. With further increase in C, the screening effect on the excluded volumes becomes intense, and thus $\langle S^2 \rangle$ and likewise $\langle r^2 \rangle$ of the polymer chain should decrease to the unperturbed values.

The scattering methods to determine $\langle S^2 \rangle$ mentioned above have been well established during the past few decades.[41] However, there were no techniques available to determine $\langle r^2 \rangle$ directly until the dielectric *normal mode* method was established and actually applied to PI and other type-A polymers by Adachi and coworkers.[42] For quantitative evaluation of $\langle r^2 \rangle$ by the dielectric method, however there still remained a crucial problem of determining μ in eq I-1 for the polymers to be examined; the value of μ must be dependent on the detailed stereochemical structure of the monomer unit and the polymer chain. In a later section we will fully discuss this problem, subdividing type-A polymers into several additional classes according to their detailed structure.

Another important problem in determining $\langle r^2 \rangle$ is to define the ratio F of the internal-to-external electric field effective for the dielectric normal mode process. For the segmental and local mode processes, there are already several fields established: the Lorentz cavity field and the Onsager reaction field, for example.[1] For the normal mode process, Adachi proposed the vacuum field of $F = 1$ to be good enough.[42,43] We will reexamine this proposal.

I-2-2. Polymer Chain Dynamics

Dynamics of a flexible polymer chain has also been one of the central problems in polymer physics in the past few decades and extensively studied both experimentally and theoretically by many authors.[5-9,28,29] Infinitely dilute solution is perhaps one of the simplest model systems for examining the dynamical features of an isolated chain. As mentioned in the previous section, the *bead-spring model* proposed by Rouse[22] and Zimm[23] was the starting point. Although there are only a few sets of experimental data on dilute solutions available,

data[14,44] of the intrinsic complex moduli [G^*], for example, were very well explained by these models, especially better by the Zimm theory[23] rather than the Rouse theory.[22]

In the range of $C^* < C < 10C^*$ the effect of chain overlapping appears to cause the distribution of viscoelastic relaxation times to approach that of the Rouse model.[14,44,45] This phenomenon was recognized theoretically as a result of shielding effect of hydrodynamic interactions among beads. With further increase in C, entanglement effect causes the appearance of the rubbery plateau region in the stress-relaxation moduli $G(t)$ and storage moduli G', if $M > M_e/\phi$ where M_e is the entanglement molecular weight specific to the polymer species in the bulk state; and ϕ, the volume fraction of the polymer. The longest relaxation time becomes proportional to $M^{3.4}$ for systems with $M > M_c/\phi$ in this entangled region where M_c is the characteristic molecular weight, another parameter specific to the polymer in the bulk state.

Experimental studies of polymer melts and concentrated solutions have a much longer history than those of dilute and/or semidilute solutions.[14] The M dependencies of zero shear viscosity η_0 and steady state compliance J_e^0 are expressed as $\eta_0 \propto M^{3.3\sim3.7}$ and $J_e^0 \propto M^0$, if $M > M_c$ and $M > M_c'$, respectively, where M_c' is still another characteristic molecular weight, representing entanglement effect.

Interpretation of these intriguing results of highly entangled polymer systems has also been a long-lasting but yet-unsettled problem in polymer rheology. In 1971 de Gennes[26] proposed an intuitive model called *reptation* model to explain the motion of a polymer chain trapped in a crosslinked network. In 1978 Doi and Edwards[28] extended de Gennes' idea to describe viscoelastic behavior of entangled polymer systems. The model called *tube* model assumes that the topological constraint to a test chain by its surrounding chains is represented as a fixed tube, in which the test chain can move only along its contour. When a part of the chain gets

out of the tube, it loses the conformational memory acquired at time $t = 0$. The time necessary for the whole chain gets out from the tube (tube disengagement time τ_d) corresponds to the longest relaxation time. The tube model predicts that both η_0 and τ_d are proportional to $M^{3.0}$, but this does *not* agree with the empirical 3.4 power law. Recently the discrepancy was explained with two modified tube models, one considering contour-length fluctuation of the test chain within the tube[46] and the other, constraint release mechanisms *via* tube reorganization.[47,48]

The dynamical features of the two extreme cases, dilute solution and entangled melt, are at least semiquantitatively explained by the Rouse-Zimm model and the modified tube models, respectively. In the semidilute regime the chain dynamics is governed by both hydrodynamic and topological interactions (the entanglement effect). Thus the semidilute solution has a nature possessing these two dynamical interactions. Dynamical scaling theory explained roughly the crossovers from dilute-to-semidilute and semidilute-to-concentrated regimes in the C dependence of the viscoelastic behavior.[49-53]

I-3. Objectives and Scope of this Thesis

The objectives of this thesis are to clarify the static and dynamical behavior of flexible polymer chains under different surroundings such as dilute and semidilute solutions, unentangled and entangled melts and blends through the dielectric *normal mode* spectroscopy of *cis*-polyisoprene (PI) and poly(lactone)s. Although the qualitative features of the polymer dynamics have so far been reasonably well understood over the whole range of C and M, there still remain many unsolved problems. This thesis intends to solve some of these problems. It consists of seven chapters including this introductory chapter.

Chapter II summarizes the theoretical background of dielectric relaxation of a type-A chain. As already noted, the classification of polymer dipoles by Stockmayer is not sufficient for detailed analyses of the dielectric behavior of the

existing type-A chains. Thus we will further classify type-A chains into three sub-types according to their molecular structure. Then the relationship between their dielectric polarization and $<r^2>$ will be discussed. The effect of internal field will also be discussed with regard to the dynamical behavior. The basic principle and the methods for determining type-A dipole moments from the dielectric relaxation strengths of such type-A chains are described.

Chapter III summarizes the methods employed in this study for preparation and characterization of PI samples including dipole-inverted PIs and also of two poly(lactone)s, poly(ε-caprolactone) (PCL) and poly(δ-varerolactone) (PVL). The principles and procedures of various experimental techniques are also described.

Chapter IV is concerned with the static behavior of PI and two poly(lactone)s investigated by the dielectric normal mode spectroscopy. As described above there exist few data of $<r^2>$. Therefore we carefully test the reliability of the method employed here to determine $<r^2>$ from dielectric measurements of particular type-A chains. First the values of $<r^2>$ and its expansion factor α determined on solutions of PI and poly(lactone)s are presented. Then this method is extended to measurement of $<r^2>$ of a probe PI chain in semidilute polybutadiene (PB) solutions. Our interest is to examine the dependence of $<r^2>$ of the test PI chains on PB concentration and molecular weight in dilute and semidilute regimes. The results are compared with the current scaling theory developed for polymer/polymer/solvent ternary solutions.

In Chapter V, the dynamic behavior of the systems described in Chapter IV are discussed. First we calculate dielectric relaxation spectra on the bases of the bead-spring and tube models. As is well known, any versions of the tube model cannot predict correct (viscoelastic) relaxation time spectra: The observed ones are usually broader than the theoretical ones. We then discuss changes of dielectric relaxation time spectra induced by changes in surroundings, namely, from dilute to semidilute solutions and from unentangled to entangled melts and blends. We also

discuss the universality of the global chain dynamics of chemically different polymer species reflected in the relaxation time spectra.

In Chapter VI the results of dielectric measurements on dipole-inverted PI chains are described. The objective of this chapter is to directly determine the eigenfunctions of the local correlation function of a flexible chain in dilute solution as well as in melt. In fact, the eigenfunctions determine the viscoelastic as well as the dielectric relaxation mode distributions. On the basis of this information, possible origins of the spectrum change described in Chapter IV are discussed in detail.

Finally Chapter VII summarizes the main results obtained, the conclusions derived therefrom, and some remarks for future work.

References

1. Böttcher, C. J. F. "Theory of Electric Polarization", Elsevier Amsterdam 1973.
2. Daniel, V. V. "Dielectric Relaxation", Academic Press : London 1967.
3. Hill, N. E. "Dielectric Properties and Molecular Behavior", Van Nestrand: London 1969.
4. Deby, P. "Polar Molecules", Chemical Catalog Co., reprinted by Dover Publisher 1929.
5. Sanders, J. K. and Huneer, B. K. "Modern NMR Spectroscopy", Oxford Univ. Press: Oxford 1987.
6. Poole, C. P. "ESR ", Wiley New York 1983.
7. Pecola, B. "Dynamic Light Scattering", Wiley New York 1976.
8. Ediger, M. D. *Ann. Rev. Phys. Chem.* **1991**, *42*, 225.
9. Stockmayer, W. H. *Pure Appl. Chem.* **1967**, *15*, 539.
10. North, A. M. *Chem. Soc. Rev.* **1972**, *1*, 49.
11. Mc Crum, N. G.; Read, B. E.; Williams, G. "Anelastic and Dielectric Effects in Polymeric Solids" Wiley, New York 1967.
12. Riande, E.; Saiz, E. "Dipole Moments and Birefringence of Polymers" Prentice Hall, Englewood Cliffs, NJ. 1992.
13. Kuhn, W. *Helvetica Chim. Acta*, **1950**, *261*, 2057.
14. Ferry, J. D. "Viscoelastic Properties of Polymets", 3rd ed.; Wiley: New York, 1980.
15. Graessley. W. W. *Adv. Polym. Sci.* **1974**, *16*, 1.
16. Adachi, K.; Kotaka, T. *Macromolecules* **1983**, *16*, 1936.
17. Fuoss, R. M.; Kirkwood, J. G. *J. Am. Chem. Soc.* **1941**, *63*, 385.
18. Kirkwood, J. G.; Fuoss, R. M. *J. Chem. Phys.* **1941**, *9*, 329.
19. Kohlrausch, R. *Prog. Ann. Phys.* **1847**, *12*, 393.
20. Williams, G.; Watts, D. C. *Trans. Faraday Soc.* **1971**, *66*, 80.
21. Havriliak, S.; Negami, S. *J. Polym. Sci. Part C* **1966**, *44*, 99.
22. Rouse, P. E. *J. Chem. Phys* **1953**, *21*, 1272.
23. Zimm, B. H. *J. Chem. Phys* **1956**, *24*, 269.
24. Van Beek, L. K. H.; Hermans, J. J. *J. Polym. Sci.* **1957**, *23*, 211.
25. Stockmayer, W. H.; Baur, M. E. *J. Am. Chem. Soc.* **1964**, *86*, 3485.
26. de Gennes, P. G., *j. Chem. Phys.* **1971**, *55*, 572.
27. de Gennes, P.-G. "Scaling Concepts in Polymer Physics"; Cornell University Press: Ithaca,

1979.

28. Doi, M.; Edwards. S. F., *J. Chem. Soc. Faraday Trans. 2.* **1978**, *74*, 1789. **1978**, *74*, 1802. **1979**, *75*, 38.
29. Doi, M.; Edwards. S. F., "The Theory of Polymer Dynamics" Oxford Science Publications, clarendon Press, Oxford, **1986**.
30. Bauer, M. E.; Stockmayer, W. H. *J. Chem. Phys.* **1965**, *43*, 4319.
31. Burke, J. J.; Stockmayer, W. H. *Macromolecules* **1969**, *2*, 647.
32. Jones, A. A.; Stockmayer, W. H. *J. polym. Sci. Polym. Symp.* **1976**, *54*, 227.
33. Adachi, K.; Kotaka, T. *Macromolecules*, **1984**, *17*, 120, **1985**, *18*, 466.
34. Flory, P. J. "Principles of Polymer Chemistry" cornell univ. Itthaca, New York 1953.
35. Yamakawa, H. "Modern Theory of Polymer Solutions"; Harper and Row: NY, 1971.
36. Flory, P. J. *J. Chem. Phys.*, **1949**, *17*, 303.
37. Le. Guillou, J. C.; Zinn-Justin, J. *Phys. Rev. Lett.* **1977**, *39*, 95.
38. Daoud,M.; Cotton, J. P.; Farnoux, B.; Jannink, G.; Sarma, G.; Benoit, H.; Duplessix, R.; Picot, C.; de Gennes, P.-G. *Macromolecules* **1975**, *8*, 804.
39. King, J. S.; Boyer, W.; Wignall, G. D.; Ulman, R. *Macromolecules* **1985**, *18*, 709.
40. Daoud,M.; Jannink, G. *J. Phys.* (*Les Vlis*) **1976**, 37, 973.
41. Pawkins, J. V. "Developments in Polymer Characterization 1." Applied Sci., London 1978.
42. Adachi, K.; Kotaka, T. *Progr. Polym. Sci.* **1993**, *18*, 585.
43. Adachi, K.; Okazaki, H.; Kotaka, T. *Macromolecules* **1985**, *18*, 1687.
44 Holmes, L. A.; Ferry, J. D. *J. Polymer Sci.*, **1968**, *C23*, 291.
45. Holmes, L. A.; Kusamizu, S.; Osaki, K. Ferry, J. D. *J. Polymer Sci. Part A-2*, **1971**, *9*, 2009.
46. Doi, M. *J. Polym. Sci., Polym. Phys. Ed.* **1983**, *21*, 667.
47. Graessley, W. W. *Adv. Polym. Sci.* **1982**, *47*, 68.
48. Watanabe, H.; Tirrel, V., *Macromolecules* **1989**, *22*, 927.
49. Takahashi, Y.; Isono, Y.; Noda, I. *Macromolecules*, **1985**, *18*, 1002.
50. Takahashi, Y.; Noda, I.; Nagasawa, M. *Macromolecules*, **1985**, *18*, 2224.
51. Adam, M.; Delsanti, M. *J. Phys.* (*Paris*) **1982**, *43*, 549.; **1983**, *44*, 1185.; **1984**, *45*, 1513.
52. Osaki, K.; Nishimura, Y.; Kurata, M. *Macromolecules* **1985**, *18*, 1153.
53. Osaki, K.; Nishizawa, K.; Kurata, M. *Macromolecules* **1982**, *15*, 1068.

II. Theories of Dielectric Relaxation of Type-A Polymers

II-1. Introduction

In this chapter we describe the theoretical background of the dielectric normal mode process. As described in Chapter I, the total type-A dipole moment $\boldsymbol{P}_A$ of a polymer chain is proportional to the end-to-end vector $\boldsymbol{r}$.

$$\boldsymbol{P}_A = \mu \boldsymbol{r} \tag{II-1}$$

where μ is a constant corresponding to the dipole moment per unit contour length. As described later, $<P_A^2>$ is determined by measurements of the dielectric relaxation strength $\Delta\varepsilon$ for the normal mode process. If the value of μ is known the absolute value of $<r^2>$ may be determined from the data of $\Delta\varepsilon$. Therefore it is important to determine μ from the chemical structure of the monomeric unit. For this purpose, it is necessary to clarify the relation between $\boldsymbol{P}_A$ and the chemical structure. Generally a chain in which there are neither symmetry elements of inversion nor mirror image belongs to type-A. Thus in the following section, we first classify the type-A polymers. Then the relationship between $<P_A^2>$ and the chemical structure of the type-A chain is discussed. Finally the basic relationship between the complex dielectric constant ε^* and P_A is described.

II-2. Classification of Type-A Polymers

Examining the chemical structure of type-A polymers, we find that actual type-A polymers are classified at least into three types. Schematic representations of them are shown in Figure II-1, in which the arrows indicate polar bonds and the lines nonpolar bonds. Here it is noted that "bond" means either a covalent bond or a virtual bond composed of a rigid chemical group such as benzene ring and -C=C- double bond. Type-A1 is a pure type-A corresponding to the original Stockmayer model.[1] Type-A2 chains are an alternating copolymer composed of polar and non-

polar bonds, while type-A3 chains are composed of more than two kinds of parallel dipoles and non-polar bonds.

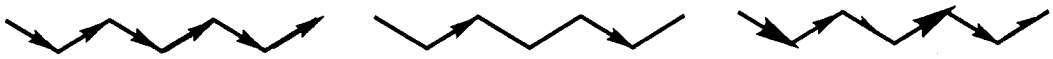

Type-A1 Type-A2 Type-A3

Figure II-1. Further classification of Type-A chain.

For an ideal type-A1 chain such as drawn in Fig.II-1, μ is exactly given by p/b where p is the bond dipole moment and b the bond length. But for type-A2 and A3 polymer chains, μ is given by an statistical average over all conformations in a certain sub-chain unit of a polymer, and eq.II-1 may be approximately rewritten as

$$P_A = <\mu> r \qquad \text{(II-2)}$$

where <···> indicates the ensemble average.

Examples of type-A1 to A3 polymers are shown in Figure II-2. Poly(2,6-disubstituted-1,4-phenylene oxide) (PPhO) shown in Fig.II-2(a) is a typical type-A1 polymer. The virtual bond connecting the two oxygen atoms is rigid and has a dipole moment parallel to this axis. Similarly, poly(substituted acetylene)s $-(CX=CH)_n-$ and poly(alkyl phosphazene)s are type-A1 polymers. For these polymers, μ can be calculated explicitly if the dipole vector of the monomer unit is known. A typical A2 polymer is *cis*-polyisoprene (PI). As shown in Figure II-2(b), this polymer consists of alternating links of the virtual bond $-C(CH_3)=CH-$ having type-A dipole moment and $-CH_2-CH_2-$ non-polar bond. Poly(lactone)s and poly(lactam)s are also typical type-A2 polymers. In these polymers the ester and amide groups are rigid and form virtual bonds. We note that these polymers possess several non-polar bonds in contrast to PI. Poly(propylene-oxide) belongs to type-A3.

(a) Type-A1

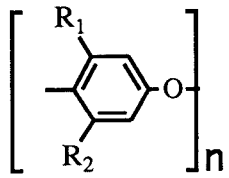

poly(2,6 disubstituted-1,4 phenylene-oxide)

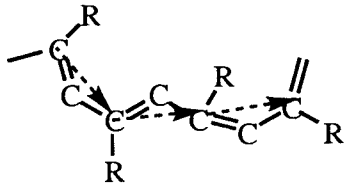

polyacetylene

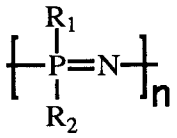

Poly(alkyl phosphazene)

(b) Type-A2

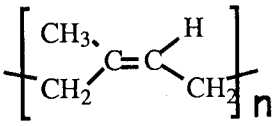

cis-polyisoprene

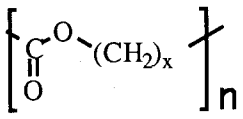

poly(lactone)

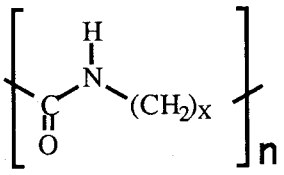

poly(lactam)

(c) Type-A3

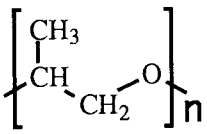

poly(propylene-oxide)

Figure II-2. Examples of Type-A1 to A3 polymers.

However, even if a polymer is not intrinsic type-A, it could possess a type-A dipole and we may call it a form type-A polymer. For example, poly(alkyl isocyanate) having the structure —[(NR)-(CO)]$_n$— is obviously not intrinsic type-A, but this polymer behaves as a type-A polymer by taking a helical structure in which the type-B dipoles due to the N-R and C=O groups align in the direction parallel to the helix axis. Alkene-sulfur dioxide alternating copolymers (poly(1-alkene sulfones)) are other examples of this type. In this thesis, however, we do not review such exceptional cases.

II-3. Calculation of Type-A Dipole Moment per Unit Contour Length

II-3-1. Separation of Polymer Dipole into Type-A and Type-B Components

For polymers having the component of type-B dipole, the total dipole vector $\boldsymbol{P}$ is written as:

$$\boldsymbol{P} = \boldsymbol{P}_A + \boldsymbol{P}_B = \langle\mu\rangle\boldsymbol{r} + \boldsymbol{P}_B \qquad \text{(II-3)}$$

where $\boldsymbol{P}_B$ is the dipole vector due to the type-B component. For the estimation of $\langle\mu\rangle$ from the polymer chemical structure, it is necessary to separate the type-A and -B components. Since the head and tail of a type-B chain are indistinguishable, there exist two conformations 1 and 2 which are completely symmetrical.[2,3]

$$\boldsymbol{P}_B(1)\cdot\boldsymbol{r}(1) = -\boldsymbol{P}_B(2)\cdot\boldsymbol{r}(2) \qquad \text{(II-4)}$$

Since the states of 1 and 2 occur with the same probability, the averaged quantities $\langle\boldsymbol{P}_B\cdot\boldsymbol{r}\rangle$ and $\langle\boldsymbol{P}_B\cdot\boldsymbol{r} / r^2\rangle$ become zero. Thus eq II-3 leads to

$$\langle\mu\rangle = \langle\boldsymbol{P}\cdot\boldsymbol{r} / r^2\rangle \qquad \text{(II-5)}$$

For all type-A2 chains this formula is applicable.

As described above, most polymers possess type-B or type-C components. In an actual experiment, we can separately observe the dielectric response of the type-A dipoles, since the relaxations of type-B or -C dipoles occur in much higher frequency (or shorter time) ranges than that of type-A dipoles.[4]

II-3-2. Calculation of Type-A Dipole by Rotational Isomeric State (RIS) Model

In the actual calculation of $<\mu>$, it is difficult to calculate the average over the whole molecule.[5] We may use two methods. One method is to approximate eq II-5 by

$$<\mu> = \frac{<\boldsymbol{P}\cdot\boldsymbol{r}>}{<r^2>} \tag{II-6}$$

If the potential for the internal rotation is known, the average values of $<\boldsymbol{P}\cdot\boldsymbol{r}>$ and $<r^2>$ are calculated by[5]

$$\begin{aligned} <\boldsymbol{P}\cdot\boldsymbol{r}> &= \Sigma_{ij}\ \boldsymbol{m}_i^{T} <\boldsymbol{T}_i \cdots \boldsymbol{T}_{j-2}\boldsymbol{T}_{j-1}>\boldsymbol{u}_j \\ <r^2> &= \Sigma_{ij}\ \boldsymbol{u}_i^{T} <\boldsymbol{T}_i \cdots \boldsymbol{T}_{j-2}\boldsymbol{T}_{j-1}>\boldsymbol{u}_j \end{aligned} \tag{II-7}$$

where $\boldsymbol{m}_i$ and $\boldsymbol{u}_i$ are the i-th bond dipole moment and bond vector, respectively, and $\boldsymbol{T}_i$ is the orthogonal matrix which transforms a vector expressed in the reference frame i+1 to that in the reference frame i. The superscript T indicates the transposed matrix. For the calculation of $<\boldsymbol{T}_i \cdots>$ we used rotational isomeric state (RIS) model developed by Flory.[5]

The other method is to perform a numerical calculation of eq II-5 for a sub-chain, *i.e.*, for a portion of he chain for which $<\mu>$ is given by

$$<\mu> = <\boldsymbol{p}\cdot\boldsymbol{b}\ /\ \boldsymbol{b}^2> \tag{II-8}$$

with $\boldsymbol{b}$ the end-to-end vector of the sub-chain. We expect that $<\mu>$ converges to a

value given by eq II-5 when $|\boldsymbol{b}|$ becomes the order of the Kuhn step length.[6,7]

The details of these methods and the results of the calculation for PI, PCL and PVL are described in Chapter IV.

II-4. Static Behavior of Type-A Polymers

II-4-1. Dielectric Constant of a System Involving Type-A Dipoles

First the relation between the macroscopic dielectric relaxation strength and dipole moment $\boldsymbol{m}$ of a molecule is considered. We assume a dilute solution in which N small molecules are dissolved in unit volume. The macroscopic polarization $\boldsymbol{M}$ is given by[8,9]

$$\boldsymbol{M} = N \frac{\int \boldsymbol{m}\, exp\,(\boldsymbol{m}\cdot\boldsymbol{E}_{eff}/k_BT)\, d\upsilon}{\int exp\,(\boldsymbol{m}\cdot\boldsymbol{E}_{eff}/k_BT)\, d\upsilon} \qquad \text{(II-9)}$$

where $\boldsymbol{E}_{eff}$ is the effective electric field and $d\upsilon$, the solid angle $d\omega$ times the differential dm of the dipole moment. Obviously the statistical average of $\boldsymbol{M}$ is proportional to $\boldsymbol{E}_{eff}$. Since the electric energy $\boldsymbol{m}\cdot\boldsymbol{E}_{eff}$ is much smaller than the thermal energy k_BT, we expand the exponential function to the first order of $\boldsymbol{m}\cdot\boldsymbol{E}_{eff}$ to a good approximation. Then the absolute value of polarization $|\boldsymbol{M}|$ reads

$$|\boldsymbol{M}| = \frac{N}{k_BT} \frac{\int (\boldsymbol{m}\cdot\boldsymbol{E}_{eff}/E_{eff})(\boldsymbol{m}\cdot\boldsymbol{E}_{eff})\, d\upsilon}{\int d\upsilon} \qquad \text{(II-10)}$$

The integral of $(\boldsymbol{m}\cdot\boldsymbol{E}_{eff})^2/E_{eff}$ equals $<m^2>E_{eff}$ $<\cos^2\theta>$ where θ is the angle between $\boldsymbol{m}$ and $\boldsymbol{E}_{eff}$. With $<\cos^2\theta>=1/3$, the the absolute value $|\boldsymbol{M}|$ is given by.

$$|\boldsymbol{M}| = NFE<m^2>/3k_BT \qquad \text{(II-11)}$$

where E is the external field and F is the ratio of the internal/external electric field.

When we use the *c.g.s. esu* unit system, the electric displacement $\boldsymbol{D}$ is defined by

$$\boldsymbol{D} = \varepsilon_\infty \boldsymbol{E} + 4\pi \boldsymbol{M} = \varepsilon_\infty \boldsymbol{E} + \frac{4\pi N \langle m^2 \rangle}{3k_B T} F \boldsymbol{E} \qquad \text{(II-12)}$$

where ε_∞ is the dielectric constant of the media. This equation with the relation of $\boldsymbol{D} = \varepsilon \boldsymbol{E}$ yields for the relaxation strength $\Delta\varepsilon$ $(=\varepsilon - \varepsilon_\infty)$

$$\frac{\Delta\varepsilon}{C} = \frac{4\pi N_A \langle m^2 \rangle}{3k_B T M} F \qquad \text{(II-13)}$$

where C is the concentration of polar molecule in mass/volume and M is its molecular weight. Equation II-13 is applicable to dilute polymer solutions. For polymer chains having type-A dipole moment P_A, $\langle m^2 \rangle$ in eq II-13 can be replaced by $\langle P_A^2 \rangle$ and thus the relation between $\langle r^2 \rangle$ and $\Delta\varepsilon$ can be written as[10]

$$\frac{\Delta\varepsilon}{C} = \frac{4\pi N_A \mu^2}{3k_B T} \frac{\langle r^2 \rangle}{M} F \qquad \text{(II-14)}$$

where μ has been defined in eq II-1. This equation means that if μ is determined either theoretically or experimentally and F is known, the absolute determination of $\langle r^2 \rangle$ is possible.

II-4-2. Internal Electric Field

The internal electric field has long been studied theoretically. The simplest expression of it is the so-called cavity field proposed by Lorentz[11] who considered the dilute solution of a polar molecule dissolved in a nonpolar solvent. Assuming that a point dipole is put at the center of a vacuum cavity of the size of the polar molecule, he expected F as

$$F = (\varepsilon_s + 2) / 3 \qquad \text{(II-15)}$$

where ε_s is the dielectric constant of the solvent. The dipole feels the external field E plus an extra field generated by the charge at the surface of the cavity due to the polarization of the solvent. In the Onsager theory,[11,12] surface charge induced by a reaction electric field due to the dipole itself is also taken into account. In the case of a non-polar solvent, F is given by

$$F = (\varepsilon_s + 2)^2 / 9 \qquad \text{(II-16)}$$

Stockmayer and Baur[10] used this equation in their theory of the normal mode relaxation. For a pure polar liquid, such as neat chlorobenzene, the Onsager theory predicts[5,7]

$$F = (n^2 + 2)^2(2\varepsilon_s + 1)/ 3(2\varepsilon_s + n^2) \qquad \text{(II-17)}$$

where n is the refractive index of the liquid.

In case of solutions of a type-A polymer, however, it is quite doubtful that any of these equations can be used for F in eq II-14 because the assumption of a vacuum cavity of the size of a random coil is not realistic. Adachi *et al.*[13] examined the ε_s dependence of $\Delta\varepsilon$ for dilute solutions of a type-A1 polymer poly(2,6-dichloro-1,4-phenylene oxide) (PDCPO) in various solvents such as chlorbenzene (ClBz) (ε_s=10.1), *o*-dichlorobenzene (DClBz) (ε_s=5.6), and carbon disulfide (CS_2) (ε_s=2.6). Using $\langle r^2 \rangle$ estimated from $[\eta]$ with an approximation of uniform expansion, they found that $(\Delta\varepsilon/C)/\langle r^2 \rangle$ is independent of ε_s in contrast to the strong dependence of F on ε_s predicted by eqs II-15 - II-17. They concluded that F is independent of ε_s for type-A dipoles and found that F is equal to unity by using eq II-14. For the validity of F=1, they further made a theoretical consideration.[14] Therefore we use F=1 hereafter.

II-5. Dynamical Features of Normal Mode Relaxation

The complex dielectric constant ε^* of macroscopic system is generally given by the Fourier-Laplace transform of the time t derivative of the response function $\Phi(t)$[15]

$$\Phi(t) = \frac{\langle \boldsymbol{M}(0)\cdot\boldsymbol{M}(t)\rangle}{\langle M(0)^2\rangle} \tag{II-18}$$

where $\boldsymbol{M}$ is the vector sum of both the permanent and induced dipole moments existing in the system. Then ε^* is written as[16-18]

$$\begin{aligned}\varepsilon^* &= \varepsilon'(\omega) - i\varepsilon''(\omega) \\ &= \varepsilon_\infty + \Delta\varepsilon \int_0^\infty (-d\Phi/dt)\exp(-i\omega t)\, dt\end{aligned} \tag{II-19}$$

where ε_∞ is the unrelaxed dielectric constant; $i^2=-1$; ω, the angular frequency; and $\Delta\varepsilon$, the relaxation strength.

We consider a solution of a monodisperse type-A polymer in a non-polar solvent. The dipoles present in this system are the permanent dipoles of the i-th polymer molecule $\boldsymbol{P}_i$, those of the solvent molecules $\boldsymbol{m}_s$, the induced dipole moments of the polymer $\boldsymbol{q}_i$, and those of the solvent $\boldsymbol{q}_s$. Then $\boldsymbol{M}$ is the sum of these dipole vectors:

$$\boldsymbol{M}(t) = \Sigma_i \boldsymbol{P}_i + \Sigma_i \boldsymbol{q}_i + \Sigma_s \boldsymbol{m}_s + \Sigma_s \boldsymbol{q}_s \tag{II-20}$$

From eqs II-18 and II-20, we obtain a quite complex expression of $\Phi(t)$. However, as far as the normal mode process of a type-A polymer is concerned, the cross-terms such as $\langle \boldsymbol{P}_i(0)\cdot\boldsymbol{q}_j(t)\rangle$ and $\langle \boldsymbol{P}_i(0)\cdot\boldsymbol{m}_j(t)\rangle$ can be ignored, because these

correlations decay much faster than $\langle \boldsymbol{P}_i(0)\cdot\boldsymbol{P}_i(t)\rangle$. We may also ignore the cross correlation function $\langle \boldsymbol{P}_i(0)\cdot\boldsymbol{P}_k(t)\rangle$ between i and k-th chains, when the dipole moment of the polymer is not large. Then $\Phi(t)$ is reduced to the molecular autocorrelation function as given by

$$\Phi(t) = \frac{\langle \boldsymbol{P}(t)\cdot\boldsymbol{P}(0)\rangle}{\langle P(0)^2\rangle} \qquad \text{(II-21)}$$

When the polymer possesses the type-A and type-B dipole moments, $\boldsymbol{P}$ is the vector sum of two dipoles $\boldsymbol{P}_A$ and $\boldsymbol{P}_B$. Similarly to the terms $\langle \boldsymbol{P}_i(0)\cdot\boldsymbol{q}_j(t)\rangle$, we can safely ignore the cross terms between the parallel and perpendicular components, *i.e.*, $\langle \boldsymbol{P}_A(0)\cdot\boldsymbol{P}_B(t)\rangle$ and $\langle \boldsymbol{P}_B(0)\cdot\boldsymbol{P}_A(t)\rangle$ because these terms also decay faster than $\langle \boldsymbol{P}_A(0)\cdot\boldsymbol{P}_A(t)\rangle$. In addition, since these terms are zero at t=0 as discussed in the previous section, its relaxation strength is considered to be small. Therefore $\boldsymbol{P}$ can be replaced by $\boldsymbol{P}_A$. Since $\boldsymbol{P}_A$ is proportional to the end-to-end vector $\boldsymbol{r}$, we finally obtain

$$\Phi(t) = \frac{\langle \boldsymbol{r}(t)\bullet\boldsymbol{r}(0)\rangle}{\langle r(0)^2\rangle} \qquad \text{(II-22)}$$

A point to note here is that μ appearing in the denominator and numerator cancel each other and hence the slow dynamic behavior is independent of the absolute value of μ.

References

1. Stockmayer, W. H. *Pure Appl. Chem.* **1967**, *15*, 539.
2. Nagai, K.; Ishikawa, T. *Polym. J. (Tokyo)* **1971**, *2*, 416.
3. Mansfield, M. L. *Macromolecules* **1986**, *19*, 1427.
4. Adachi, K.; Kotaka, T. *Prog. Polym. Sci.* **1993**, *18*, 585.
5. Flory, P. J. *Statistical Mechanics of Chain Molecules*. Wiley, New York **1969**
6. Eyring, H. *Phys. Rev.*, **1932**, *39*, 746.
7. Kuhn, W. *Kolloid-Z* **1934**, *68*, 2; **1936**, *76*, 258; **1939**, *87*, 3
8. Oka, S "Yuudentairon" Iwanami-shoten: Tokyo, 1954.
9. Saito, N. "Koubunshi Butsurigaku" Shoukabou: Tokyo, 1976.
10. Stockmayer, W. H.; Baur, M. E. *J. Am. Chem. Soc.***1964**, *86*, 3485.
11. Bottcher, C. J. F. "Theory of Electric Polarization", Elsevier: Amsterdam 1973.
12. Onsager, L.,*J. Am. Chem. Soc.* **1936**, *58*, 1486.
13. Adachi, K. ;Okazaki, H.; Kotaka, T. *Macromolecules* **1985**, *18*, 1486.
14. Adachi, K.; Kotaka, T. *Prog. Polym. Sci.* **1993**, *18*, 585.
15. Adachi, K.; Kotaka, T. *Macromolecules* **1988**, *21*, 157.
16. Cole, R. H. *J. Chem. Phys.* ***1965***, *42*, 637.
17. Nee, T.-H.; Zwanzig, R. *J. Chem. Phys.* **1970**, 52, 6353.
18. Williams, G.; Watts, D. C. *Trans. Faraday Soc.* **1970**, 66, 80.

III. Sample Preparation and Methods

III-1. Introduction

For experimental studies of the conformational and dynamical properties of flexible polymers, we need well characterized narrow distribution samples. In this chapter, methods of sample preparation and characterization are summarized.

In this work the dielectric method was mainly used. Measurements of light scattering and intrinsic viscosity were also used to characterize the dilute solution properties. The methods and principles of these measurements are also explained.

III-2. Sample Preparation

III-2-1. Polyester Samples

Four poly(ε-caprolactone) (PCL) and three poly(δ-varerolactone) (PVL) samples with narrow molecular weight distribution (MWD) were prepared with a catalyst of lanthanide compounds by Prof. Yasuda of Hiroshima University. The details of the polymerization are given in ref. 1. The two MW PCL samples with M_w(the weight-average molecular weight) =1.58 x 10^5, 2.57 x 10^5 (see Table I) were obtained by fractionation from a sample having slightly broad MWD with M_w/M_n (the weight to number-average molecular weight ratio) = 1.2. The fractionation was made by using benzene and *n*-heptane as the solvent and non-solvent, respectively, according to Koleske and Lundberg.[2]

III-2-2. Polyisoprene and Polybutadiene Samples

All *cis*-Polyisoprene (PI) and polybutadiene (PB) samples were prepared via anionic living polymerization in *n*-heptane at 20± 5 °C. As an initiator of polymerization, *sec* -butyllithium (*s*-BuLi) was used normally. For determination of molecular weight (MW) of PB samples by the end group analysis, *tert*-BuLi was used as the initiator.

III-2-3. Dipole Inverted Polyisoprene Samples

PI samples with *symmetrically* inverted dipoles were prepared *via* coupling of

monodisperse PI anions with a prescribed amount of *p*-xylyrene dichloride (XDC) and successive fractionation using benzene/methanol as a solvent/non-solvent.[3] Five PI samples with *asymmetrically* inverted dipoles were synthesized by a *multi-step* coupling method as summarized in Scheme 1.

As shown in Scheme 1, the method splits the coupling of two living PI precursors of molecular weights M_1 and M_2 into several steps. In the first step, to a vigorously stirred dilute heptane solution of the first PI precursor anions (with $M_1 > 24 \times 10^3$) added at -78°C was a large amount of XDC ($\cong$ 30-40 times excess to the anions) diluted with tetrahydrofuran (THF) was added at -78°C. Immediately after the addition, single-chain termination was completed and the first precursors with chlorinated ends (PI-Cl) were obtained as a major product. When necessary, the living ends of the precursors were converted to diphenyl ethylene (DPE) anions through a reaction with about 2 times excess of DPE just before the addition of XDC (case II of Scheme 1).

In the second step, the first-step-product was precipitated into pure acetone (a non-solvent for PI) to largely reduce the amount of unreacted XDC left with the product. After removal of the supernatant containing the excess XDC, the precipitated product was thoroughly dried and then re-dissolved in pure THF. The whole precipitation/re-dissolution procedure was repeated in high vacuum for several times,[4,5] and the PI-Cl/THF solution containing only a small amount of residual XDC was recovered (cf., part b of Scheme 1).

In the third step, the PI-Cl chains were allowed to couple with 2-3 times excess of the second precursor PI anions (with $M_2 < M_1$) at $\cong$ 30°C for 2-3 days to yield dipole-inverted PI chains (cf., part c of Scheme 1). (Dimers of the second precursors were also formed as a minor product due to residual XDC, but they were removed by later fractionation.) For convenience for later characterization, the living ends of the second precursors were converted to DPE anions when DPE was not used in the first step (case I of Scheme 1), and vice versa (case II).

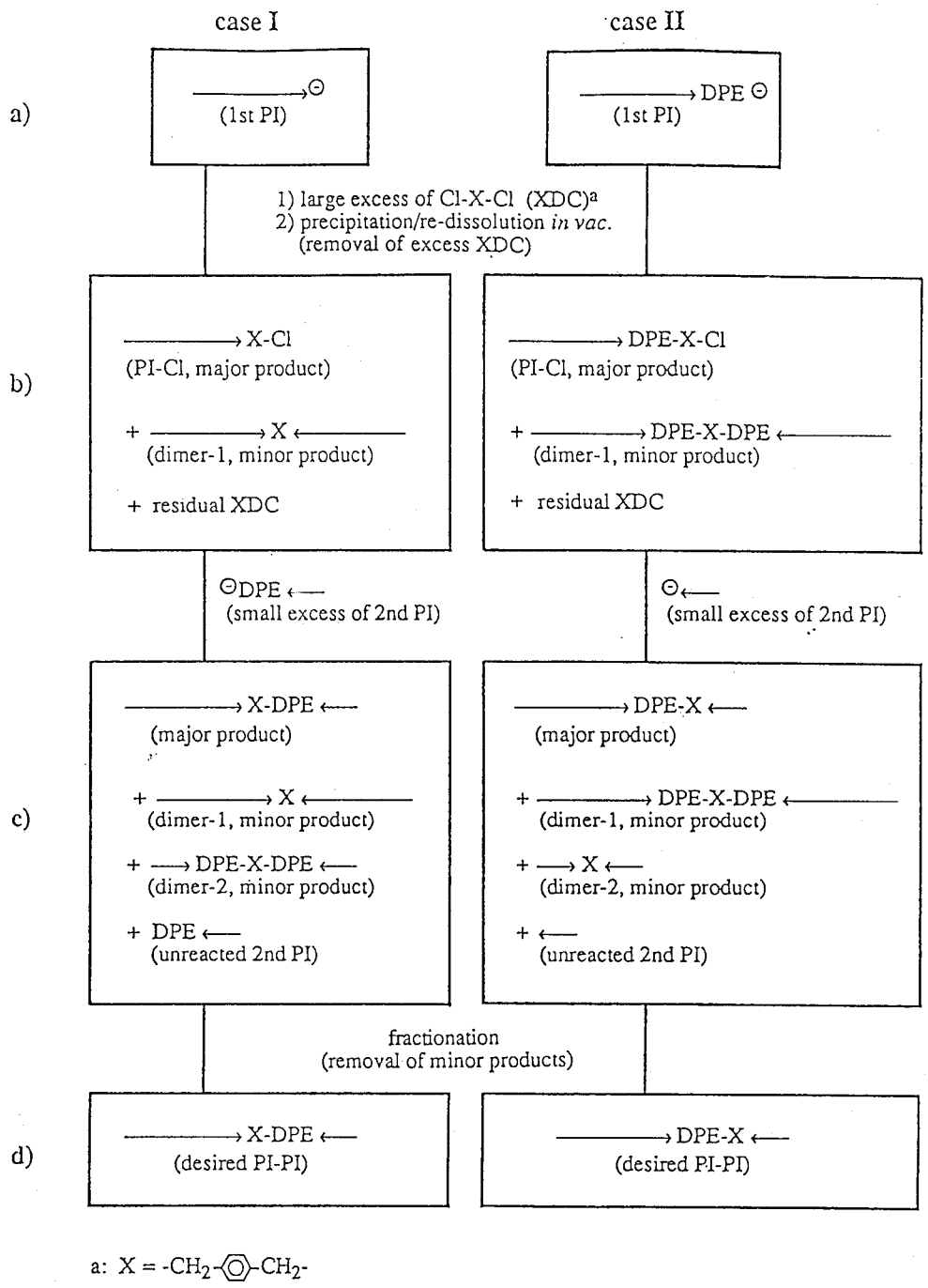

a: X = -CH_2-⬡-CH_2-

Scheme 1. Synthesis of PI chains with asymmetrically inverted dipoles *via* multi-step coupling.

Finally, after fractionation of the third-step-product from benzene/methanol solutions, we obtained dipole-inverted PI chains composed of two PI blocks of the molecular weights M_1 and M_2: The direction of the parallel dipoles is the same in each block but inverted at the junction between the two blocks.

III-3. Characterization

III-3-1. Gel Permeation Chromatography

The weight-average molecular weights, M_w, of all samples except for the four high MW PI and four low MW PB samples were determined by gel permeation chromatography (GPC: Tosoh Co., Model HLC-801A) equipped with refractive index (RI), ultraviolet (UV) absorption (Tosoh, UV-8011) and low angle light scattering (LS) (Tosoh, LS-8000) monitors. The eluent was tetrahydrofuran (THF). The M_w/M_n ratio was calculated from the GPC diagram by using the calibration curves of M_w vs.elusion volume. The characteristics of the PCL and PVL samples are listed in Table I, and those of PI and PB in Table II. The resulting MW values for four high MW PIs from light scattering and for oligo-PBs from NMR are also listed in Table II (see III-2-3 for NMR measurement).

Table I. Characteristics of PCL and PVL Samples

code	$10^{-3}M_w$	M_w/M_n	$[\eta]^a/g^{-1}cm^3$	code	$10^{-3}M_w$	M_w/M_n	$[\eta]^a/g^{-1}cm^3$
PCL09	9.12	1.07	25.4	PVL14	13.9	1.08	22.2
PCL17	16.6	1.09	37.3	PVL24	23.8	1.07	29.8
PCL38	38.0	1.09	65.7[b]	PVL38	38.0	1.07	44.2
PCL158	158	1.09	170				
PCL257	257	1.10	223				

a: determined in benzene at 25°C

b: calculated from the equation $[\eta]=6.4\times10^{-2}\ M_w^{0.66}$

Table II. Characteristics of PI and PB Samples

code	$10^{-3}M_w$	M_w/M_n	$[\eta]^a$/g^{-1}cm^3
PI-86	86	1.06	
PI-140	140	1.05	88.1
PI-222	222[b]	1.07	
PI-542	542[b]	1.06	
PI-651	651	1.19	
PI-743	743[b]	1.07	249.6
PI-1230	1230[b]	1.07	

code	$10^{-3}M_w$ or M_n	M_w/M_n	$[\eta]^a$/g^{-1}cm^3
PB-0.7	0.711[c]		
PB-01	1.25[c]		
PB-03	2.70[c]		
PB-05	5.40[c]		
PB-06	5.95	1.05	
PB-09	9.24	1.07	
PB-13	13.0	1.05	20.9
PB-20	19.9	1.06	
PB-33	33.1	1.06	39.7
PB-63	62.9	1.04	64.8
PB-89	89.0	1.05	
PB-211	211	1.03	127
PB-521	521	1.15	225

a: determined in heptane at 22°C

b: determined from LS measurement

c: number average molecular weight determined from NMR measurement

III-3-2. Characterization of Products by Multi-Coupling Reaction

The products of the dipole-inverted PI samples were characterized with the GPC apparatus mentioned in the previous section. Monodisperse PI chains[3] were used as elution standards for the products synthesized by the multi-coupling reaction.

Through the multi-step coupling, a UV-active coupler-unit composed of *p*-xylyrene and DPE groups was attached to each PI chain (cf., part d of Scheme 1). This low-MW unit had no detectable contribution to the RI and LS signals for the

high-MW PI chains made in this study. However, since the isoprene unit has very weak UV absorption (at λ = 254 nm), even one coupler-unit per chain drastically increased the UV signal intensity. Using this feature, we examined the coupler/isoprene composition at various stages of the multi-step coupling through the UV signal.

As an example of the UV and RI signals of the products at various stages of the reaction, Figure III-1 shows those for the case II (cf., Scheme 1) with M_1 = 34.7 x 10^3 and M_2 = 13.7 x 10^3. The signal sensitivities are the same for all GPC traces a-e, so that the changes in coupler/isoprene composition during the reaction are seen in the figure as the differences of the UV/RI signal ratios for the traces. For the main peaks of the traces a and b obtained before and after the reaction of the first PI precursor with DPE and XDC, we find that the RI signal is the same but the UV signal is much larger for the latter. Thus, the coupler-units were successfully attached to the precursor ends to obtain the PI-Cl chains as the main product. Although a small amount of the dimers was seen for the trace b at a location corresponding to $2M_1$ (the solid arrow), they were removed by later fractionation.

The GPC trace b of the first-step product was not affected by the precipitation/re-dissolution procedure, and changed to the trace d after the reaction with the second precursor PI anions (trace c). The UV/RI signal ratio for the main peak of the trace d is certainly smaller than that for the main peak of the trace b. In addition, we found that the former peak appeared at a location corresponding to $M = M_1+M_2$ (shown by the diamond-shaped arrow). These results indicate a successful coupling of the two precursors. Finally, a small amount of undesired components, unreacted second precursors, their dimers (dashed arrow for the trace d), and the dimers of the first precursors (solid arrow), were removed by fractionation to obtain the final product.

The weight-average molecular weights M_w and polydispersity indices M_w/M_n for the PI precursors and the dipole-inverted PI chains (final product), were

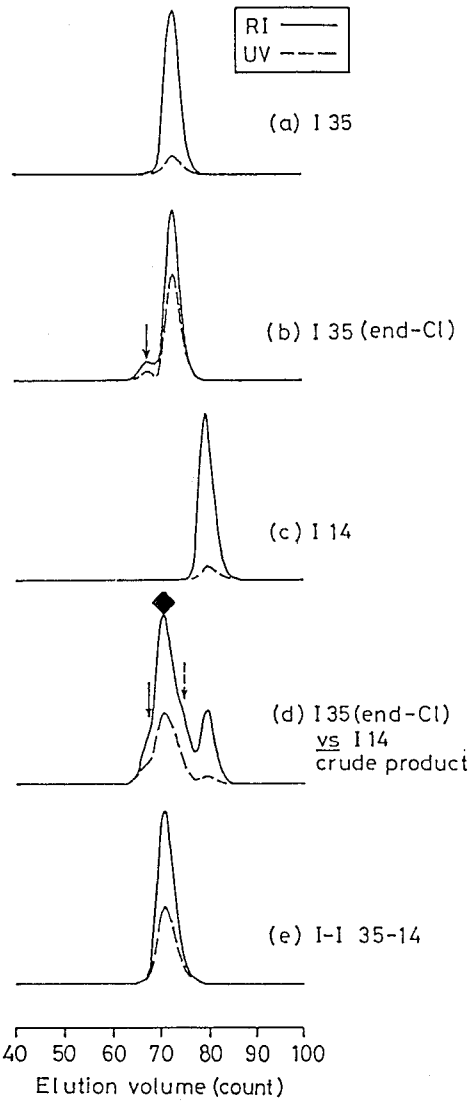

Figure III-1. GPC traces for products obtained at various stages of the synthesis of a dipole-inverted PI sample with $M_1 = 34.7\times10^3$ and $M_2 = 13.7\times10^3$. The solid and dashed arrows for the part b and d indicate the dimers of the first and second precursors, respectively. These minor components were formed through a bimolecular termination of living precursor anions by *p*-xylyrene dichlorides. The diamond shaped arrow for the trace d indicates the dipole-inverted PI chain having $M = M_1 + M_2$.

evaluated from their RI signals with an elution volume calibration. The M_w values were also determined from the LS signals, and good agreements were observed. The results of the characterization are summarized in Table III. As seen there, the molecular weights for all the PI samples (except I-I 415-415) are nearly the same.

In addition to the RI and LS signals, the UV signals were analyzed to evaluate a quantity

$$r_{UV} = \frac{A_c + A_1 + A_2}{A_f} \qquad \text{(III-1)}$$

Here, A_1 and A_2 are the *molar* UV absorption for the first and second PI blocks involved in the final product (cf., part d of Scheme 1), and A_c and A_f are the molar absorption for the coupler unit and the final product, respectively. We should have $r_{UV} = 1$, if the final product contains only the desired PI chains with asymmetrically inverted dipoles. Thus, the quantity r_{UV} was used as a measure for a purity of that product.

A_1 and A_2 were evaluated from the UV data and molecular weights of the PI precursors recovered before the reaction with DPE and XDC (cf., Scheme 1). Similarly, A_f was evaluated from the UV data and MW for the final product. For evaluation of A_c for the cases I of Scheme 1, we measured the molar UV absorption A_x for *p*-xylene and $A_{2\text{-DPE}}$ for the end-modified second precursor recovered after the reaction with DPE. The difference $\Delta A_2 = A_{2\text{-DPE}} - A_2$ represents the molar absorption of the DPE unit involved in that precursor, and A_c was evaluated as $\Delta A_2 + A_x$. For the cases II, we replaced the chlorine atom at the end of the first precursor by isoprene-pentamer through an end-capping reaction with a large amount of living pentamer anions. 100% replacement was easily achieved within 1*h* for this reaction involving oligo-anions. From the molar UV absorption $A_{1\text{-c-p}}$ for the resulting end-capped precursor, A_c was evaluated as $A_{1\text{-c-p}} - A_1$.

The r_{UV} values calculated from the A values are summarized in Table III together with the other measure for the product-purity, $r_M = (M_1 + M_2)/M$ with M_1, M_2, and M being the molecular weights of the two PI precursors and the final product, respectively. As seen there, both r_{UV} and r_M values are identical to unity within experimental uncertainties, indicating that the desired PI chains with asymmetrically inverted dipoles were successfully obtained.

Table III. Characteristics of Dipole-Inverted PI Samples.

Code	$10^{-3}M_w$	M_w/M_n	r_{UV}[b]	r_M[c]	first precursor		second precursor	
					$10^{-3}M_1$[a]	M_w/M_n	10^3M_2[a]	M_w/M_n
I-I 49-0[d]	48.8	1.05	------	------	48.8	1.05	------	------
I-I 50-6	55.4	1.06	1.03	1.01	49.9	1.05	6.12[f]	1.08
I-I 35-9	44.4	1.05	1.04	1.00	35.0	1.04	9.48	1.04
I-I 35-14	47.6	1.07	0.96	1.02	34.7	1.05	13.7	1.04
I-I 33-16	48.9	1.07	0.98	0.99	32.6	1.07	15.7	1.04
I-I 28-18	47.4	1.06	0.96	0.96	27.5	1.04	18.0	1.04
I-I 24-24	47.7	1.06	------	------	23.9	1.05	------	------
I-I 415-415[e]	828[g]	1.08	------	------	415[g]	1.07	------	------

a: weight-average molecular weight
b: $r_{UV} = (A_c + A_1 + A_2)/A_f$
c: $r_M = (M_1 + M_2)/M$
d: regular PI without dipole-inversion
e: this sample is used in section V-3.
f: this sample is used in section V-5.
g: determined from the GPC calibration using the PI samples characterized by LS measurement (listed in Table II).

III-3-3. Nuclear Magnetic Resonance (NMR)

The number average molecular weight M_n of oligo-PB samples were determined from the molar ratio of protons in the backbone to the *tert*-butyl group by ^{1}H-NMR (JEOL GSX-400 at 400 MHz). NMR measurements were carried out at 30°C for 20 wt % $CDCl_3$ solutions, and a small amount of $CHCl_3$ was used as an internal standard. Figure III-2 shows the representative ^{1}H-NMR spectrum of PB-01.

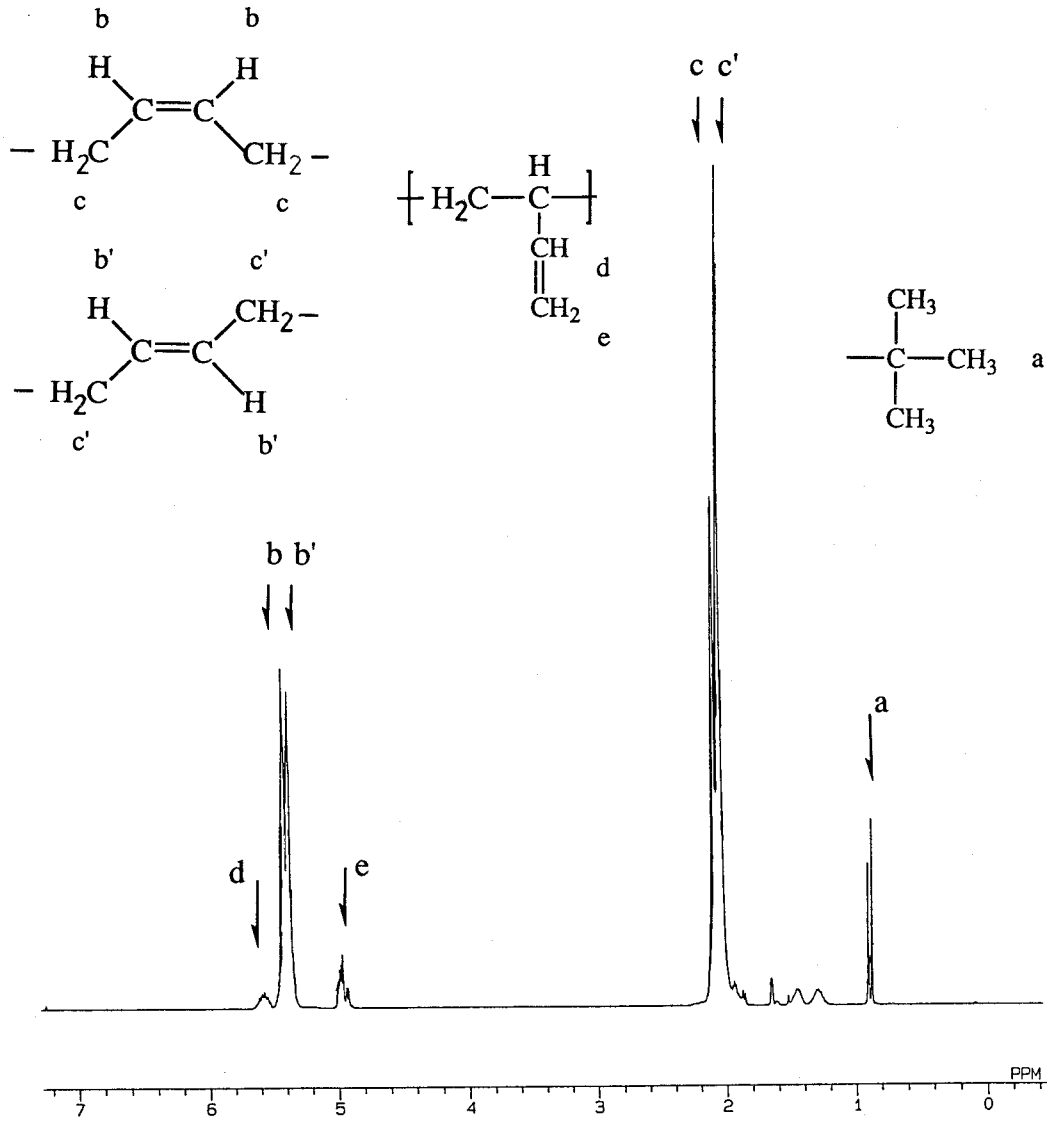

Figure III-2. NMR spectrum of PB-01.

The assignment of NMR peaks of each proton in the structure of *cis*-, *trans*-, *vinyl*- and in *t*-butyl group was made according to the references 6 and 7 and shown in this figure. From the NMR peak intensity I of each protons, number average molecular weights were determined from the following equation:

$$M_n = \frac{(I_b+I_{b'})/2+(I_d+I_e)/3}{I_a/9} \times 54 + 57 + 1 \qquad \text{(III-2)}$$

where the subscripts correspond to each proton in Figure III-2. The results are listed in Table II.

III-4. Methods

III-4-1. Dielectric Spectroscopy

When alternating voltage V^* (= $V_0\, e^{i\omega t}$) is applied to a capacitor of vacuum capacitance C_0 filled with a dielectric of ε^* (=ε'- $i\varepsilon''$). The complex admittance is $i\omega C_0\varepsilon^*$ and the current I^* (= $I_0\, e^{i(\omega t+\pi/2-\delta)}$) traversing the capacitor is given by[8]

$$I^* = i\omega C_0\varepsilon^* V^* \qquad \text{(III-3)}$$

When the capacitor is equivalent to a parallel combination of a pure capacitor with capacitance C and a pure resistor with conductance G, ε' and ε'' are given by

$$\varepsilon' = \frac{C}{C_0}, \quad \varepsilon'' = \frac{G}{\omega C_0} \qquad \text{(III-4)}$$

These two quantities, C and G, were measured with capacitance bridges; in the range from 100 Hz to 20 kHz and 20kHz to 1MHz with two capacitance bridges[9] (General Radio 1615A and Ando TR-IBK Type respectively) and 20kHz to 1 MHz with an LCR meter (Yokogawa Hewlett-Packard 4284A) and those from 1MHz to 100MHz with a twin-T type bridge (Fujisoku DLB 1101D).

Two type of capacitance cells (i) and (ii) were used. Sketches of the cell and

(i)

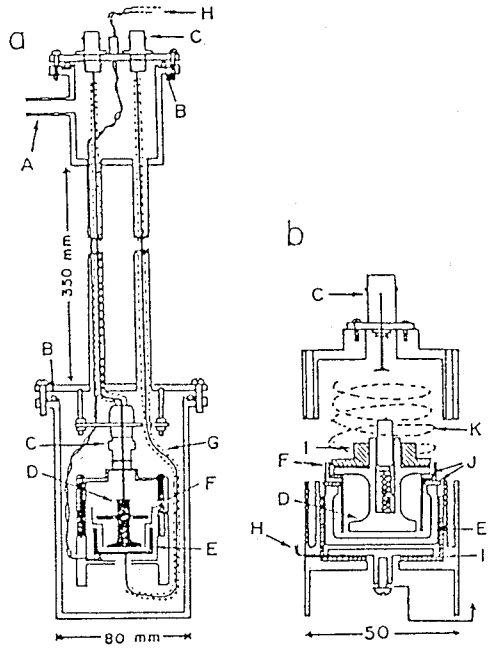

(ii)

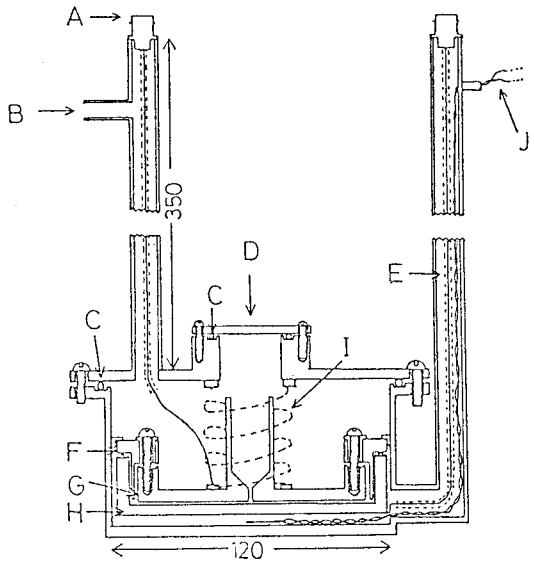

Figure III-3. Sketches of the capacitance cell: (i) standard cell, (ii) large cell.

the cryostats are shown in Figure III-3. For measurements on dilute solutions of PI, the cell (ii) with $C_0 \cong 130$ pF was used. The other samples were measured with the standard type cell (i) $C_0 \cong 25$ pF. The cell (ii) was designed to detect a weak signal from a trace amount of PI in dilute solution in such a way that liquid samples could be introduced into the cell from the inlet D without dismantling the cell in order not to change C_0.

Since values of ε'' for dilute solution of PI were of the order of 10^{-4}, careful data correction was needed. The measurements were carried out twice on the pure solvent and then on a sample solution. The ε'' value was corrected by subtracting the ε'' value for the pure solvent from that for the solution. Figure III-4 shows the representative data of ε'' measured with the General Radio and Ando bridges before and after this correction.

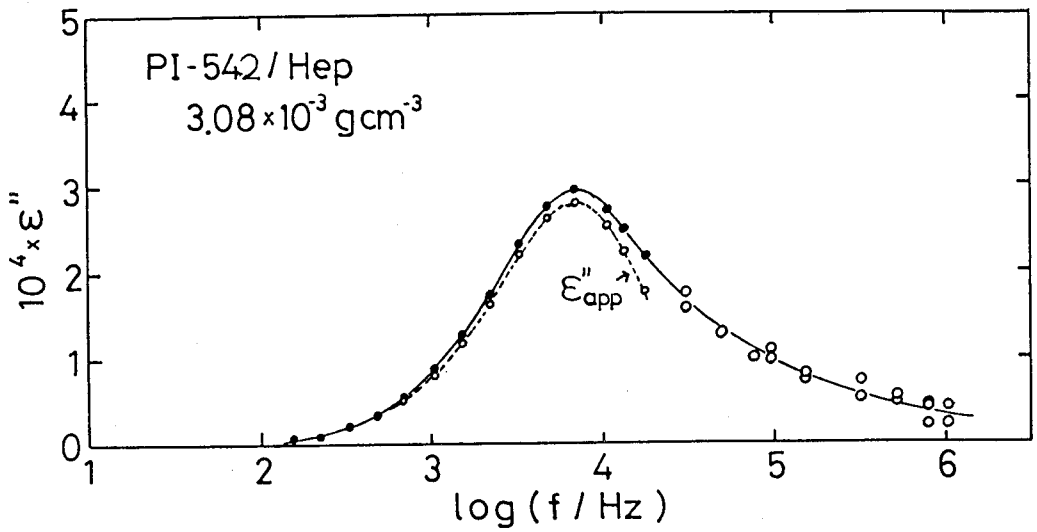

Figure III-4. Representative data of ε'' for PI-542/heptane solution. The smaller open circles represent apparent (uncorrected) value measured with GR bridge and the filled circles are the data after collection of subtracting the ε'' of pure solvent. The larger unfilled circles in the high f range are those measured with the Ando bridge and corrected by the same method.

The relaxation strength $\Delta\varepsilon$ was determined from the area under the ε'' curve by

$$\Delta\varepsilon = \frac{2}{\pi}\int_{-\infty}^{\infty} \varepsilon'' \, d\ln f \qquad \text{(III-5)}$$

When the measured frequency range was limited, we assumed that $\Delta\varepsilon$ is proportional to the loss maximum value ε''_{max} of the loss multiplied by the half width δ, i.e., $\Delta\varepsilon = K'\varepsilon''_{max}\delta$. The constant K' was estimated to be 1.8 from the ε'' curves measured over wide frequency range. The error in the determination of $\Delta\varepsilon$ is estimated to be within 5%.

III-4-2. Viscometry

Intrinsic viscosities $[\eta]$ were determined by using a Ubbelohde type capillary viscometer. The results are listed in Tables I and II.

The relative viscosity of PB solutions was also measured with the Ubbelohde type viscometer. The results will be used for the discussion about the relation between dielectric relaxation time and medium viscosity for PI/PB/heptane ternary systems in section V-4.

III-4-3. Light Scattering Measurements

In order to determine the mean square radius of gyration $\langle S^2 \rangle$ for PI in cyclohexane and in heptane, light scattering measurements were made with a scattering photometer (Fica 50) using cylindrical cells in the angular range from 30 to 150°. The vertically polarized light of 436nm was used as the incident beam. With pure benzene as the reference liquid, reduced scattering intensities R_θ for polymer solutions was calculated.[10]

At infinite dilution, R_θ is expressed by

$$\left(\frac{KC}{R_\theta}\right)_{C=0} = \frac{1}{M_W}\left[1+\frac{1}{3}\left(\frac{4\pi}{\lambda}\right)^2 \langle S^2 \rangle_z \sin^2\frac{\theta}{2} + O\left(\sin^4\frac{\theta}{2}\right)\right] \qquad \text{(III-6)}$$

where λ is the wave length of incident light in the scattering medium and K is the optical constant defined by

$$K = 4\pi^2 n_0^2 \, (\partial n/\partial C)^2 \, / \, N_A \lambda_0^4 \qquad \text{(III-7)}$$

with λ_0 and $\partial n/\partial C$ being the wavelength of incident light in vacuum and the specific refractive index increment in units of $cm^3 g^{-1}$, respectively. The value of $\partial n/\partial C$ for PI/heptane solutions at 25°C was determined to be 0.165 $cm^3 g^{-1}$ by using a modified Schulz-Cantow type differential refractometer. For $\partial n/\partial C$ of cyclohexane solutions, the value reported by Takano *et al.* (0.115 $cm^3 g^{-1}$) was used.[11] Figure III-5 shows the plots of $(KC/R_\theta)^{1/2}$ vs. $sin^2(\theta/2)$ at infinite dilution for PI samples in cyclohexane and heptane at 25°C. For any samples, the intercepts for the two solutions are quite close to each other, showing a good agreement of M_w value in the two solvents (see eq II-6). The value of $<S^2>$ of PI determined from the initial slopes of the plots are compared with the dielectric relaxation strength data in section IV-2.

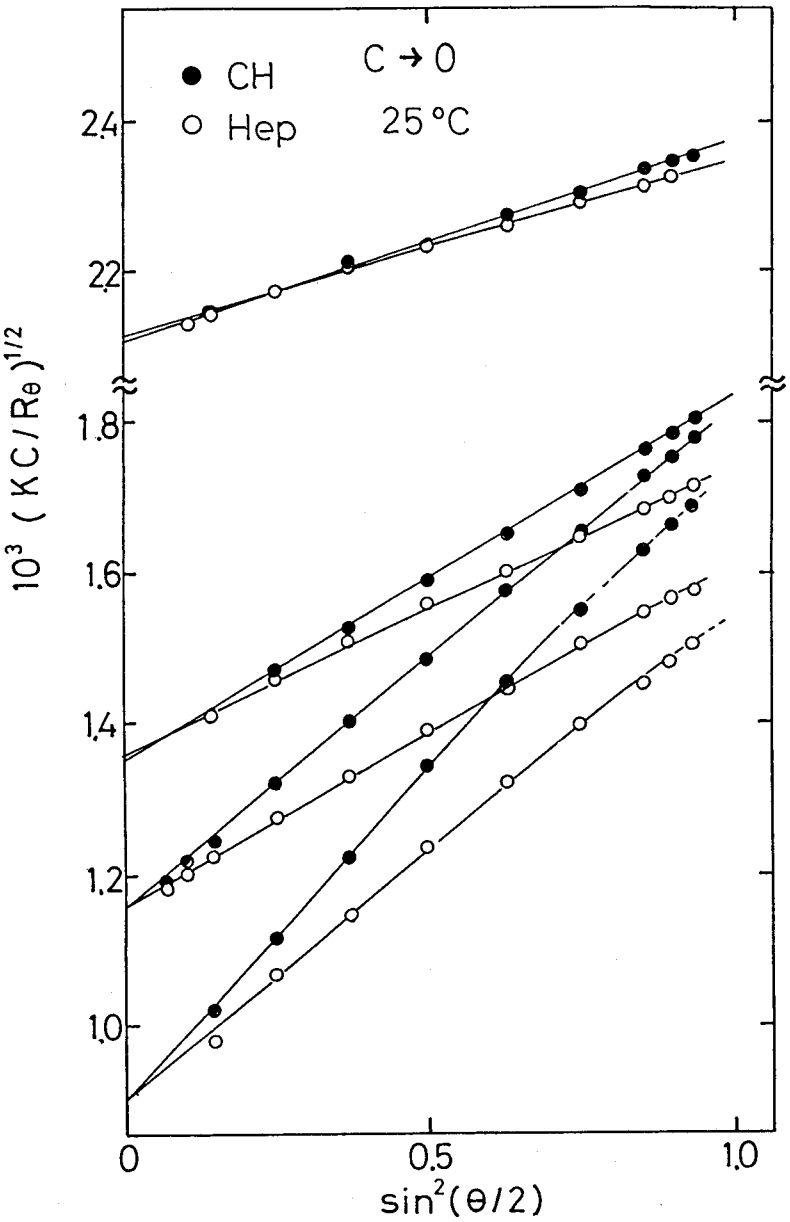

Figure III-5. Plots of $(KC/R_\theta)^{1/2}$ vs.$sin^2(\theta/2)$ for solutions of PI samples in heptane and cyclohexane at the infinite dilution. Samples; PI-222, PI-542, PI-743, and PI-1230 from top to bottom.

References

1. Yasuda, H. "Proc. of 1st International Symp. on Nontraditional Polymerization Method" Alma-Ata, 1990, *4*.
2. Koleske, J. V.; Lundberg, R. D. *J. Polym. Sci.* **1969**, *A-2*, 7, 897.
3. Yoshida, H.; Watanabe, H.; Adachi, K.; Kotaka, T. *Macromolecules* **1991**, *24*, 2981.
4. Watanabe, H.; Urakawa, O.; Kotaka, T. *Macromolecules* **1993**, *26*, 5073.
5. Watanabe, H.; Shimura, T.; Kotaka, T.; Tirrell, M. *Macromolecules* in press.
6. Okamoto, T. "Unique Structure and Catalysis of Novel Group 5A Metal Complexes" Master Thesis, Faculty of Science, Osaka University 1988.
7. Yoshida, H. "Dynamics of Star Shaped Polymer Chains" Doctoral Thesis, Faculty of Science, Osaka University 1991
8. Oka, S.; Nakata, O. "Kotaiyuudentairon";.Iwanami-shoten: Tokyo, 1960.
9. Hedvig, P. "Dielectric Spectroscopy of Polymers, 1st Ed.; Hilger: Bristol, 1977.
10. Miyaki, Y., Doctoral Thesis, Faculty of Science, Osaka University "*Dilute Solutions of Polystyrene* " **1981**
11. Takano, N.; Einaga, Y.; Fujita, H. *Polym. J.* **1985**, *17*, 1123.

IV. Dipole Moment and End-to-End Distance

IV-1. Introduction

In this chapter, the end-to-end distances of PI,[1] PCL, and PVL chain[2] in dilute and semidilute solutions are studied on the basis of eq II-14. As pointed out in the introductory chapter, the dielectric method is unique in the sense that it provides information on $\langle r^2 \rangle$. There have been no experimental studies on the comparison between $\langle r^2 \rangle$ and $\langle S^2 \rangle$ although several theoretical calculations were made.[3,4] For this purpose it is needed to examine the reliability and the limit of applicability of eq.II-14 to types A1, A2, and A3 chains. Obviously $\langle r^2 \rangle$ is uniquely determined for type-A1 chains if μ is determined theoretically or experimentally. The μ value so determined can be used irrespective of the condition such as solvent quality. On the other hand, for type-A2 or A3 polymers, $\langle \mu \rangle$ of eq II-2 may depend on the solvent nature. Therefore strictly speaking, we have to determine $\langle \mu \rangle$ for each solvent or medium to evaluate $\langle r^2 \rangle$. This will be a rather laborious work. However, optimistically speaking, the solvent effect on $\langle \mu \rangle$ may be small and $\langle \mu \rangle$ calculated in vacuum may be used in a good approximation. The two-parameter theory[3] of polymer solutions assumes that the dimension of a random coil is described by the excluded volume parameter and the step length b. The value of b is usually insensitive to solvent quality. If so, this must also be the case for μ. In fact, the data of the unperturbed dimensions of polymers listed in Polymer Handbook[5] indicate that the values of the characteristic ratio C_∞ for a given polymer are independent of solvent nature within a scatter of 10%. In an effort to settle these problems, we compare our experimental P_A with the theoretical dipole moments calculated by *ab initio* molecular orbital[6] and rotational isomeric methods[7] in section IV-2 of this chapter.

The end-to-end distance of a polymer chain decreases with increasing C by the shielding effect of excluded volume.[8,9] For type-A polymers this effect is

expected to be reflected to the change in $\Delta\varepsilon/C$. We investigate the C dependence of $\Delta\varepsilon/C$ for PI and PCL solutions and compared with the scaling theory proposed by Daoud and Jannink.[8,9]

The study of PI semidilute solution is extended to $<r^2>$ of probe PI chains in semidilute PB solutions in section IV-3. We investigate the excluded volume effect in the ternary system. The purpose of this investigation is to clarify how the excluded volume of the probe PI chain is shielded by its matrix PB chains in this system, especially the effect of PB molecular weight M_B and PB concentration C_B.

IV-2. End-to-End Distance of Several Type-A2 Chains in Dilute Solution

IV-2-1. Calculation of μ by the MO and RIS Models

In this section we attempt to calculate μ for PI and PCL. The *ab-initio* method[6] was used for calculation of the monomer dipole moment and the rotational isomeric state (RIS) model for determination of $<\mu>$ with eqs II-6 and II-7.

First we calculate the absolute value and the angle to the backbone of the monomer dipole moment for PI and poly(lactone)s by *ab-initio* molecular orbital method. In this calculation we adopt the bond lengths and the bond angles given in reference 7 and the rotational angles are all fixed to trans as shown in Figure IV-1. The calculated dipole vectors are indicated by arrows in this figure. The dipole moment of -COO- unit of 1.19 D is ca. 34% smaller than the observed value of 1.81 D for *n*-propylpropionate.[10] The discrepancy suggests that the *ab-initio* method is not so reliable for a molecule containing hetero-atoms such as oxygen and nitrogen. Thus we will use 1.81 D for the dipole moment of the ester group and only the direction of the dipole vector obtained by the *ab initio* calculation was employed. For PI, the calculated value may be reliable, since PI has no such hetero atom.

Next we tried to calculate $<\mu>$ with eqs II-6 and II-7 by the RIS model. The potentials for internal rotation were taken from reference 7 were adopted.

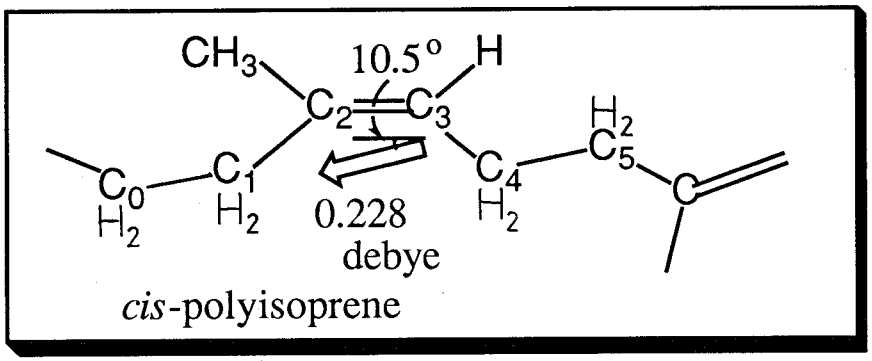

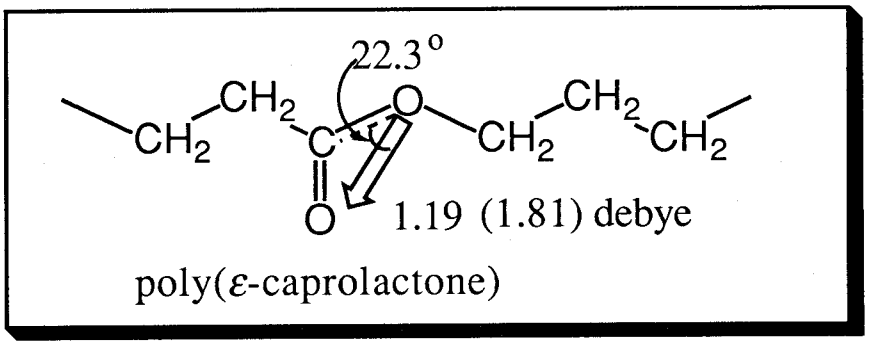

Figure IV-1. Result of MO calculation for PI and PCL.

Figure IV-2 shows the results of calculation on PI and PCL. The converged values of μ were taken as $<\mu>$ at $N \rightarrow \infty$ and listed in Table IV.

On the other hand we experimentally evaluated the value of $<\mu>$ by the following procedures. From eq II-14, $<\mu>$ is given by $(3k_BTM\Delta\varepsilon/4\pi N_AC<r^2>)^{1/2}$ with $F = 1$. The $<r^2>$ value was evaluated from the data of $<S^2>_\theta$[11,12] for PI assuming $<r^2> = 6<S^2>_\theta$, and for PCL and PVL $<S^2>$ was calculated from $[\eta]$ assuming the Flory-Fox equation $[\eta]=\Phi\ (<r^2>^{3/2}/M_w)$ with $\Phi = 2.5\times10^{23}$.[13] From the dielectric data of $\Delta\varepsilon$ and the value of $<r^2>$ thus evaluated, we determined $<\mu>$ for each polymer. The results are listed in Table IV. We see that the calculated and observed $<\mu>$ values agree within 25%. The discrepancy is attributed to the uncertainty in the dipole moments and the RIS potentials. Especially a large error may be involved in the RIS potentials of PCL since Flory and Williams[7] estimated them assuming the similarity of the ester and amide groups. Therefore a detailed calculation remains as future work.

Table IV. Comparison of $<\mu>$ values between the observed and calculate ones.

	calculated μ / esu	observed μ / esu
cis-Polyisoprene	4.99×10^{-12}	5.39×10^{-12}
poly(ε-caprolactone)	8.98×10^{-12}	11.3×10^{-12}

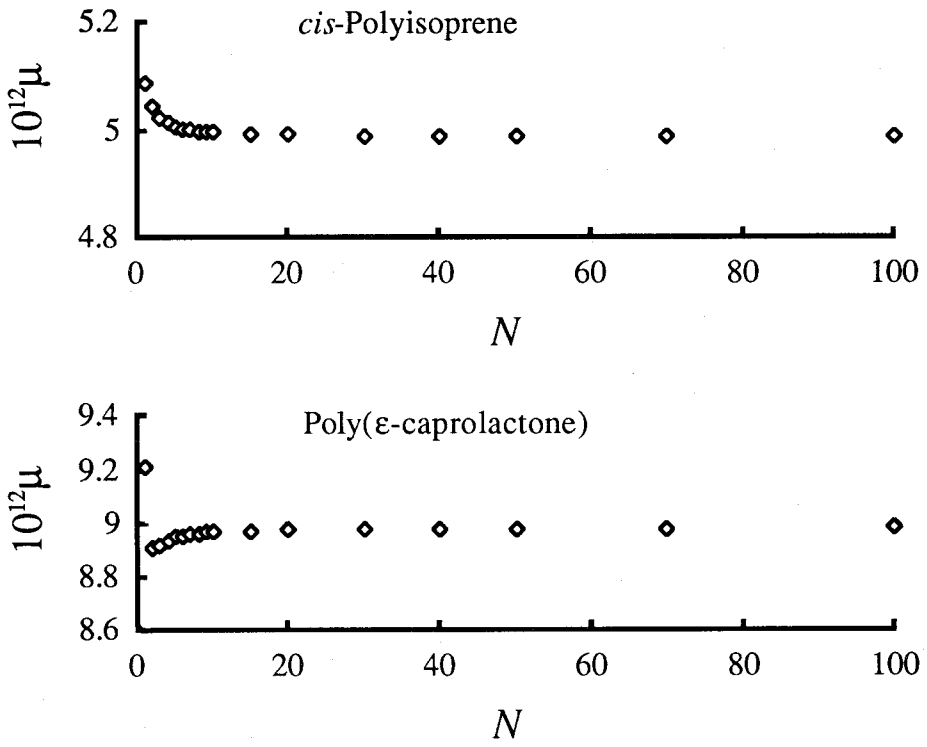

Figure IV-2. Result of the RIS calculation. Dependence of $<\mu>$ on the degree of polymerization N for PI and PCL.

IV-2-2. Relation between Local Dipole Vector and Conformation

Figure IV-3 shows the local conformations of PI and PCL. For PI, it is noted that carbon atoms 1, 2, 3 and 4 locate on a plane because the internal rotation of the -C=C- double bond is forbidden. Thus PI is composed of the virtual bond indicated by the dashed line and bond C_4-C_1. This figure also shows the potential energy E for the internal rotation angle ϕ around the C_3-C_4 bond calculated by a computer program "Molecular Mechanics 2" MM2.[14] It is seen that in the range of $100<\phi<250°$, E is very high. This indicates that the direction of C_4-C_1 bond is confined in a relatively narrow region of ±80°. Thus the fluctuation of the end-to-end vector $\boldsymbol{u}$ of the monomer unit against the monomer dipole vector $\boldsymbol{p}$ is relatively small. This suggests that PI is approximately a type-A1 chain. Contrary, in the case of PCL, the $\boldsymbol{u}$ fluctuates randomly against $\boldsymbol{p}$. Thus it is expected that μ of PCL depends more strongly on the local conformation than that of PI.

IV-2-3. Summary of Applicability of the Dielectric Method to Study of $\langle r^2 \rangle$

In this section we summarize the applicability of eq II-14 to studies of end-to-end vector. We may utilize eq II-14 in two ways, namely the determination of the absolute value of $\langle r^2 \rangle$ and the expansion factors α. The α for $\langle S^2 \rangle$ and $\langle r^2 \rangle$ are defined by

$$\alpha_S^2 = \langle S^2 \rangle / \langle S^2 \rangle_\theta \qquad \text{(IV-1a)}$$

$$\alpha_r^2 = \langle r^2 \rangle / \langle r^2 \rangle_\theta \qquad \text{(IV-1b)}$$

where the subscript θ indicates the unperturbed state. In studying the MW dependence of α_r in a solvent, no the exact value of μ is required, so that eq II-14 is applicable in this case. Similarly, the exact value of μ is unnecessary in the C dependence of α_r in semidilute solutions where the local chain conformation may be same in dilute solution. However for either comparison of the absolute $\langle r^2 \rangle$ among different solvent systems or determination of the absolute value of $\langle r^2 \rangle$, we have to determine $\langle \mu \rangle$ for each system.

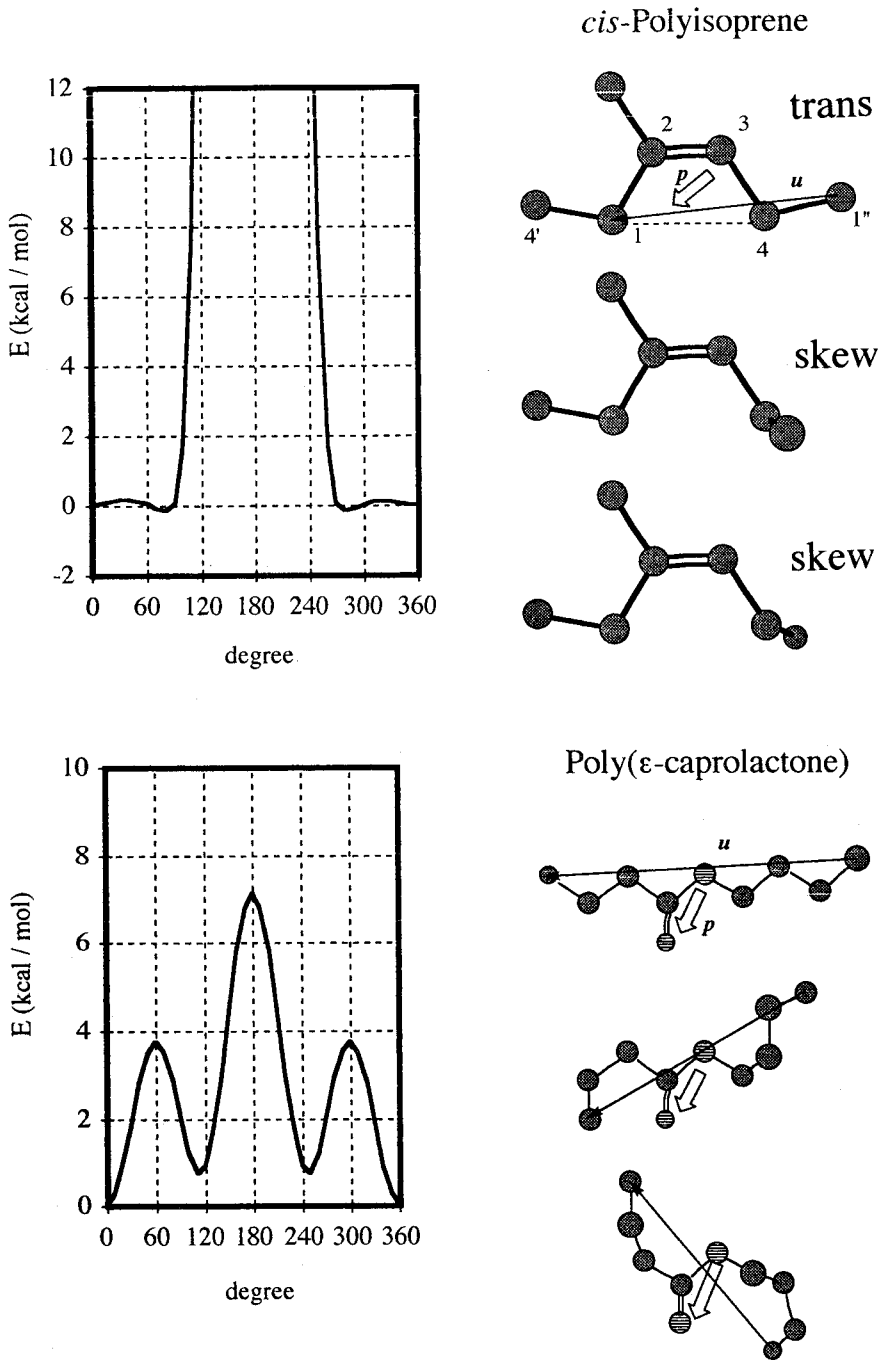

Figure IV-3. Monomer conformation and rotational potential energy for PI and PCL.

From eq.II-14 we can also define the "dielectric expansion factor" α_ε by

$$\alpha_\varepsilon^2 = (\Delta\varepsilon/C)/(\Delta\varepsilon/C)_\theta = \alpha_r^2\,(\mu^2/\mu_\theta^2) \qquad \text{(IV-1c)}$$

where μ_θ denotes μ in a theta state.

We have already shown that in type-A1 polymers μ/μ_θ is always unity. However in type-A2 or A3 polymers, μ/μ_θ may change with the potential of the RIS which changes by polymer-solvent interactions. In Table V the applicability for the determination of $<r^2>$ for type-A1, A2, and A3 polymers is summarized. In this table ○ indicates that μ is uniquely determined or the absolute value of μ is not necessary and × denotes that μ depends on the solvent. In the case of ×, we have to determine μ either by experiments or by the RIS potential determined by taking into account the polymer-solvent interactions.

Table V. Applicability of the determination of $<r^2>$

	Relative values			
	M_w dependence at constant C	C dependence in Semidilute solution	Comparison of $<r^2>$ among solutions in different solvent	absolute value
A1	○	○	○	○
A2 and A3	○	(○)*	×	×

*: If μ is determined by the local chain conformation and the conformation does not change against C, the applicability becomes good. In semidilute regime the local chain conformation is expected to be the same as that in dilute solution but in concentrated regime it may change so that the applicability will be limited in semidilute regime.

As mentioned above, PI can be approximately regarded as a type A1 chain. Thus $\mu/\mu_\theta \cong 1$ for PI. In section IV-3, we will compare $\alpha_\varepsilon^2 (\cong \alpha_r^2)$ and α_S^2 for PI solutions. In the later sections the M_w and C dependence of α_ε^2 is discussed.

IV-3. Dielectric Relaxation Strength and the Type-A Dipole Moments

IV-3-1. *cis*-Polyisoprene (PI) in Cyclohexane and Heptane Solutions

Figures IV-4(a) and (b) show ε''/C for dilute cyclohexane (good solvent) and heptane (marginal solvent) solutions of PI. We see that the peak area increases with increasing molecular weight. The relaxation strengths $\Delta\varepsilon/C$ calculated from the area under the ε'' curves (cf. eq III-5) are plotted against M_w in Figure IV-5. In this figure we have also plotted the data of dioxane (θ solvent) solutions. We can see clearly the excluded volume effects in this figure.

For the comparison between $<S^2>$ and $<r^2>$, we made light scattering (LS) measurements on the cyclohexane and heptane solutions. The z averaged mean square radius of gyration $<S^2>_z$ divided by M_w is plotted against M_w in Figure IV-6. Here the $<S^2>_z$ for PI/dioxane solutions reported by Hadjichristidis *et al.*[11] and Tsunashima *et al.*[12] are also plotted. We note that the slopes for each solvent in figures IV-5 and IV-6 agree well.

Now we consider the expansion factors α_S^2 and α_r^2 assuming $\alpha_r \cong \alpha_\varepsilon$. Since α_r^2 thus calculated corresponds to the number average, we corrected α_r^2 to the z-average value by assuming Zimm-Schulz distribution.[15] However the correction factor was only 3%. Figure IV-7 compares α_r^2 and α_S^2 It can be seen that $\alpha_r \propto \alpha_S$ and $\alpha_r > \alpha_S$ in the M_w range studied. The relations between α_r^2 and α_S^2 in the two solvents expressed by

$$\alpha_S^2 = 0.95\ \alpha_r^2 \quad \text{for heptane}$$
$$\alpha_S^2 = 0.82\ \alpha_r^2 \quad \text{for cyclohexane} \qquad \text{(IV-2)}$$

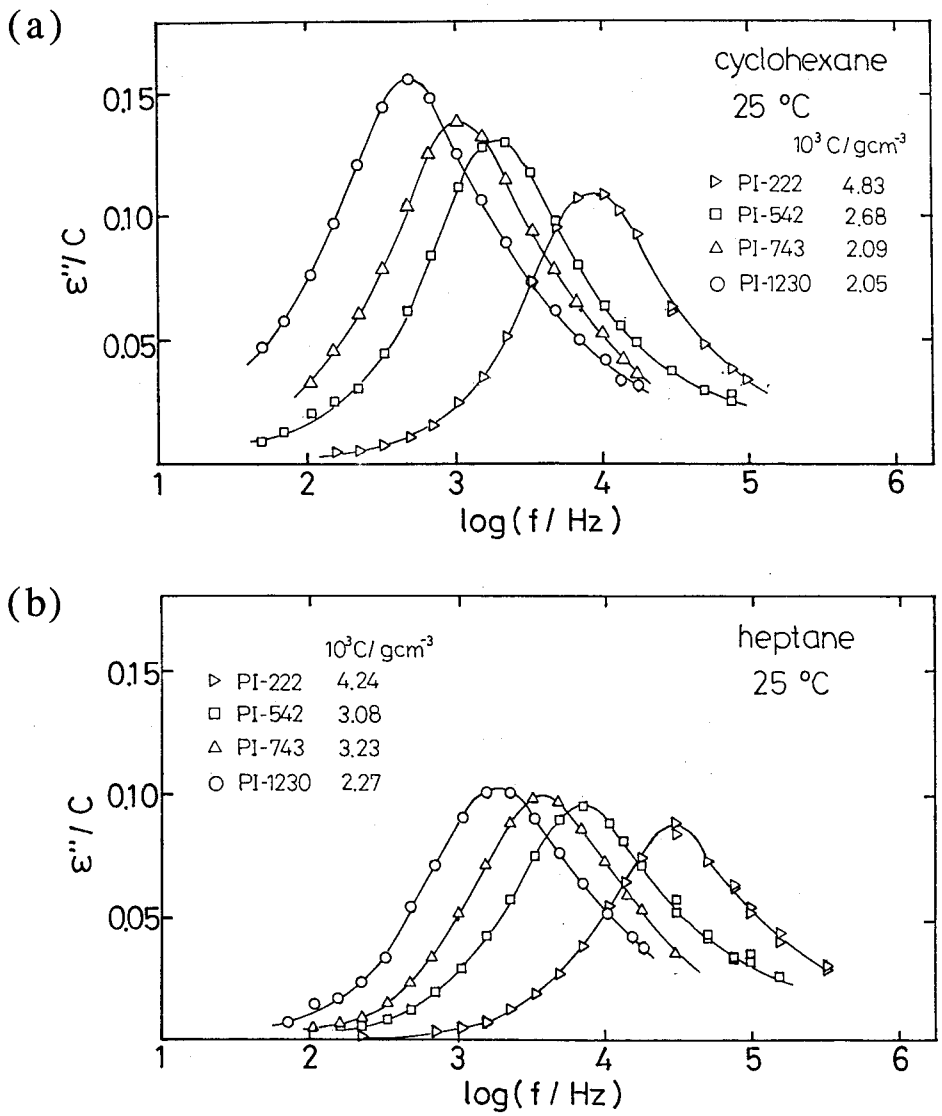

Figure IV-4. Dielectric loss curves reduced by PI concentration in dilute solution, (a) in cyclohexane and (b) in heptane.

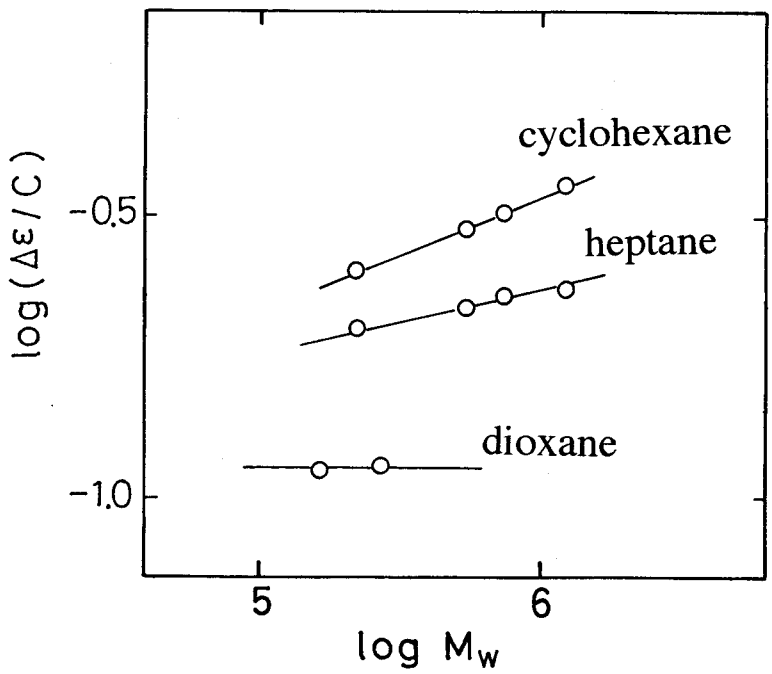

Figure IV-5. Double logarithmic plots of $\Delta\varepsilon/M_w$ vs. M_w for solutions of PI in cyclohexane (good solvent), heptane (marginal solvent), and dioxane (θ solvent).

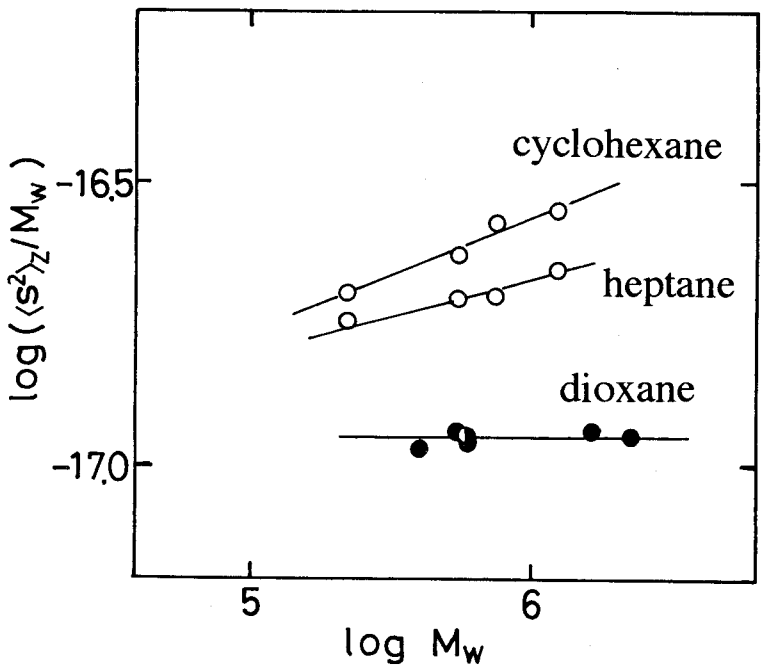

Figure IV-6. Double logarithmic plot of $<S^2>_z/M_w$ vs. M_w for the same solutions as shown in Fig. IV-5. For the dioxane solution the data reported by Hadjichristidis *et al.* and Tunashima *et al.* are plotted by filled and half filled circles.

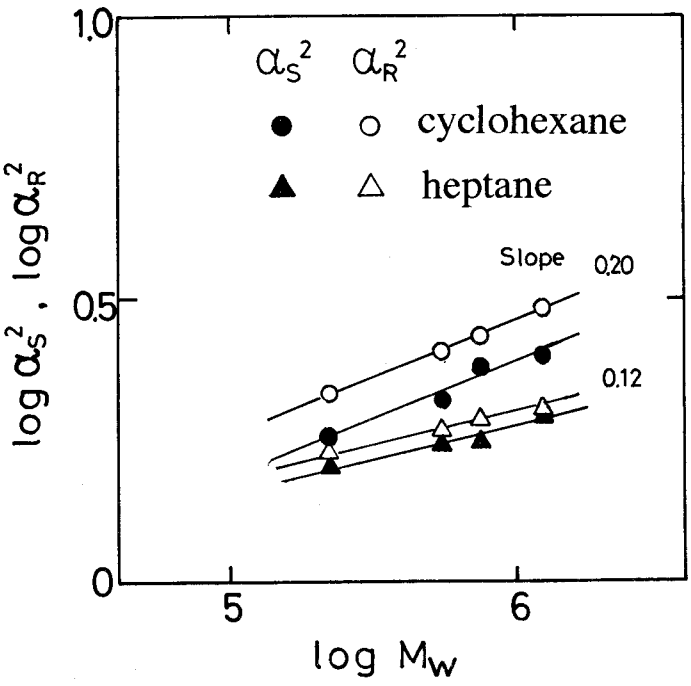

Figure IV-7. Comparison of the expansion factors for $<S^2>$ and $\Delta\varepsilon$ of PI in cyclohexane and heptane by taking the values in dioxane solution as standard.

Domb *et al.*[4] obtained the relation between α_S^2 and α_r^2 by a computer simulation of self-avoiding random flight chains, with the result that $\alpha_S^2 = 0.93\alpha_r^2$ for infinitely long chains. Our results are consistent with their simulation. However the proportionality constant 0.82 for cyclohexane solution (good limit solvent) is smaller than their result by 11%.

Since μ is constant in a given solvent, the M_w dependence of α_r can be determined explicitly. It is a reasonable result that the slopes of the log $\Delta\varepsilon/C$ vs. log M_w for cyclohexane and heptane solutions agreed well with those of log $<S^2>_z/M_w$ vs. log M_w.

IV-3-2. Poly(ε-caprolactone) and Poly(δ-varerolactone) in Benzene Solutions

In this section, we examine the dielectric relaxation strength of dilute benzene solutions of PCL and poly(δ-varerolactone) (PVL), both of which are similar in structure as shown in Fig. II-3.

The $[\eta]$ data listed in Table I can be cast into the Mark-Houwick-Sakurada equations:[13]

$$[\eta] = 6.4\times10^{-2}\, M_w^{0.66} \qquad \text{for PCL / benzene}$$
$$[\eta] = 3.0\times10^{-2}\, M_w^{0.69} \qquad \text{for PVL / benzene} \qquad \text{(IV-3)}$$

From the relation of $[\eta] \propto M_w^{3\nu-1}$, the excluded volume exponent ν is determined to be 0.55 for PCL and 0.56 for PVL. We see that benzene is a marginal solvent for both polymers.

Figure IV-8 shows the M_w dependence of $\Delta\varepsilon/C$ for PCL and PVL solutions. Using the value of ν evaluated from $[\eta]$, we predict the exponent for $\Delta\varepsilon/C$ ($\propto <r^2>/M_w \propto M_w^{2\nu-1}$) to be 0.10 for PCL and 0.12 for PVL. The actual slopes of the plots for PCL and PVL in Figure IV-8 are 0.11 for both and agree approximately with this prediction. This indicates that the weak M_w dependence of $\Delta\varepsilon/C$ reflects the change in $<r^2>/M_w$ with excluded-volume.

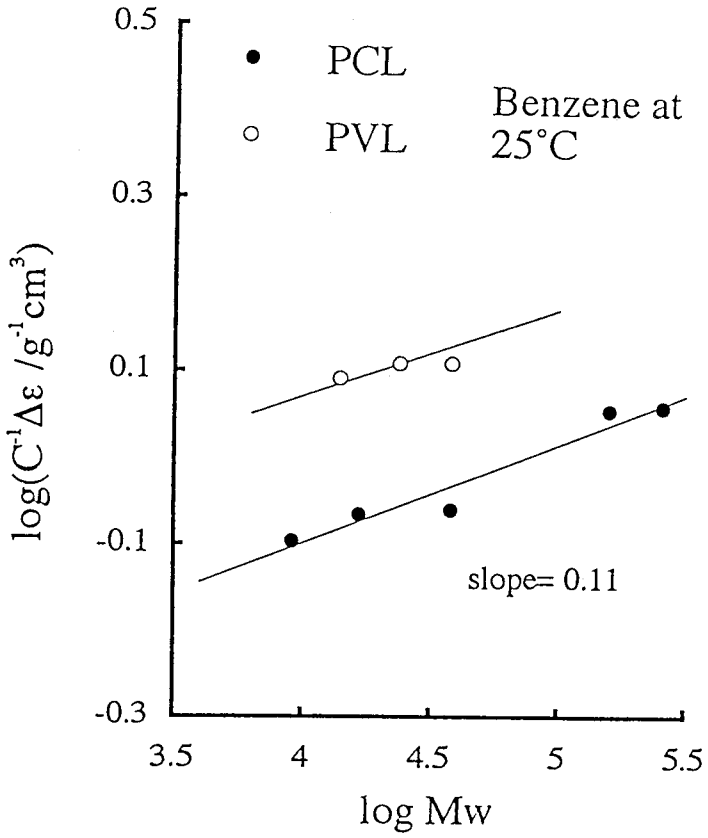

Figure IV-8. Molecular weight dependence of $\Delta\varepsilon/C$ for dilute benzene solutions of PCL and PVL at 25°C.

IV-4. End-to-End Distance in Semidilute Solutions

IV-4-1. C dependence of $\Delta\varepsilon$ in solutions of *cis*-Polyisoprene

Figure IV-9 shows the C dependence of $\Delta\varepsilon/C$ for PI-743 and PI-140 /heptane solutions. It is seen that $\Delta\varepsilon/C$ begins to decrease with C when C exceeds C^* ($\cong 1/[\eta]$). This may be considered to be the onset of screening of the excluded volume effect.

Comparison with Scaling Theories

According to Daoud and Jannink,[8] the M and C dependence of $\langle r^2\rangle$ in the semidilute regime is given by

$$\langle r^2\rangle \propto MC^{(2\nu-1)/(1-3\nu)} \tag{IV-4}$$

where ν is the excluded volume exponent equal to 3/5 in a good solvent and 1/2 in a θ solvent. Eq IV-4 predicts that $\langle r^2\rangle/M$ is independent of M and proportional to $C^{(2\nu-1)/(1-3\nu)}$. As is seen in Figure IV-9, the data of $\langle r^2\rangle/M$ for PI-743 and PI-140 in the range of $C > 5C^*$ coincide and fall on a straight line with a slope of -0.152, which corresponds to ν=0.56 in eq IV-4. This value of ν agrees with that (ν=0.56) estimated from the M_w dependence of $\langle S^2\rangle$ or $\Delta\varepsilon/C$ in dilute solution.

Scaling theory predicts that the ratio $\langle r^2\rangle/\langle r^2\rangle_0$ becomes a universal function of C/C^*:

$$\langle r^2\rangle/\langle r^2\rangle_0 = 1 \qquad C < C^* \tag{IV-5}$$

$$\langle r^2\rangle/\langle r^2\rangle_0 = (C/C^*)^{(2\nu-1)/(1-3\nu)} \qquad C > C^* \tag{IV-6}$$

Here $\langle r^2\rangle_0$ denotes the mean-square end-to-end distance in the dilute regime and $C^* \propto M^{1-3\nu}$. Figure IV-10 shows double-logarithmic plots of $\langle r^2\rangle/\langle r^2\rangle_0$ vs. C/C^* for PI-743 and PI-140 solutions. We see that all data are successfully superposed and well represented by eqs IV-5 and 6 except for the crossover region of $C \cong C^*$.

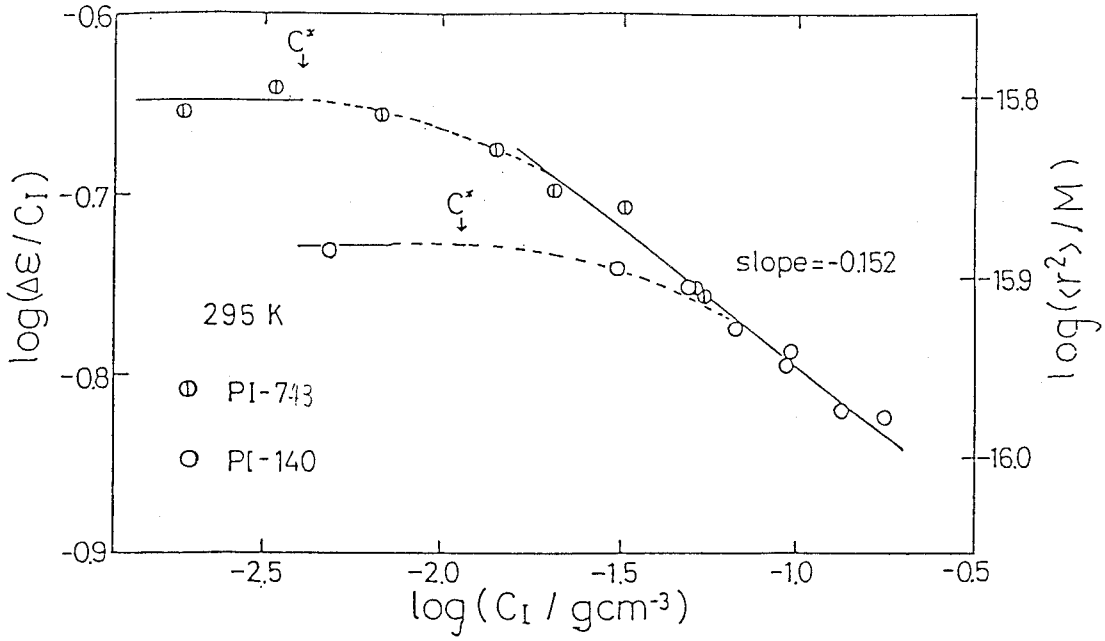

Figure IV-9. Double logarithmic plots of $\Delta\varepsilon/C$ vs. C at 295K for PI/heptane solutions. The arrows indicate the overlap concentration determined as $1/[\eta]$.

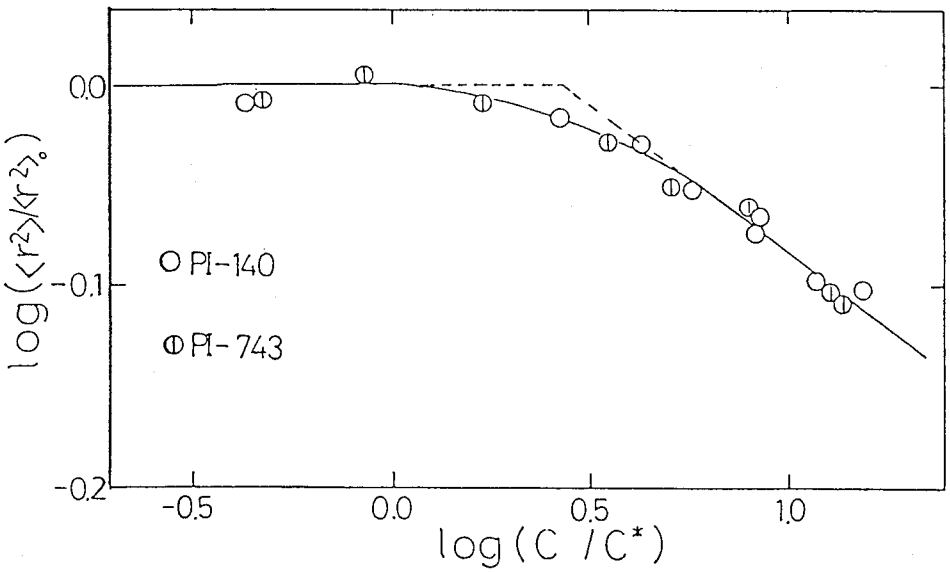

Figure IV-10. Reduced plot of $\langle r^2 \rangle / \langle r^2 \rangle_0$ vs. C/C^*. Here $\langle r^2 \rangle_0$ represents $\langle r^2 \rangle$ in the dilute regime. The dashed line represents the theoretical prediction from eqs (IV-5, 6).

IV-4-2. C Dependence of $\Delta\varepsilon$ in Solutions of Poly(ε-caprolactone)

In Figure IV-11, the C dependence of $\Delta\varepsilon/C$ is shown for the PCL-158 / benzene system. With increasing C above 7×10^{-3}gcm^{-3}, log $\Delta\varepsilon/C$ ($\propto$ log $\langle r^2\rangle/M_w$) decreases. in proportion to $C^{(2\nu-1)/(1-3\nu)}$. The indicated straight line approximately fitting the data points for $C > 7\times10^{-3}$gcm^{-3} has a slope of -0.146 which yields ν=0.547 when eq IV-4 is used. This ν value agrees well with that (ν=0.55) determined from $[\eta]$ vs. M_w relation. This behavior is quite similar to semidilute solutions of PI. From such results, we can conclude that the C dependence of μ is not so important in semidilute regime.

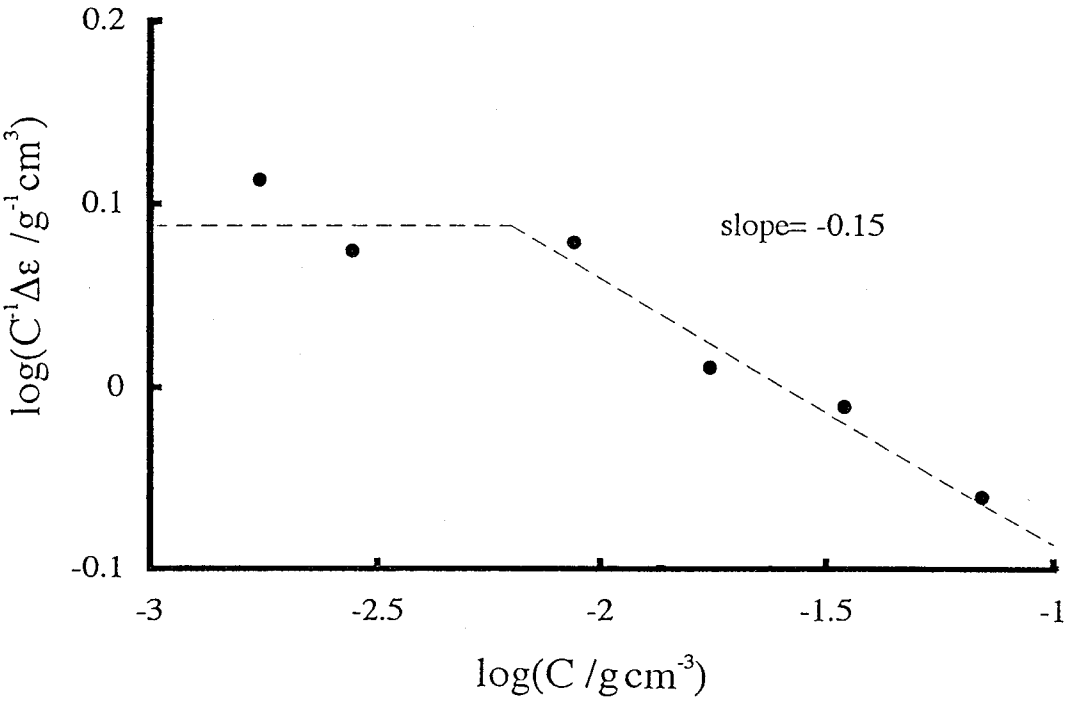

Figure IV-11. Double logarithmic plot of $\Delta\varepsilon/C$ vs. C for PCL/benzene solutions at 25°C.

IV-5. End-to-End Distance of a Probe Chain in Polymer /Polymer /Solvent Ternary Systems

This section deals with $<r^2>$ ($\propto \Delta\varepsilon$) of the PI probe chain in PI/PB/heptane ternary solutions determined as a function of the molecular weights (M_I) of the PI chain, M_B of PB, and its concentration C_B. Especially two aspects are examined: How the ratio M_I/M_B and the interaction parameter χ between PI and PB affect the $<r^2>$ of PI. The results for the dependence on M_I/M_B and χ are compared with those for PI/heptane binary solutions which is regarded as a system of $M_I=M_B$ and $\chi=0$.

IV-5-1. Background of this Problem

In ternary solutions consisting of a trace amount of probe chains (N chain) with DP = N, matrix chains (P chain) with DP= P and a good solvent, the dimensional features of the N chains are classified into two regimes. If $N >>$ P, the P chains behave as a solvent and the screening effect will hardly act on the N chain. On the other hand, in the case of $N \leq P$, the screening effect is similar to semidilute binary solutions is expected.

Flory [16] first calculated the excluded-volume effect of a long N chain in a matrix of homologous short P chains (a binary blend). He concluded that the P chains behave as a good solvent and the N chain is expanded when their DPs satisfy a condition of $N^{1/2} > P$. Joanny et al [17,18] applied a scaling treatment and extended the Flory theory to a ternary system composed of a single N chain, matrix P chains of the chemically same kind, and an athermal solvent. They reported that the Flory condition for the binary blend is replaced by $(N/g_P)^{1/2} > P/g_P$, where g_P is the blob size and the suffix P denotes the P chain. From the relation $g_P \propto C_P^{1/1-3\nu}$, they calculated that in $1 < C_P/C_P^* < (N/P)^{3\nu-1}$, the excluded-volume effect between the blobs of the N chain is not fully screened and hence the N chain exhibits an "anomalous" behavior due to the inter-blob excluded volume effect. For example, even in the semidilute regime $<r^2>$ is proportional to $N^{2\nu}$ and differs with P. For

$N/P < 1$, on the other hand, $<r^2>$ of the N chain is equal to that in a semidilute binary solution in which $N = P$.

Recently Nose[19] extended the theory of Joanny *et al.* to a more general case. He calculated the dimension of a single test chain (N chain) in a matrix consisting of chemically different P chains in an athermal solvent. The interaction parameter between N and P chains is χ. He discussed the dimensional behavior of a single N chain for the cases of (i) $N >> P$ and (ii) $N \leq P$. To survey the whole aspect of the theory, we first consider the simplest case of $\chi = 0$ which is equivalent to the theory of Joanny *et al.*[17,18].

In the case (i) of $N >> P$, the Nose theory predicts that there are three regimes in which C_p dependence of $<r^2>$ are different. In regime I, the P chains do not overlap each other and hence $C_p/C_p^* < 1$. In this regime the dimension of the N chain is nearly equal to that in the pure solvent:

$$<r^2> \equiv a^2 N^{2\nu} \qquad \text{Regime i-I} \qquad \text{(IV-7)}$$

where a is the length of a monomer unit. In regime II, the short P chains are partially overlapped, $1 < C_p/C_p^* < (N/P)^{3\nu-1}$:

$$<r^2> \equiv a^2 N^{2\nu} (C_p/C_p^*)^{2(2\nu-1)/(1-3\nu)} \qquad \text{Regime i-II} \qquad \text{(IV-8)}$$

In this regime, the excluded-volume effect between blobs in the N chain is still prevailing and the value of the exponent of C_p/C_p^* is two times larger than the polymer/solvent binary system (eq.IV-4). The reduced end-to-end distance $<r^2>/<r^2>_0$ can be expressed by a universal function of C_p/C_p^*. In regime III, $C_p/C_p^* > (N/P)^{3\nu-1}$:

$$<r^2> \equiv a^2 N\, C_p^{(2\nu-1)/(1-3\nu)} \qquad \text{Regime i-III} \qquad \text{(IV-9)}$$

In this regime the excluded-volume effect between blobs is completely screened, so that the N dependence of $<r^2>$ is of the Gaussian type and the exponent to C_P is equal to that of eq.IV-4. This equation can be rewritten as in Table VI. Thus $<r^2>$ in the regime III can not be reduced by C_P^*.

In the case (ii) of $N \leq P$, two regimes appear: The regime of $C_P < C_N^*$ is referred to as regime-I where $<r^2>^{1/2}$ of the N chain is smaller than the screening length ξ_P of the matrix solution. Thus the N chain expands as in the pure solvent and its $<r^2>$ is given by

$$<r^2> \equiv a^2 N^{2\nu} \qquad \text{Regime ii-I} \qquad \text{(IV-10)}$$

When $C_P < C_N^*$ referred to as regime-II, $<r^2>^{1/2} > \xi_P$. Thus the excluded volume effect is screened and $<r^2>$ is given by

$$<r^2> \equiv a^2 N\, C_P^{(1-2\nu)/(3\nu-1)} \qquad \text{Regime ii-II} \qquad \text{(IV-11)}$$

In these regimes (ii-I,II), $<r^2>$ is completely independent of P and cannot be reduced by C_P^*. These theoretical classifications are summarized in Table VI.

When $\chi>0$, we have to take into account the θ concentration C_θ where the two-body interaction between the N chains changes from repulsive to attractive. When $C_P >> C_\theta$, the intra-chain excluded-volume effect in the N chain becomes attractive and hence the chain collapses;

$$<r^2> \equiv a^2 N^{2/3}\, C_P^{-2/3} \chi^{-2/3} \qquad \text{(IV-12)}$$

At C_P below C_θ, the regimes discussed for the case of $\chi=0$ still exist, and especially in the regimes i-I and II, the universality with respect to C_P/C_P^* still holds well. However the dependence on C_P becomes slightly stronger.

For excluded volume problems in such ternary systems, however, few experiments [20-24] have been reported so far. A purpose of the study in this section is to provide a reliable experimental basis on which these theories can be tested.

Table VI. Theoretical classification of the dimension of guest chain.

(i) $N >> P$

Concentration	$\langle r^2 \rangle / \langle r^2 \rangle_0$	regime
$C_p/C_p^* < 1$	1	i-I
$1 < C_p/C_p^* < (N/P)^{3\nu-1}$	$(C_p/C_p^*)^{2(1-2\nu)/(3\nu-1)}$	i-II
$C_p/C_p^* > (N/P)^{3\nu-1}$	$(C_p/C_N^*)^{(1-2\nu)/(3\nu-1)}$	i-III

(ii) $N < P$

Concentration	$\langle r^2 \rangle / \langle r^2 \rangle_0$	regime
$C_p/C_N^* < 1$	1	ii-I
$C_p/C_N^* > 1$	$(C_p/C_N^*)^{(1-2\nu)/(3\nu-1)}$	ii-II

IV-5-2. End-to-End Distance of Tracer PI Chain in PB / Heptane Solutions

As mentioned in the above section we are interested in the following two aspects: (1) the effect of the molecular weight of surrounding PB and (2) the interaction between PI and PB on $\langle r^2 \rangle$ of the guest PI chain.

Figure IV-12 shows $\Delta\varepsilon/C_I$ ($\propto \langle r^2 \rangle/M$) for PI-140 plotted against PB concentration C_B in matrices of PB-13, PB-63 ,PB-211, and PB-521. Figure IV-13 shows similar plots for PI-743 in solutions of PB-33, PB-211, and PB-521. C_I was fixed to be 2×10^{-3} gcm^{-3} for PI-743/PB/heptane system and 4×10^{-3} gcm^{-3} for PI-140/PB/heptane. These concentrations are less than C^* of PI. Thus the PI chains are not overlapped each other though the PB chains are in the semidilute regime. In Figs IV-12 and IV-13, the data for PI/heptane binary solutions are also plotted against the PI concentration C_I.

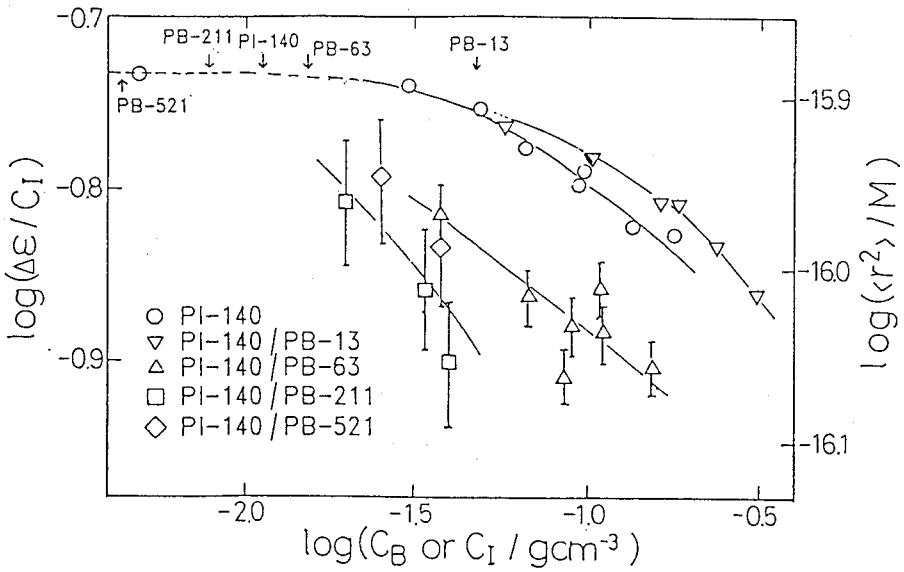

Figure IV-12. Double-logarithmic plot of $\Delta\varepsilon/C$ of PI-140 vs.PB concentration C_B. The data of PI/heptane binary solutions (reproductions from Figure IV-10) are also plotted against log C_I. The arrows indicate the C^* for each matrix solution. The large error bars in high MW PB solutions are due to the lack of data of the half width δ for ε'' curves because the peak located high frequency. Errors in the PI-140/heptane (o) and PI-140/PB-13/heptane (∇) systems are similar to those of the PI-140/PB-63/heptane (Δ) system. The solid lines are guides for the eyes.

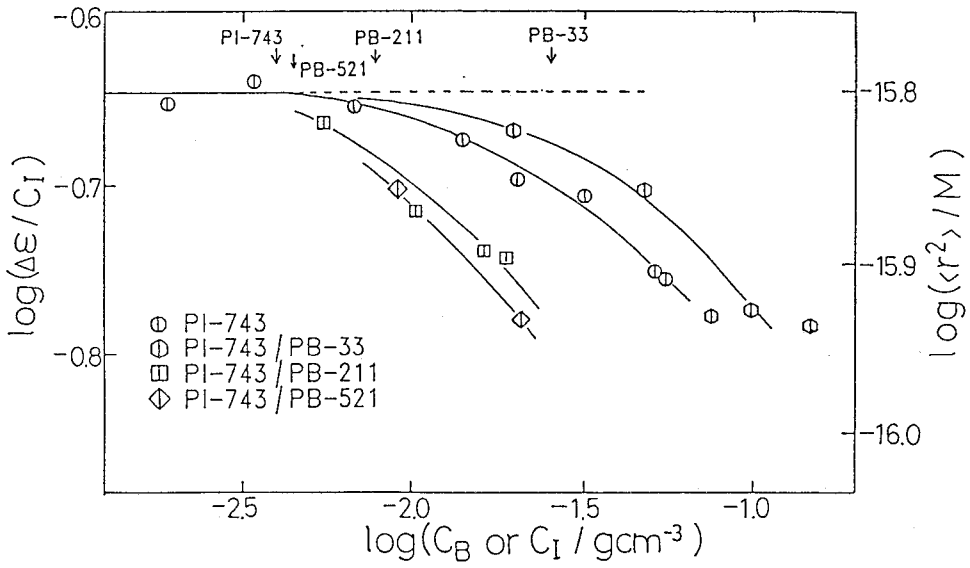

Figure IV-13. Double-logarithmic plots of $\Delta\varepsilon/C$ of PI-743 vs. C_B. The arrows indicate C^*. The solid lines are guides for the eyes.

We see that curves of $<r^2>$ lower with increasing M_B, but when M_B/M_I is larger than unity, $<r^2>$ of PI becomes independent of M_B (see data of PI-140/PB-521 in Fig.IV-12). Thus the matrix molecular weight affects strongly the guest chain dimension as predicted by the theories of Joanny *et al.* and Nose. For the case of $M_I/M_B > 1$, the C where $<r^2>$ of PI begins to decrease is close to C_B^*. Thus we tried to reduce the data of Figures IV-12 and 13 by $<r^2>_0$ and C_B^* as shown in Figure IV-14. We can see that all the curves approximately converge to one universal curve except for PI-140/PB-521 system. This indicates that when a PB matrix solution is regarded as a "*solvent*", the quality is determined by C_B/C_B^* for the case of $M_I/M_B > 1$.

In the opposite case of $M_I/M_B<1$, the screening length ξ_B in PB solutions can be larger than $<r^2>^{1/2}$ of PI since $<r^2>^{1/2}$ of PI is smaller than that of PB, . In such a case the screening effect does not act upon the PI chain. Thus the PI chain expands as in a pure good solvent. But when ξ_B becomes nearly equal to $<r^2>^{1/2}$ of PI, the PI chain begins to shrink by the screening effect.

Figure IV-15 shows the schematic representation of the guest PI chain beginning to shrink for the cases of (a) $M_I/M_B >1$ and (b) $M_I/M_B < 1$. In the cases-a and -b, the shrinkage starts respectively at $C_B \cong C_B^*$ and $C_B \cong C_I^*$ where $<r^2>^{1/2}$ of the PI chain becomes nearly equal to ξ_B. In case-b the dimension of the PI chain does not depend on M_B and depends only on the mesh size (screening length) which is proportional to $C_B^{1/1-3\nu}$, so that the curves of $<r^2>/M_w$ vs. C_B are considered to become universal as was seen in PI/heptane semidilute solutions shown in Figure IV-9. In Figure IV-16 we plotted $\Delta\varepsilon/C_I$ against C_B for PI-140/PB-211, PI-140/PB-521, and PI-743/PB-521 solutions and also the data of PI/heptane binary solutions against C_I for comparison. We can see that these data for ternary solutions fall on a single curve. This result indicates that in the case of $M_I/M_B < 1$, $<r^2>$ is independent of M_B and determined only by C_B.

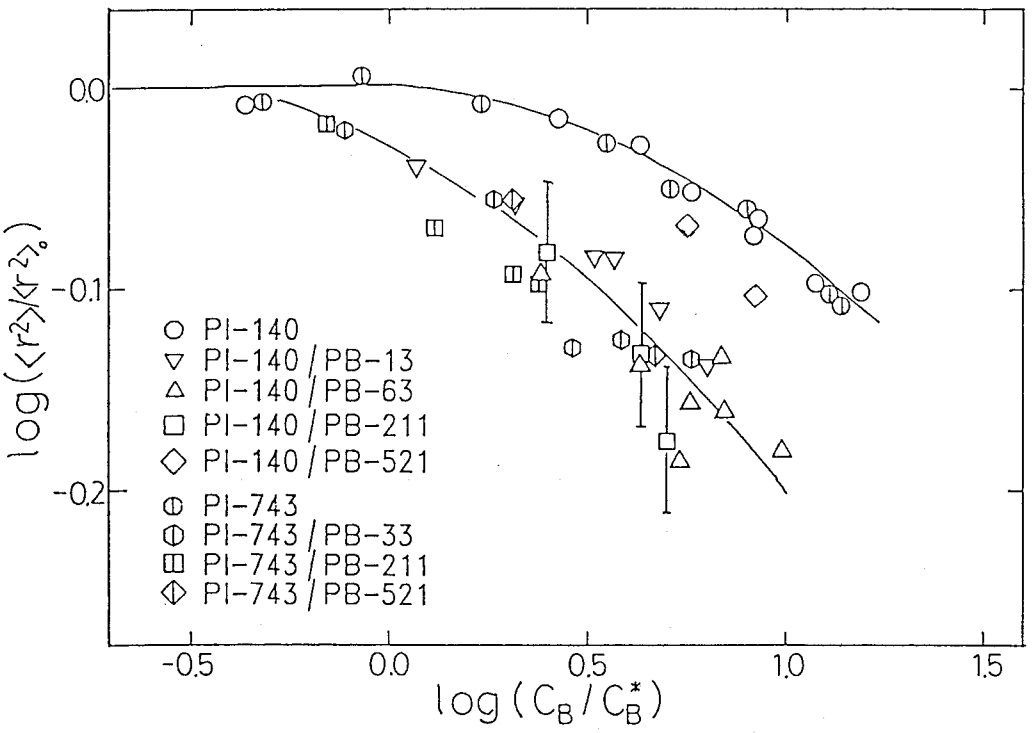

Figure IV-14. Reduced plot of $\langle r^2\rangle/\langle r^2\rangle_0$ vs. C_B/C_B^* for PI/PB/heptane solutions. The solid lines indicate guides for eyes.

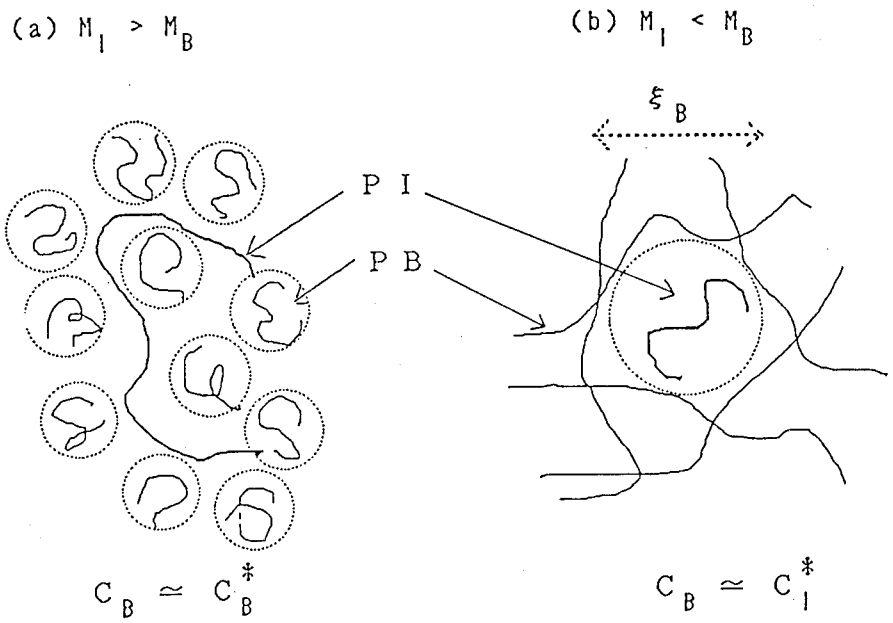

Figure IV-15. Schematic representation of a single guest PI chain in semidilute PB solution. The PI chain begins to shrink at (a) $C_B \approx C_B^*$ when $M_I > M_B$ and at (b) $C_B \approx C_I^*$ when $M_I < M_B$. In (b), ξ_B is equal to the end-to-end distance of the PI chain.

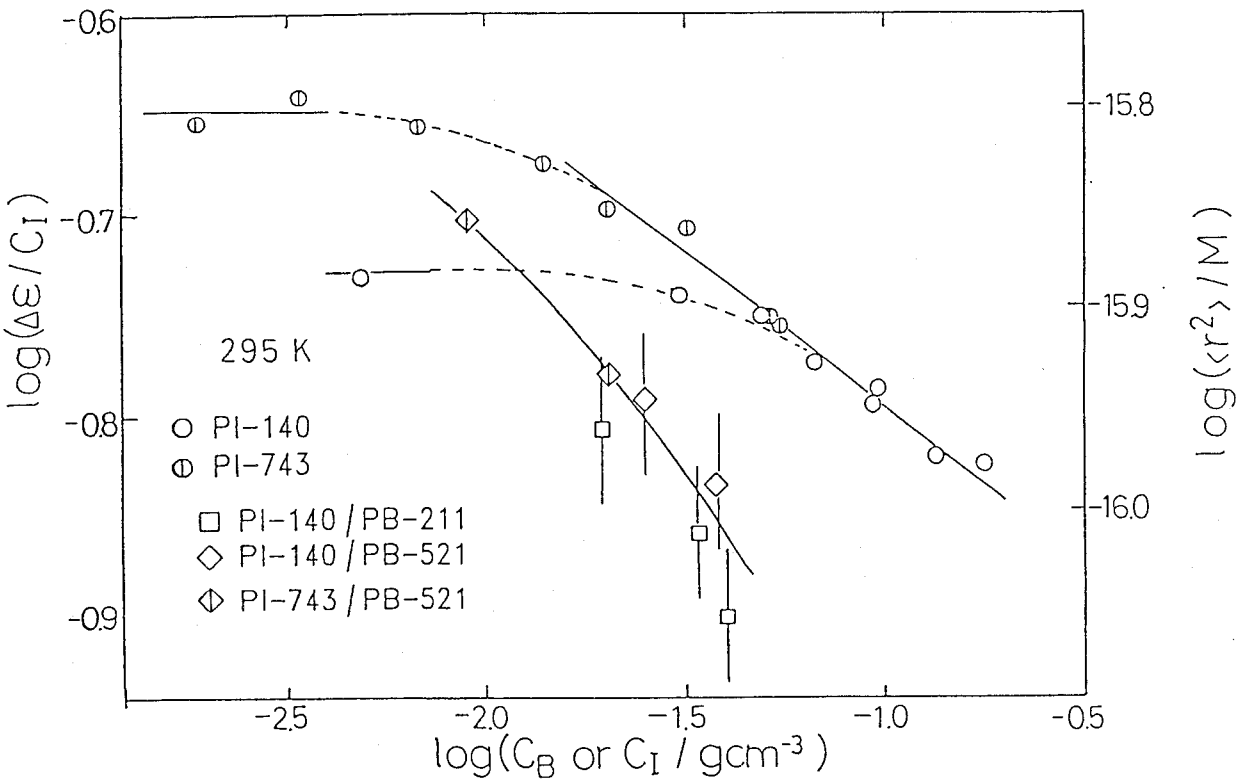

Figure IV-16. Double-logarithmic plot of $\Delta\varepsilon/C$ of PI for PI-743/PB-521, PI-140/PB-211, and PI-140/PB-521 solutions. The data of PI/heptane solutions are also plotted in this figure.

Kuhn *et al.*[20,21] and Lin and Rosen[22] measured $<S^2>$ of high MW polystyrene (PS) chains immersed in isorefractive poly(methylmethacrylate)(PMMA)/solvent system by light scattering. They found that the second virial coefficient A_2 of PS decreased with C_{PMMA} and the θ concentration C_θ at which A_2 becomes 0 was proportional to $1/[\eta]$ ($\propto C^*$). And the C_{PMMA} dependence of radius of gyration $<S^2>$ was successfully expressed by the universal form, $<S^2>/<S^2>_0 \cong f(C/C_\theta)$ in the case of $M_{PS}>M_{PMMA}$. Our result is consistent with theirs provided that $C_B^* \propto C_\theta$. The case of $M_{PS} < M_{PMMA}$ was investigated by Numasawa *et al*,[23] who made similar light scattering measurements.[20] They reported that at a matrix concentration where $\xi \propto <S^2>^{1/2}$, A_2 became zero but $<S^2>$ of the PS chain was expanded as in a good solvent because the intra-chain excluded-volume effect was not screened out. In such a case C_θ is not proportional to C^* of the matrix solution and independent of the molecular weight of the matrix polymer. Thus the universality of the C_B/C_B^* dependence of $<r^2>$ does not hold. In Fig.IV-14 we can see the data for PI-140/PI-521 locate above the universal curve and this is consistent with their result.

Another noteworthy point is the difference between PI/PB/heptane and PI/heptane solutions being due to the interaction between PI and PB. In Fig.IV-12, we see that $<r^2>$ of PI-140 in the binary PI/heptane system is larger than that in the ternary systems except for the case where M_B is much lower than M_I. This is also the case for solutions of PI-743 in Fig.IV-13. Thus $<r^2>$ of a PI chain in solutions of the same PI chains is larger than that in solutions of PB . If we regard the PI or PB solution surrounding a test chain as a "solvent", the quality of PI solution is better than PB solution at the same concentration: The interaction parameter between the PI and PB chains is positive. In Figs IV-13 and 15, the difference in $<r^2>$ between PI/PB/heptane and PI/heptane is also ascribed to the interaction between PI and PB chains.

IV-5-3.Comparison with Scaling Theories

As is seen in Fig.IV-14, $\langle r^2\rangle/\langle r^2\rangle_0$ vs. C_B/C_B^* converges on one curve in the case of $M_I > M_B$. The theory predicts that if $N >> P$, the C dependence of $\langle r^2\rangle/\langle r^2\rangle_0$ is given by eqs IV-7 and 8 and hence the data of $\langle r^2\rangle/\langle r^2\rangle_0$ in solutions of PI with various M_B fall on a universal curve of C_B/C_B^*. Thus our experimental results may be explained by considering that the present system is in the regimes i-I (eq.IV-7) and i-II (eq.IV-8). However there are two disagreements with the theory. One is that the slope in Figure IV-14 is expected to be two times larger than that in PI/heptane binary systems (compare eq IV-8 with IV-6). Actually we see that the slope is almost the same between binary and ternary systems. This may be explained as follows. Since our experiment did not cover the wide range of C_B, the observed slope has not reached the asymptotic value. Second, the theory predicts that the regime i-II appears only when $N >> P$ say $N/P > 10$. But as seen in Fig.IV-14 the data of $M_I/M_B < 10$ converge. This result is not explained by the theory.

In Figure IV-16, three curves for PI-140/PB-211, PI-140/PB-521, and PI-743/PB-521 approximately coincide within the experimental error. This behavior may be explained assuming that these solutions are in the case ii. We conclude that the theory explains roughly the experimental result, but does not quantitatively.

IV-5-4. M_I dependence of $\langle r^2\rangle$

In this section, the M_I dependencies of $\langle r^2\rangle$ for dilute PI in a PB matrix solution in which C_B=4.84x10^{-2} gcm^{-3} and M_B=3.3x10^4 are discussed. Figure IV-17 shows the comparison of $\langle r^2\rangle/M$ for dilute PI in *n*-heptane and that in the PB/heptane semidilute solution. We see that the slope is almost the same. This indicates that the excluded-volume effect for the PI chain is not screened out even in the semidilute matrix solution. The Nose theory mentioned above predicts that the excluded-volume effect between blobs still prevails in the regime i-II but the absolute value of $\langle r^2\rangle$ is smaller than $\langle r^2\rangle_0$ by the factor of $(C_P/C_P^*)^{2(2\nu-1)/(1-3\nu)}$ (eq.IV-8). The prediction agrees with this experimental result.

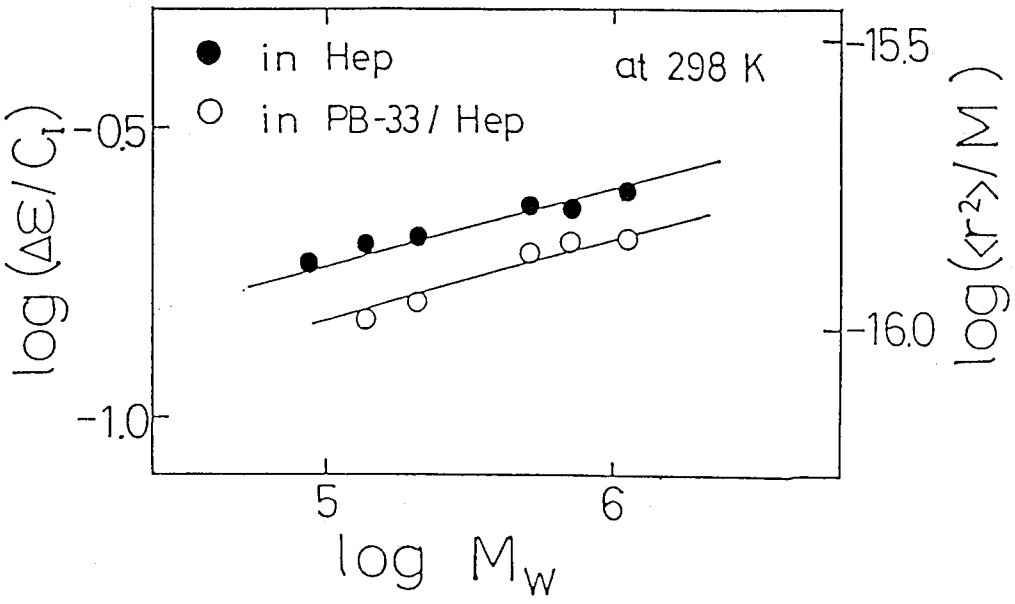

Figure IV-17. Dependence of $\Delta\varepsilon/C$ on molecular weight of PI in heptane dilute solution and PB-33/heptane semidilute solution (C_B=4.84×10^{-2} gcm^{-3}).

IV-5-5. Conclusions

The main results for the PI/PB/heptane ternary systems are summarized as follows.

1. The mean square end-to-end distance $\langle r^2 \rangle$ of PI chain in PB semidilute solutions changes with PB concentration C_B and PB molecular weight M_B, it decreases with increasing C_B at fixed M_B. In the case of $M_I/M_B > 1$, $\langle r^2 \rangle$ decreases with increasing M_B at fixed C_B and $\langle r^2 \rangle/\langle r^2 \rangle_0$ is approximately expressed by a universal function of C_B/C_B^*. In the case of $M_I/M_B < 1$, $\langle r^2 \rangle$ is independent of M_B.

2. In semidilute solutions of low molecular weight PB, the excluded volume effect between blobs is not screened as predicted by the theories of Nose and Joanny *et al.*

3. $\langle r^2 \rangle$ of a PI chain in semidilute solutions of the same PI chains is larger than that of the PI chain in solutions of PB. This is due to the interaction between PI and PB.

References.

1. Urakawa, O.; Adachi, K.; Kotaka, T. *Macromolecules* **1993**, *26*, 2036, 2042.
2. Urakawa, O.; Adachi, K.; Kotaka, T.; Takemoto, Y.; Yasuda, H. *Macromolecules* in preparation.
3. Yamakawa, H. "Modern Theory of Polymer Solutions"; Harper and Row: NY, 1971.
4. Domb, C.; Hioe, F. *J. Chem. Phys.* **1969**, *51*, 1915.
5. Brandrup, J. and Immergut, E. H. "Polymer Hand Book, 2nd Ed." Wiley; New York 1975.
6. Nishimoto, K.; Imamura, A. "Bunsi sekkei no tame no ryoushi kagaku" Koudansha; Tokyo 1990.
7. Flory, P. J. "Statistical Mechanics of Chain Molecules" Wiley New York 1969.
8. Daoud,M.; Jannink, G. *J. Phys. (Paris)* **1976**, *37*, 973.
9. de Gennes, P. G., "Scaling Concept in Polymer Physics" Cornell Univ. Press, Ithaca N.Y. 1979.
10. Smith, J. W. "Electric Dipole Moments" Butterworths Scientific Publications, London, 1955.
11. Hadjichristidis, N.; Roovers, J. E. L. *J. Polym. Sci., Polym. Phys. Ed.* **1982**, *20*, 2163
12. Tunashima, Y.; Hirata, N.; Nemoto, N.; Kurata, M. *Macromolecules* **1988**, *21*, 1107
13. Flory, P. J. "Principle of Polymer Science" Cornell Univ. Press, Ithaca N.Y. 1953
14. Allinger, N. L. *J. Am. Chem. Soc.* **1977**, *99*, 8127.
15. Peebles, Jr. L. H. "Molecular Weight Distributions in Polymers" Interscience Publishers, New York 1971.
16. Flory, P. *J. J. Chem. Phys.* **1949**, *17*, 3, 303.
17. Joanny, J. F.; Grant, P.; Turkerich, L. A.; Pincus, P. *J. Phys.* **1981**, *42*, 1045.
18. Joanny, J. F.; Grant, P.; Pincus, P.; Turkerich, L. A. *J. Appl. Phys.* **1981**, 52, 5943.
19. Nose, T. J. Phys. 1986, 47, 517.
20. Kuhn, R.; Cantow, H. J .; Burchard, W. *Angew. Makromol. Chem.* **1968**, *2*, 146.
21. Kuhn, R.; Cantow, H. J. *Makromol. Chem.* **1969**, *122*, 65.
22. Lin, C. Y.; Rosen, S. L. J. *Polym. Sci., Polym. Phys. Ed.* **1982**, *20*, 1497.
23. Numasawa, N.; Hamada, T.; Nose, T. *J. Polym. Sci., Polym. Lett. Ed.* **1985**, *23*, 1.
24. Cotts, D. B. *J. Polym. Sci., Phys. Ed.* **1983**, *21*, 13, 81.

V. Dynamic Properties

V-1. Introduction

Molecular dynamics of a flexible polymer chain is affected by several factors, *i.e.*, hydrodynamic interaction, excluded volume effect, and entanglement. Influences of these interactions on polymer dynamics change with C and MW. At infinite dilute solution there is no inter-chain interaction and hence hydrodynamic interaction and excluded volume effects within a chain play an important role. With increasing C such interactions are screened and the inter-chain interactions such as topological interaction begin to exert. Changes of polymer dynamics with C have been studied mainly by viscoelastic experiments.[1]

It was almost established that dilute solution properties such as the relaxation times τ and the relaxation spectrum can be explained by the Zimm model[2] rather than the Rouse model.[3] In a system in which $C > C^*$ but chains are not entangled yet, it is known that the hydrodynamic effect is screened by an increase in C and as the result the Rouse model becomes applicable to such an intermediate state.[1] However there remains a problem in such application of the Rouse model because this model essentially assumes an isolated chain. For detailed discussion of polymer dynamics in such a C regime, it is necessary to study the dynamics of non-entangled chains in dense systems.

On the other hand for well entangled systems, there is no successful theories to explain viscoelastic properties since the molecular dynamics in such a system is a very complicated many-body problem. Especially no theories so far succeeded to explain the relaxation spectrum. Although the tube model[4] or its modifications[5,6,7] explain qualitatively the viscoelastic properties, these models are not sufficient for quantitative explanation. Especially for the relaxation spectrum (the distribution of τ) these models predict a sharper distribution than experimental results.[8,9] This means that in order to apply such models to dense systems (semidilute or

concentrated solutions), further modification of the models or wholly an entirely new concept is necessary. To summarize, the Zimm model is applicable to dilute solution but the theory of the dynamics in dense polymeric systems has not been established.

From these views, it is significant to examine systematically the polymer dynamics over wide C and MW ranges from the Zimm like regime to the entanglement regime. In this chapter the dielectric normal mode process of type-A chains in various conditions is described. We will also compare the dielectric and viscoelastic properties as a test of theories.

V-2. Dynamics of Polymers in Dilute Solution

V-2-1. Rouse and Zimm Theory

Rouse modeled a flexible polymer chain by $N+1$ beads connected by N springs.[3] According to this model, the correlation function of $\boldsymbol{r}$ in eq II-22 is given by

$$\langle \boldsymbol{r}(0)\cdot\boldsymbol{r}(t)\rangle = \frac{8\langle r^2\rangle}{\pi^2} \sum_{p:\mathrm{odd}} \frac{1}{p^2} exp\,(-t/\tau_p) \qquad \text{(V-1)}$$

$$\tau_p = \zeta N^2 b^2 / (3\pi^2 k_B T\, p^2) \qquad \text{(V-2)}$$

where τ_p is the relaxation time for the p-th normal mode; ζ, the friction coefficient per bead; b, the average distance between beads; and $k_B T$ the thermal energy.

Taking into account hydrodynamic interactions Zimm extended the Rouse model.[2] According to his theory, $\langle \boldsymbol{r}(0)\cdot\boldsymbol{r}(t)\rangle$ is expressed by the same form as eq V-1 but with different τ_p given by

$$\tau_p = \pi^{3/2}\eta_s b^3 N^{3/2} / (12^{1/2} k_B T\, \lambda_p) \qquad \text{(V-3)}$$

where η_s is the solvent viscosity and λ_p, the p-th eigenvalue tabulated by Zimm *et al.*[2]

The *log* ε'' vs. *log* ω curve predicted by the Zimm and Rouse theories are shown in Figure V-1. The difference in ε'' between the two models is small around the loss maximum but increases with increasing ω. On the other hand the difference in storage modulus G' and loss modulus G'' between these models are appreciable as shown in Figure V-2.

V-2-2. Molecular Weight Dependence of Dielectric Relaxation Times τ

The ε'' curves of PI in dilute cyclohexane and heptane solutions at 25°C have already been shown in Fig.IV-4. We evaluated the normal mode relaxation time τ by the relation $\tau = 1/(2\pi f_m)$ where f_m is the loss maximum frequency. The resulting τ values are plotted against M_w in Figure V-3. They almost correspond to the first normal mode relaxation time τ_1. The results of PCL and PVL in benzene solution were also shown in this figure.

According to the Rouse-Zimm theory, the theoretical τ_1 (the first normal mode relaxation time) is rewritten by using the intrinsic viscosity as

$$\tau_1 = KM_w[\eta]\eta_s / RT \qquad \text{(V-4)}$$

where K is a constant which equals 1.22 for the free-draining Rouse model and 0.85 for the non-draining Zimm model. In Figure V-4, the observed τ for PI, PCL and PVL solutions in various solvents are replotted against $M_w[\eta]\eta_0/RT$. Here for PI, cyclohexane and benzene are good solvents, heptane is a marginal solvent and dioxane (38°C) is a theta solvent, while for both PCL and PVL, benzene is a marginal solvent. No appreciable difference among the systems can be seen in the figure. This finding indicates that though the excluded-volume effect affects $[\eta]$, it hardly affects the functional form of eq V-4. The front factor K is estimated to be *ca.* 1.4±0.3, which is close to the value predicted by the Rouse model (1.22) rather than the Zimm model (0.85).

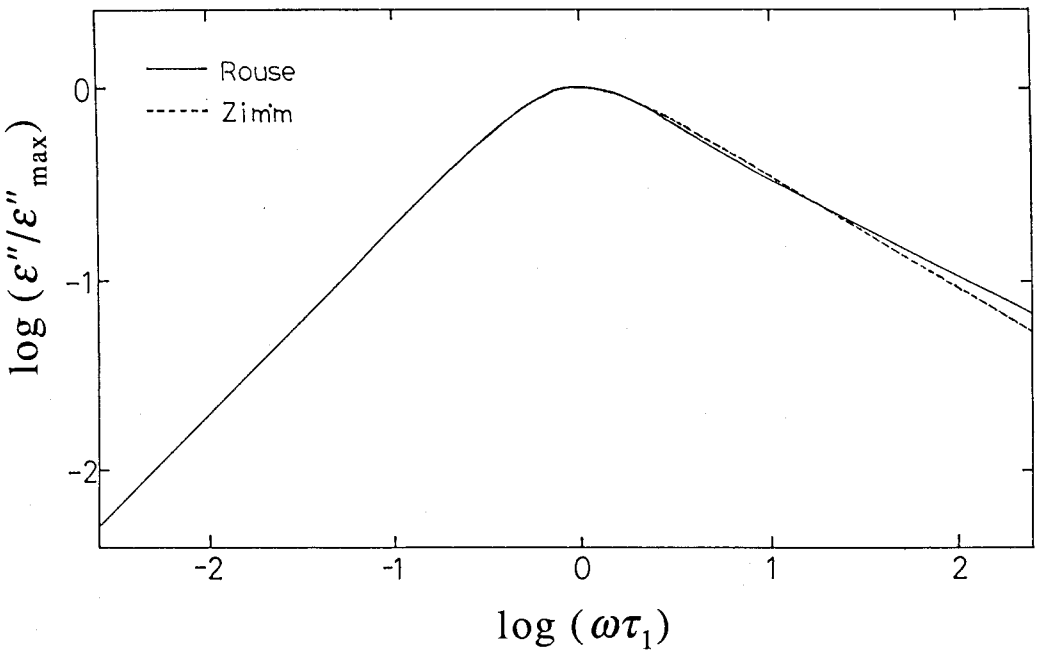

Figure V-1. Logarithmic plots of ε'' against $\omega\tau_1$ for the Rouse and Zimm theories.

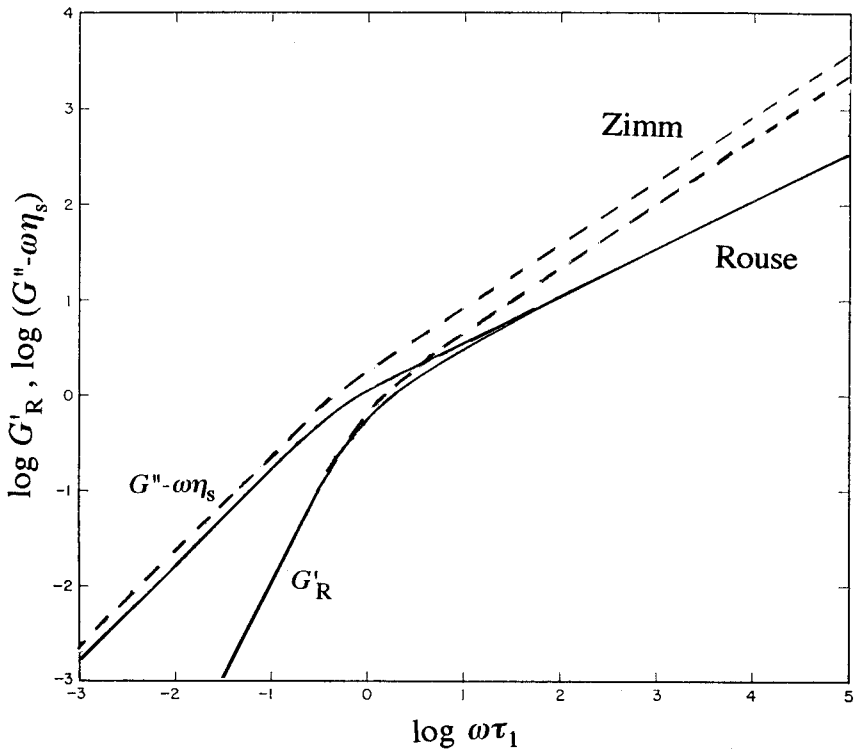

Figure V-2. Logarithmic plots of G' and $G''-\omega\eta_s$ against $\omega\tau_1$ predicted the Rouse and Zimm theories.

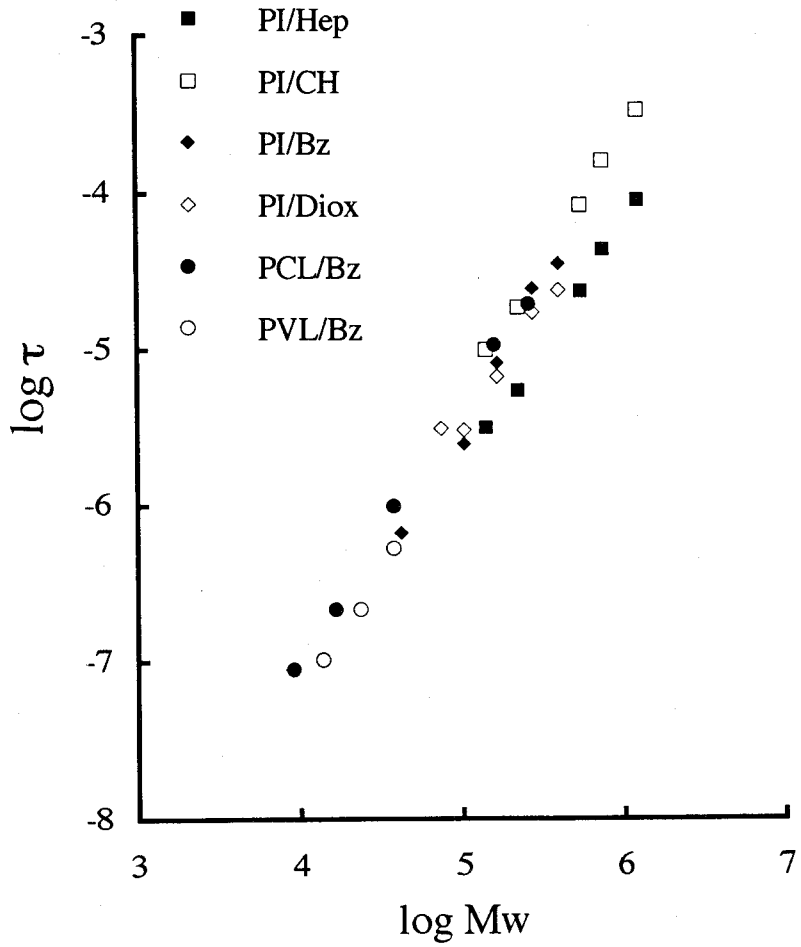

Figure V-3. M_w dependence of τ for dilute solutions of PI, PCL, and PVL.

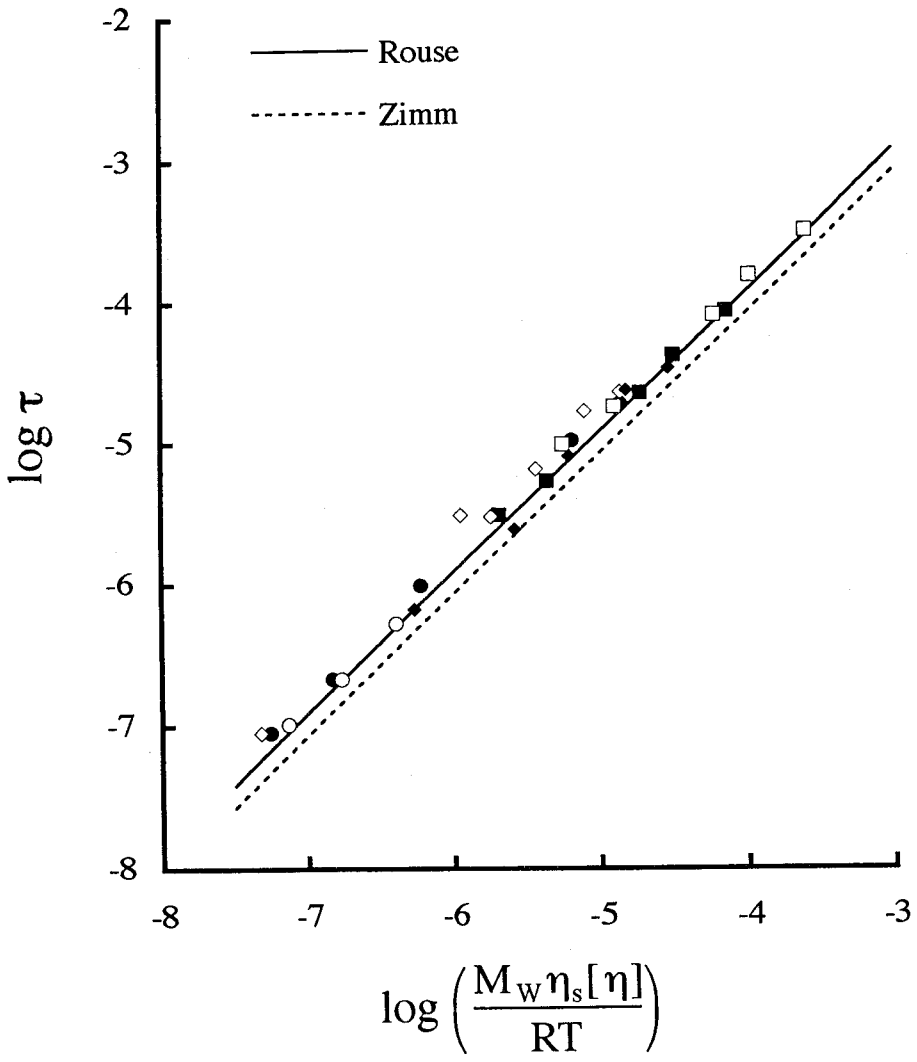

Figure V-4. Dependence of τ on the reduced Rouse, Zimm parameter $\eta_s[\eta]M_w/RT$. The symbols are the same as those used in Figure V-3.

V-2-3. Mode Distribution: Shape of Dielectric Loss ε'' Curves

The ε'' curves for PI in heptane and cyclohexane solutions are compared in Figure V-5. Their shape does not depend on MW and solvent nature. The ε'' curves calculated by the Zimm theory (from eqs II-19,22 and V-1,3) is shown by the solid line in the figure. It agrees with the experimental ones. This corresponds well to the result of the viscoelastisity.[1]

Figure V-6 shows *log* ε'' vs. *log* f plots for dilute solutions of PCL and PVL solutions. The C is mostly ca. $0.5C^*$ and is regarded to be dilute. The data reported by Jones *et al.*[11] for dioxane solutions of PCL are also shown in this figure by a solid line. We see that our ε'' curves are much narrower than theirs. The discrepancy may be due to the polydispersity of the samples used and the polymer concentration studied by Jones *et al.*; their PCL samples had $M_w/M_n \cong 4/3$ and C of 3wt% is not low enough to be regarded as a dilute solution. Effect of C on loss curves are discussed in the following sections.

In the same figure, the PCL data are compared with those of PI indicated by the dashed line. The shapes of the ε'' curves for PCL and PI are seem to be the same within the experimental uncertainty, indicating that the mode distribution for global motions is not affected by the local chemical structure and well represented by the Zimm model.

V-3. Dynamics of Polymers in Semidilute Solution

V-3-1. Theories of C Dependence of τ

V-3-1-1. Dynamic Scaling Theory

In this section we briefly summarize the dynamic scaling theory.[10] In entangled regime τ is empirically expressed as

$$\tau \propto \zeta b^2 N^{3.5} \qquad \text{(V-5)}$$

where the meaning of the parameters are the same as that in eq V-3.

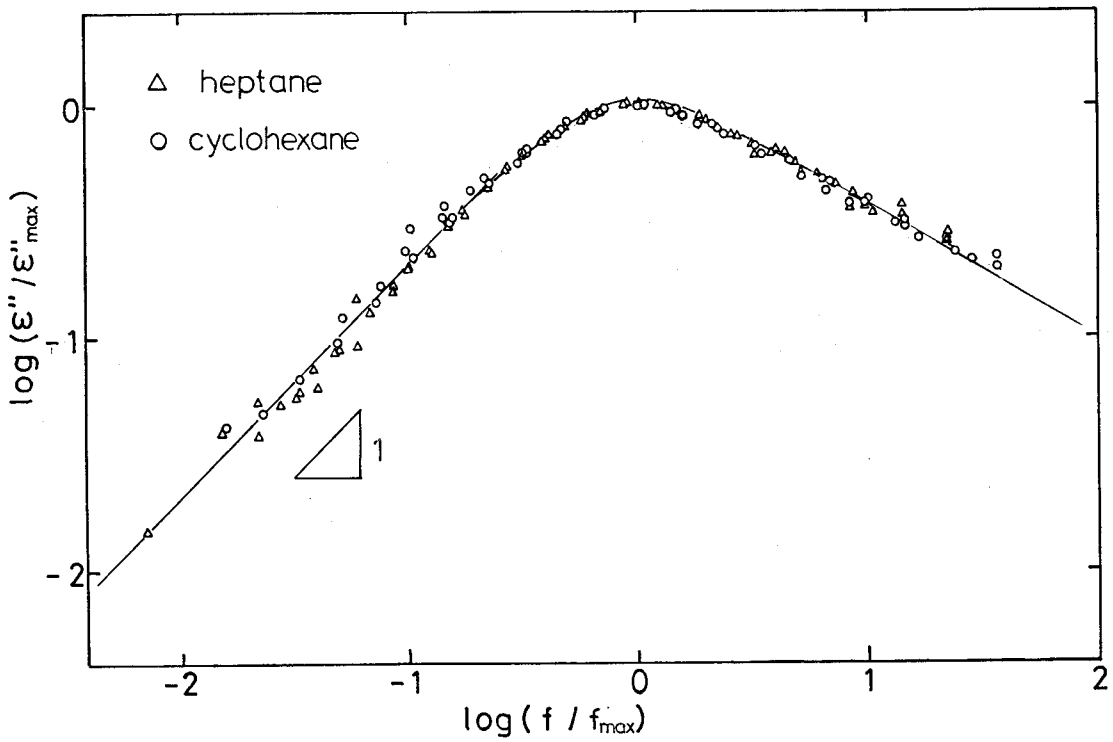

Figure V-5. Comparison of the shape of the ε'' curves for PI/cyclohexane and PI/heptane dilute solutions. The solid line indicates the theoretical curve by Zimm.

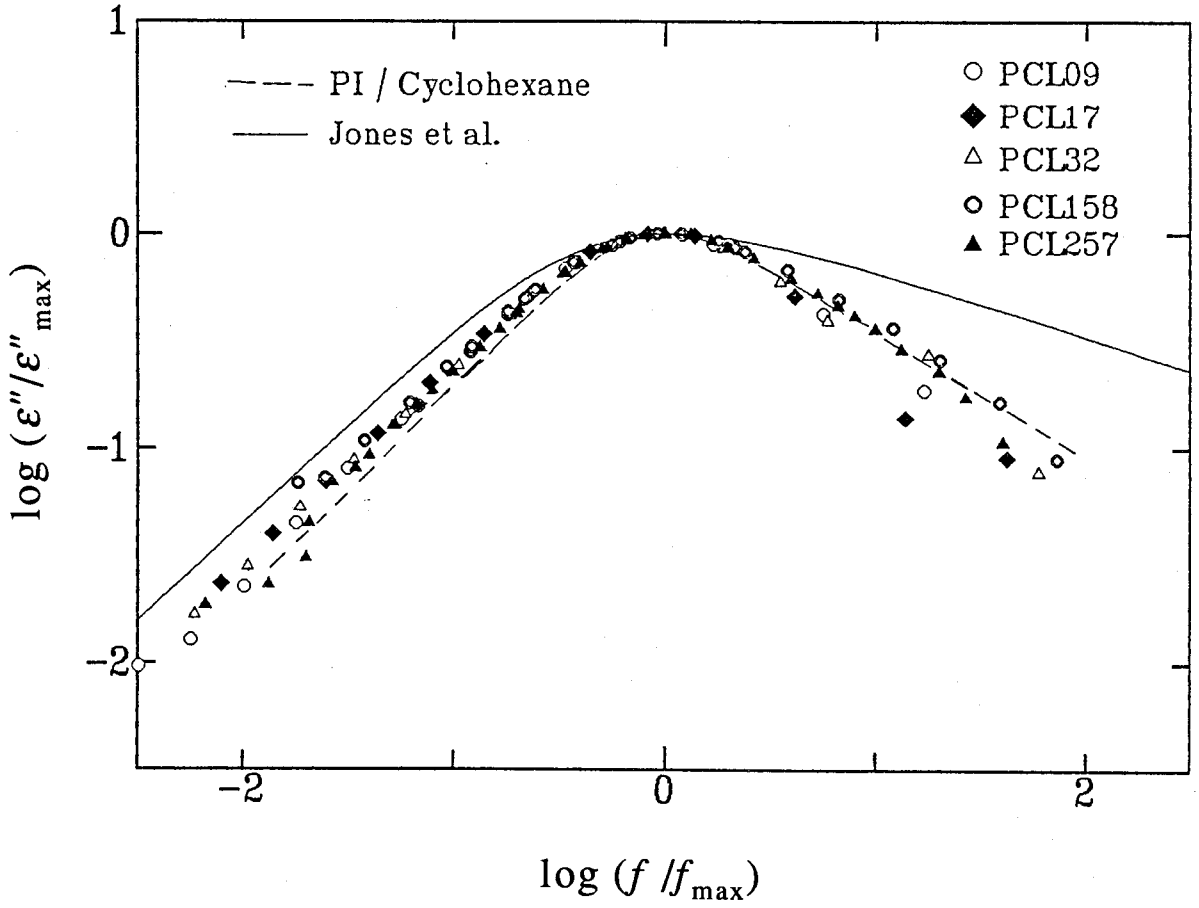

Figure V-6. Comparison of the shape of the ε'' curves for dilute benzene solutions of PCL and PVL. The data for PCL/dioxane solutions reported by Jones *et al.* are shown by the solid line.

If one assumes that the bead corresponds to a blob of radius ξ in which there are g segments, then N and b should be replaced by N/g and ξ, respectively. Here we note that $g \propto C^{1/(1-3\nu)}$ and $\xi \propto C^{\nu/(1-3\nu)}$. With the Stokes theory the friction coefficient for one blob is given by $\zeta = 6\pi\eta_s\xi$. From eq. V-5, τ is given by[10]

$$\tau \propto \eta_s N^{3.5} C^{(3\nu-3.5)/(1-3\nu)} \qquad \text{(V-6)}$$

On the other hand the relaxation time τ_0 in dilute solution is given by a modified Zimm model as[4]

$$\tau_0 \propto \eta_s N^{3\nu} \qquad \text{(V-7)}$$

Validity of this equation has been demonstrated by the fact that the proportionality between τ_0 and $M_w[\eta]$ ($\propto N^{3\nu}$) holds as described in the previous section. From eqs V-6 and V-7 τ/τ_0 can be written as

$$\tau/\tau_0 \propto (C/C^*)^{(3\nu-3.5)/(1-3\nu)} \qquad \text{(V-8)}$$

This equation provides a criterion to check whether chains are entangled or not in a semidilute solution.

V-3-1-2. Tube Model

The tube model is applicable to well entangled systems . According to Doi and Edwards[4] it is assumed that a test chain is confined in a tube with diameter a which is equal to $\langle r^2\rangle^{0.5}$ of the chain with $M = M_e$. The longest relaxation time τ_d is given by

$$\tau_d = L^2 / (\pi^2 D_C) \qquad \text{(V-9)}$$

where L is the curvilinear length of the tube and D_C the diffusion coefficient of the

chain along the tube. If the chain is represented by the Rouse model, eq V-9 is written as[4]

$$\tau_d = \zeta N^3 b^4 / (\pi^2 k_B T a^2) \qquad \text{(V-10)}$$

The higher mode relaxation times are expressed by $\tau_p = \tau_d / p^2$ and the end-to-end correlation function $\langle \boldsymbol{r}(0) \cdot \boldsymbol{r}(t) \rangle$ has the same form as the Rouse model represented by eq. V-1. It is noted that the relaxation spectra predicted by the Rouse and tube models are the same. Thus these two models predict the same shape of ε'' curves.

V-3-1-3. Muthukumar-Freed Theory

Muthukumar and Freed[12,13] proposed a theory to represent the C dependence of the p-th normal mode (Rouse-Zimm mode) relaxation time τ_p in the crossover region from dilute to semidilute regime considering the inter-chain hydrodynamic interaction effect. Their expression is

$$\tau_p = \tau_{p0} [1 + CAp^{-\kappa} - 2^{0.5}(CAp^{-\kappa})^{1.5} + 2(CAp^{-\kappa})^{2.0} + \ldots] \qquad \text{(V-11)}$$

where τ_{p0} is the p-th relaxation time at infinite dilution, A is a constant proportional to $M^{3\nu-1}$, and κ is equal to 3ν-1; note that A is proportional to $[\eta]$. Eq. V-11 can be approximated by similar to the Martin equation which is

$$\tau_p = \tau_{p0} \exp (A' C[\eta]) \qquad \text{(V-12)}$$

This equation predicts that log τ is proportional to $C[\eta]$ in the crossover region.

According to the Muthukumar-Freed theory, τ_p is different from that predicted by Rouse model but the end-to-end correlation function $\langle \boldsymbol{r}(0) \cdot \boldsymbol{r}(t) \rangle$ is the same as Rouse model function represented by eq. V-1. Thus the relaxation spectrum predicted by Muthukumar-Freed theory is also almost the same as that by the Rouse model. Since, as can be seen in Figure V-1, the Rouse and Zimm spectra are

similar, the difference among the four models, *i.e.*, the Rouse, Zimm, Tube and Muthukumar-Freed models, is small.

V-3-2. C Dependence of τ

At C is above C^*, the dielectric response changes as shown in Figure V-7 in which the data for (a) PI-743/heptane and (b) PI-140/heptane solutions are shown. The ε'' curves shift to low frequency with C indicating that the increase of C slows down the polymer mobility.

Figure V-8 shows the C dependence of τ for solutions of PI in (a) heptane and(b) cyclohexane. In order to determine the critical C above which PI chains are entangled, we used eq V-6 and $\tau/M_w^{3.5}$ is plotted against C in Figure V-9. If polymer chains are well entangled, a universal straight line may be expected for different MW data. From the slopes of the indicated bold straight lines, we determined the value of ν to be 0.54 and 0.59 for heptane and cyclohexane solutions respectively. These values agree well with the ν values of 0.544 in heptane and 0.58 in cyclohexane determined from the $[\eta]$ vs. M_w relations.

Figure V-10 shows the double-logarithmic plots of τ/τ_0 vs.$C[\eta]$ ($\approx C/C^*$) for (a)PI/heptane and (b)PI/cyclohexane. In spite of the relatively large difference of MW, all data points for each solvent fall on a single curve. The thick straight lines correspond to those in Fig V-9. Although the onset of entanglement is rather ambiguous, the crossover may be seen to occur at $C[\eta] \cong 10$ for both heptane and cyclohexane solutions.

V-3-3. Comparison with Muthukumar-Freed's Theory

The Muthukumar-Freed theory[12,13] is tested in Figure V-11 with the data of log τ for solutions of PI-743 and PI-140 in heptane. In the low concentration region, log τ data varies linearly with C_I as expected from eq V-12. The parameter A is determined from the slopes of straight lines to be 70.0 for PI-743 and 26.2 for PI-140. These values of A conform to $0.29[\eta]$ within an error of 6%, so that $A'=0.29$.

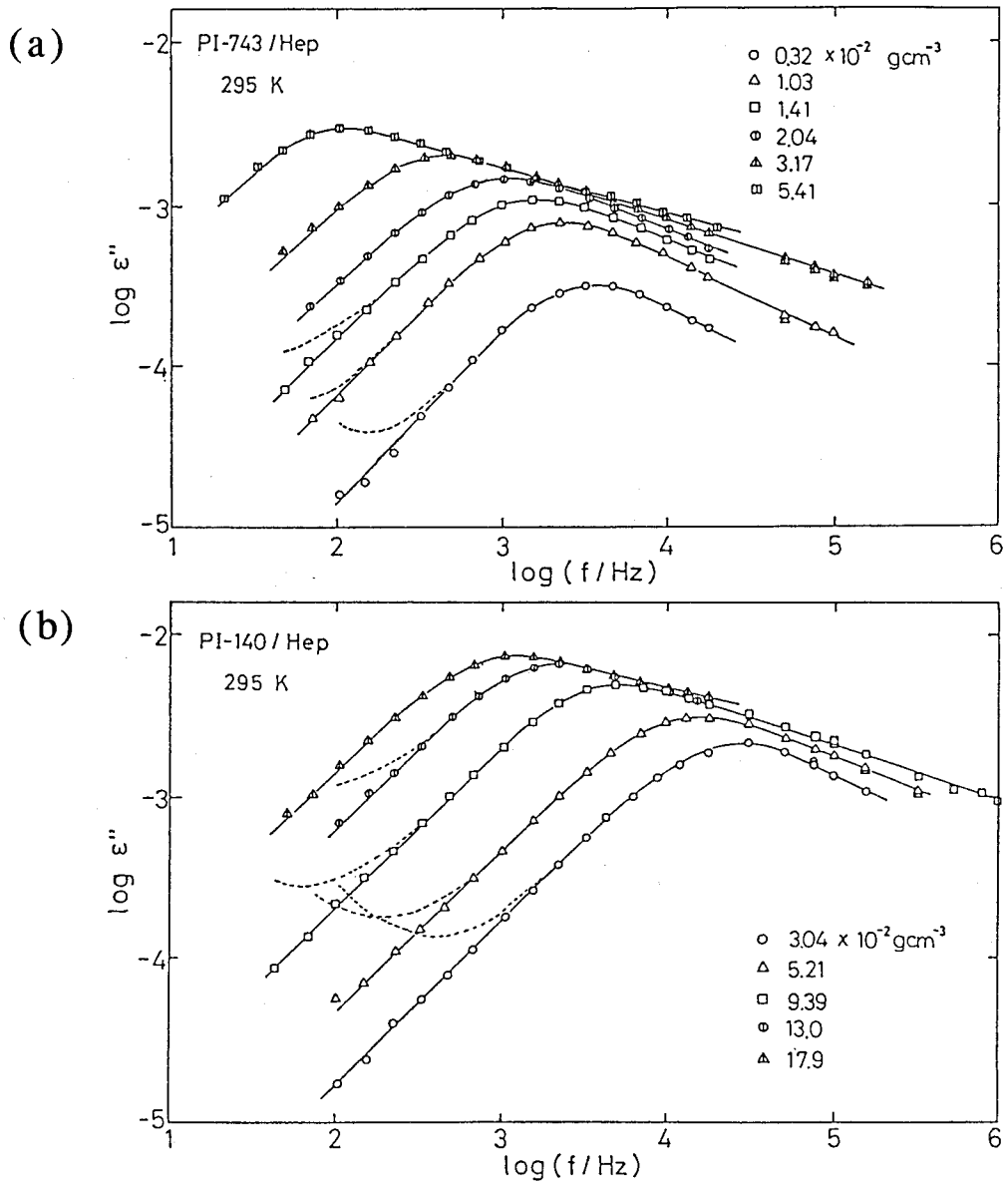

Figure V-7. Representative ε'' curves for (a) PI-743 and (b) PI-140 in heptane solutions of various concentrations. The dashed lines indicate raw data in which the increase of ε'' in the low frequency range was due to ionic conduction. The contribution of the ionic conduction g_{dc} to ε'' was estimated by plotting alternating conductivity g against f^2. The value of g at $f = 0$ was estimated by linear extrapolation and was assumed to be the direct current conductivity The data points shown here are the corrected ones.

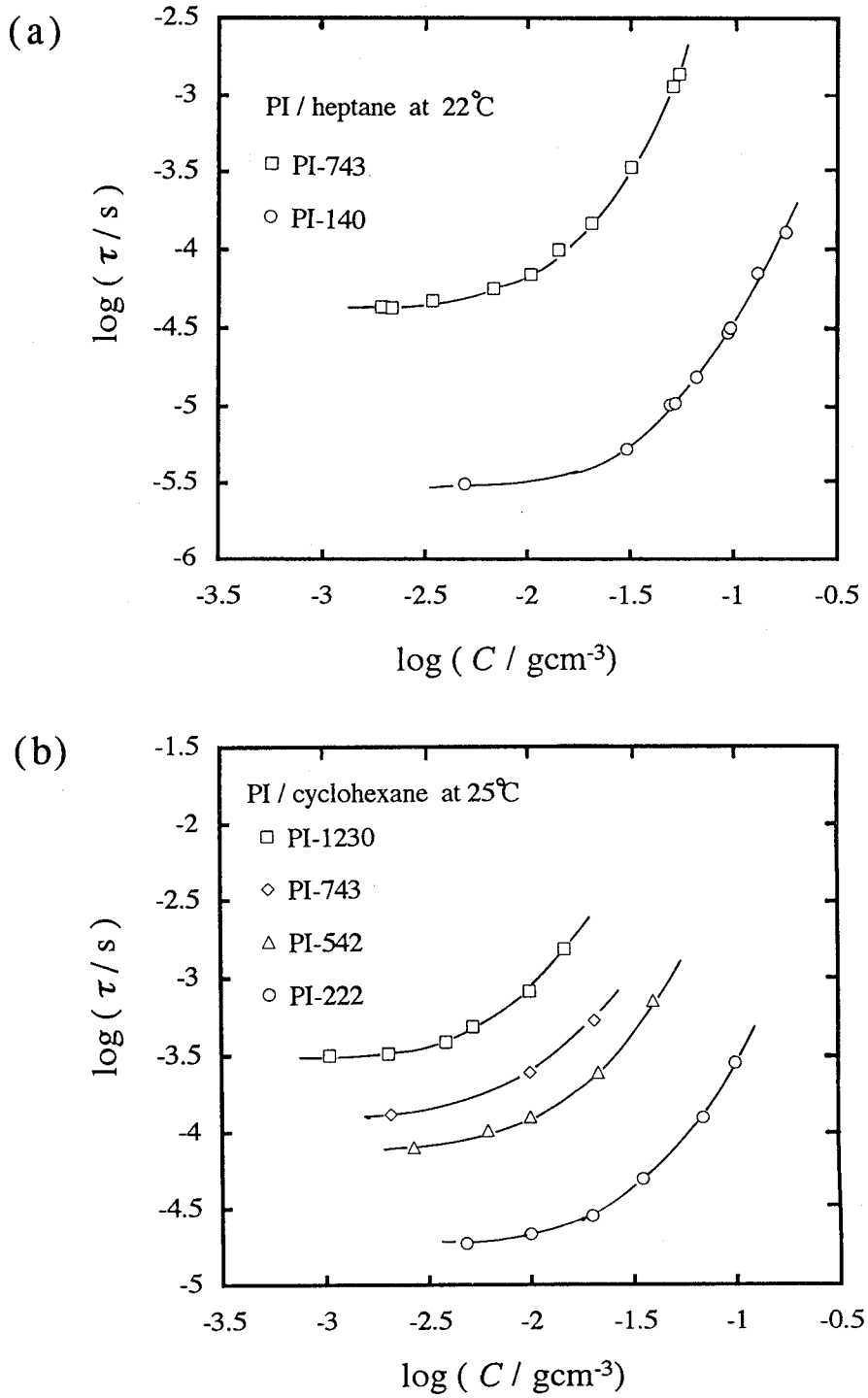

Figure V-8. Concentration dependence of normal mode relaxation time τ in (a) heptane and (b) in cyclohexane solutions of PI with different M_w.

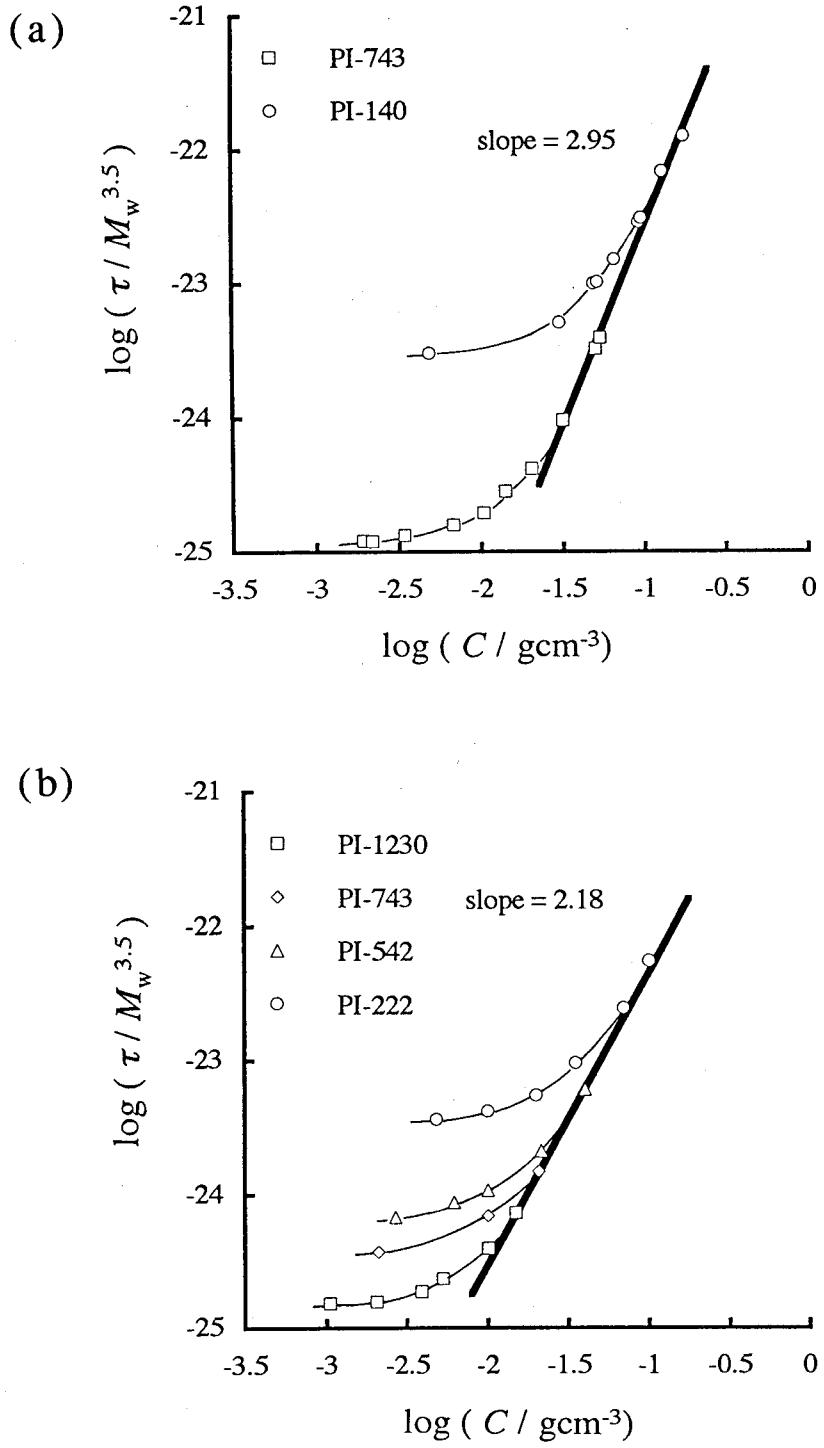

Figure V-9. Double-logarithmic plots of $\tau/M_w^{3.4}$ vs. C for (a) PI/heptane and (b) PI/cyclohexane solutions.

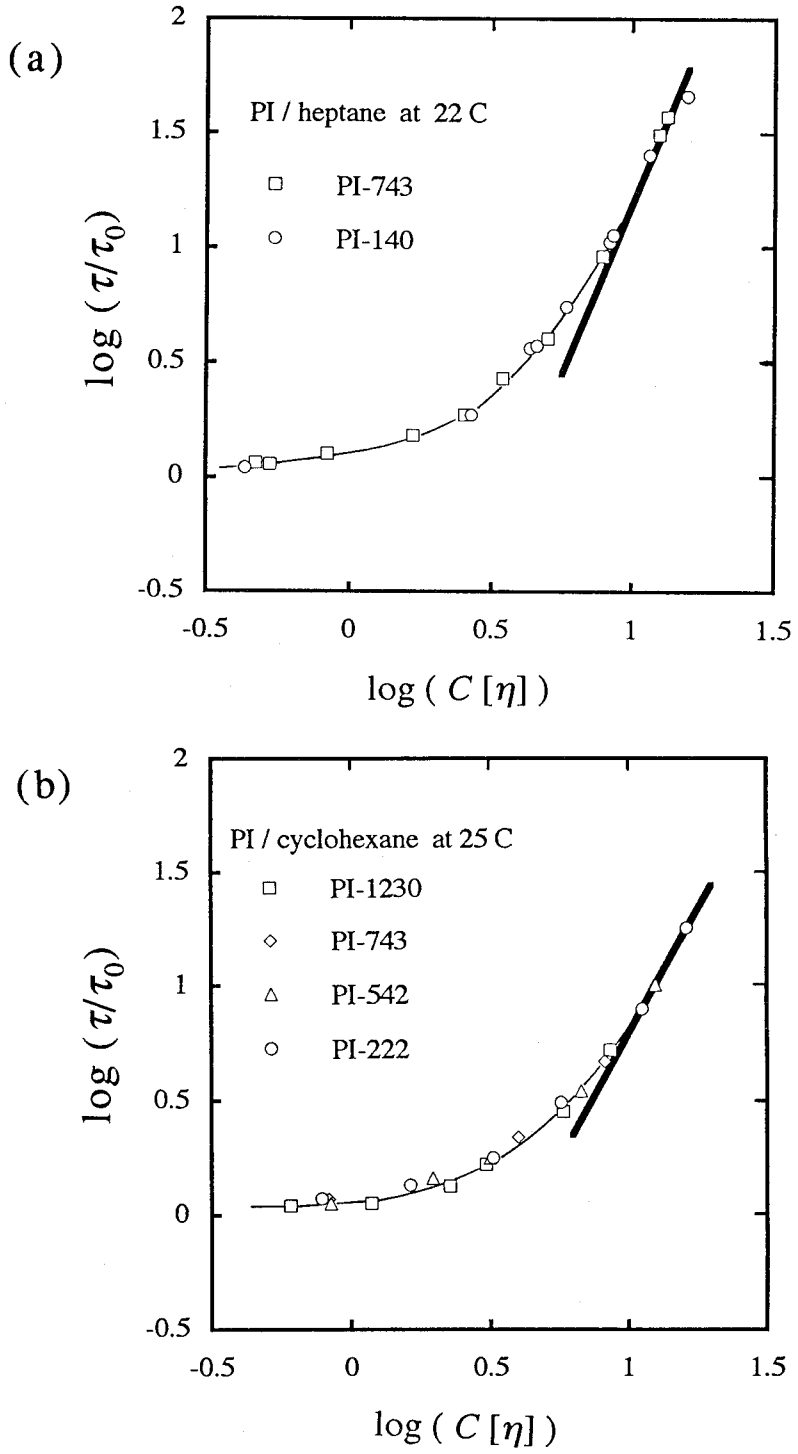

Figure V-10. Double-logarithmic plots of τ/τ_0 vs. $C[\eta]$ for (a) PI/heptane and (b) PI/cyclohexane solutions. The solid lines indicate the prediction by the scaling theory in entangled region.

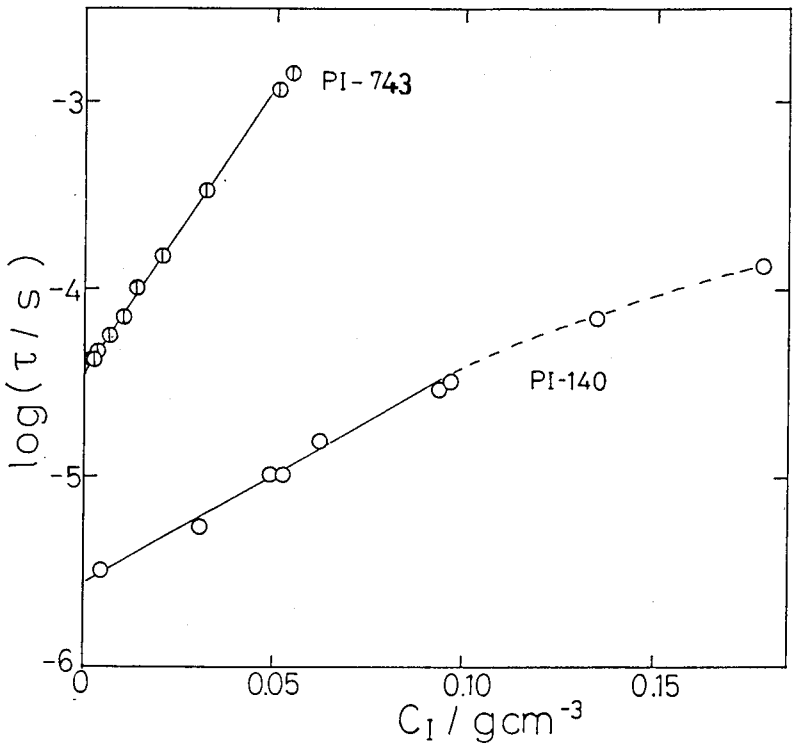

Figure V-11. Semi-logarithmic plots of τ vs. C for PI/heptane solutions.

For cyclohexane solutions of PI , we got A'=0.20 which is smaller than A' of heptane solutions. This means the dependence of τ on C is more gentle in cyclohexane (good solvent) than in heptane (marginal solvent). This result well corresponds to the scaling prediction, *i.e.*, the exponent in eq. V-6 decreases with increasing solvent quality.

Figure V-12 compares theoretical and experimental τ for (a)PI/heptane and (b) PI/cyclohexane solutions. The solid lines in this figure show the theoretical τ_1 calculated from eq. V-11 with p = 1 and $A = A'[\eta]$. We see that the agreement is good for cyclohexane solutions but not for heptane solutions in which τ is better described by the exponential equation (eq. V-12) than eq. V-11.

For PCL-158/benzene solutions we obtained A' = 0.26 which is intermediate between the values for PI/heptane and PI/cyclohexane solutions. We find that A' is related to the solvent quality as shown in Table VII where ν and A' are compared.

Table VII. List of Muthukumar parameter A' and excluded volume exponent.

A'	ν determined from $[\eta]$	system
0.29	0.54	PI/heptane
0.20	0.58	PI/cyclohexane
0.26	0.55	PCL/benzene

V-3-4. *C* Dependence of τ for the First and Second Modes

From the dielectric normal mode process of PI with the symmetrically inverted dipole, the relaxation time τ_2 of the second mode was measured. The theoretical background will be described in Chapter VI. We discuss the result of τ_2 in semidilute solutions of PI.

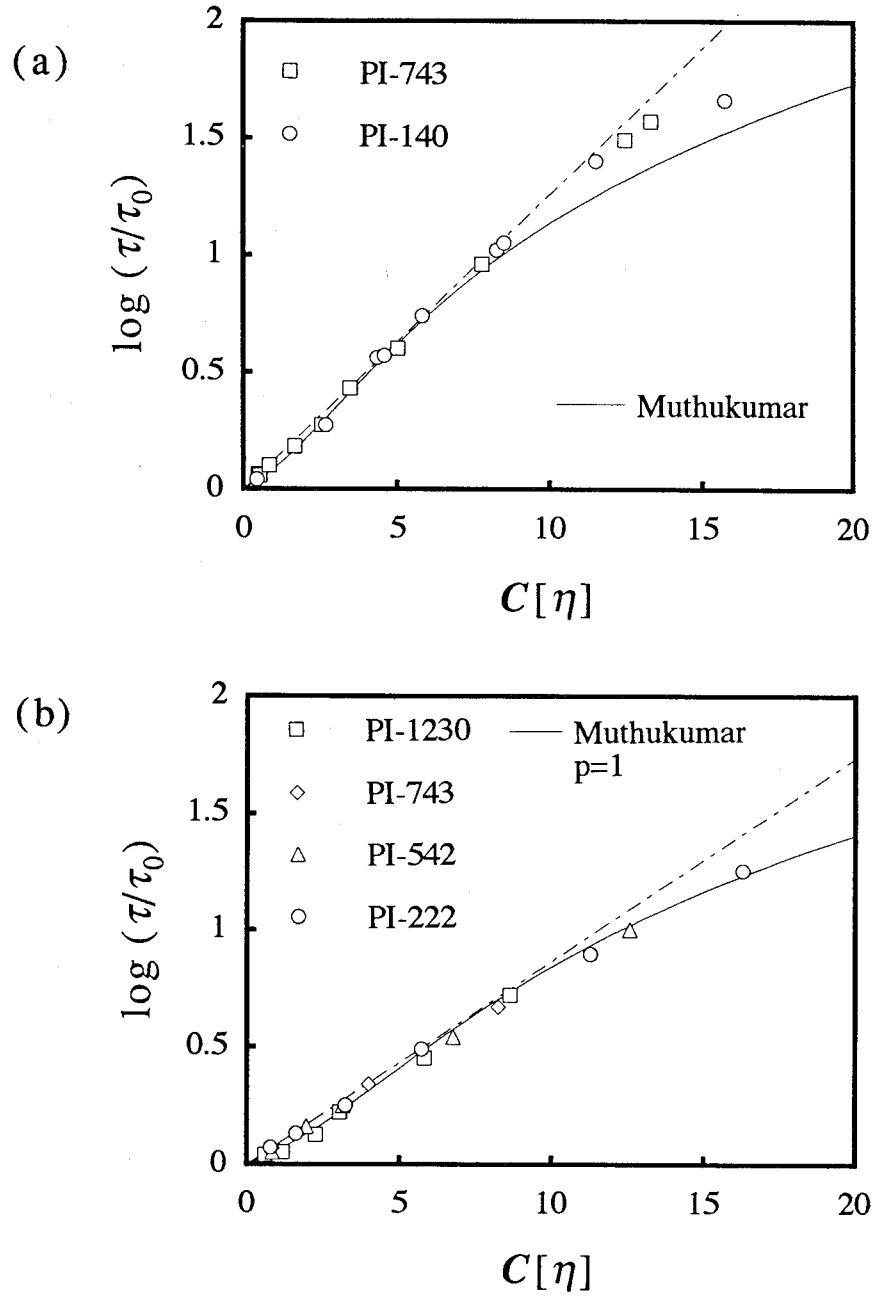

Figure V-12. Comparison with the Muthukumar and Freed theory for $C[\eta]$ dependence of τ/τ_0. (a) Heptane and (b) Cyclohexame solution.

We examined the normal mode of dipole inverted PI (I-I 415-415) in cyclohexane solutions and determined τ_2 from the peak frequency of ε''. Figure V-13 shows the $C[\eta]$ dependence of $\tau_2/\tau_{2,0}$ determined and τ/τ_0 ($=\tau_1/\tau_{1,0}$) replotted for Fig. V-12, where $\tau_{2,0}$ is the second normal mode relaxation time extrapolated to $C \rightarrow 0$. The Muthukumar theory for τ_2 is also shown in this figure, along with the theoretical curve for $p=1$. The agreement between theory and experiment is not good, though the τ_1 data in cyclohexane were well described by their theory.

Figure V-14 shows the $C[\eta]$ dependence of τ_1/τ_2. In this figure the experimental error are as large as about 20% since the τ_1/τ_2 data were determined after many reduction procedures. However the tendency of the increasing ratio with increasing C is seen. The Zimm, Rouse, and Tube theories predict the ratio to be 3.17 , 4.00, and 4.00, respectively. Experimental values of τ_1/τ_2 in dilute solution are close to the prediction of the Zimm model but tend to approach with C to 4.0 predicted by Rouse and Tube models. This finding may be interpreted by the idea that the hydrodynamic interaction is screened and topological interaction becomes intense as C increases.

V-3-5. C Dependence of the Shape of ε'' Curves

Figure V-15 shows the reduced ε'' curves for (a) PI-743 / heptane and (b) PI-222 / cyclohexane solutions, where ε'' is reduced by the ε''_{max} and f by f_{max}. We see that the curves become broader with increasing C. For dilute solutions, the shape is nearly the same as that predicted by the Rouse or Zimm theories as mentioned in the previous section. For semidilute solutions, the curves become broader with increasing C in the high frequency side of the loss peak. The log ε'' vs. log f relation is linear over a range of 0.5 decade above f_{max}. With increasing C, the slope α ($= d\log \varepsilon''/d\log f$) in the high frequency side of the loss curve increases (the absolute value of α decreases.) Such a change in α is equivalent to that in relaxation spectrum and hence the fashion of chain motion becomes different with increasing C due to the inter-chain interaction. However, this phenomenon can

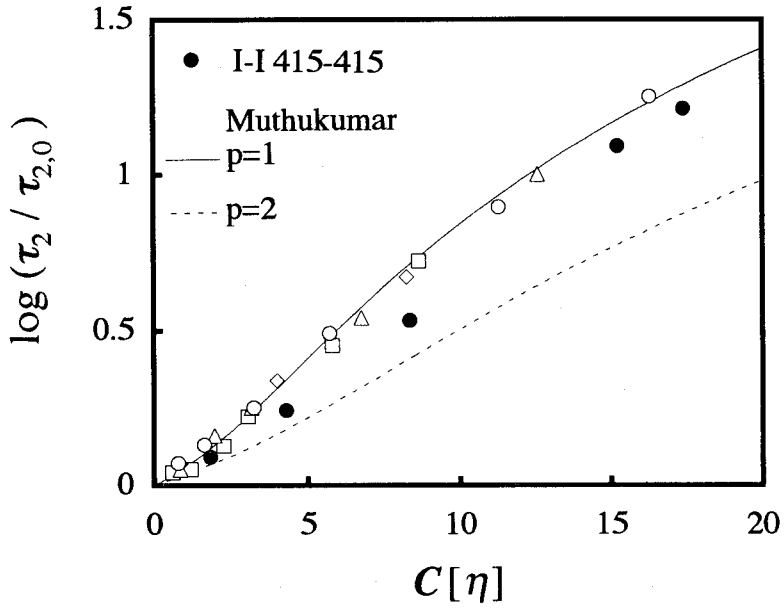

Figure V-13. $C[\eta]$ dependence of the ratio of the second mode relaxation time at C to that at infinite dilution for I-I 415-415 in cyclohexane. For the comparison the data of $\tau/\tau_0(=\tau_1/\tau_{1,0})$ shown in Figure V-12(b) are also plotted. The solid and dashed lines represent the theoretical prediction for the first and the second mode respectively by Muthukumar-Freed theory.

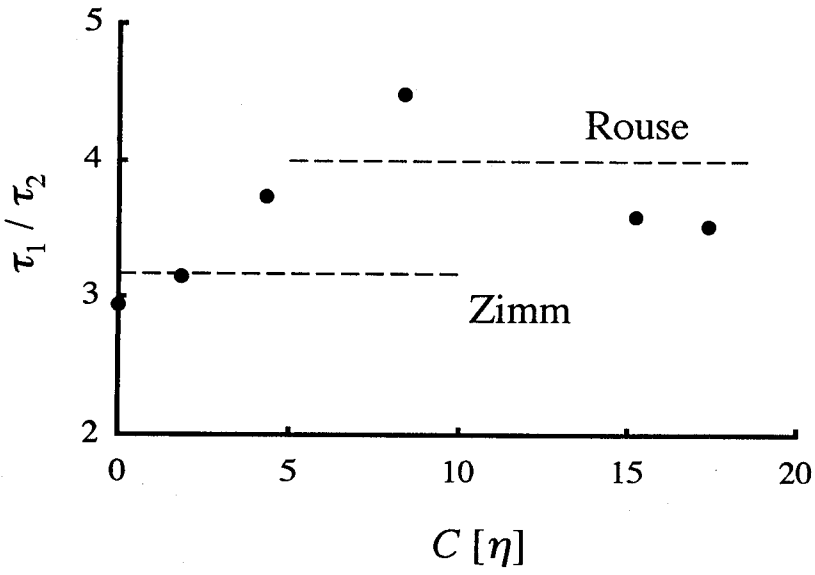

Figure V-14. $C[\eta]$ dependence of τ_1/τ_2 for PI/cyclohexane solutions.

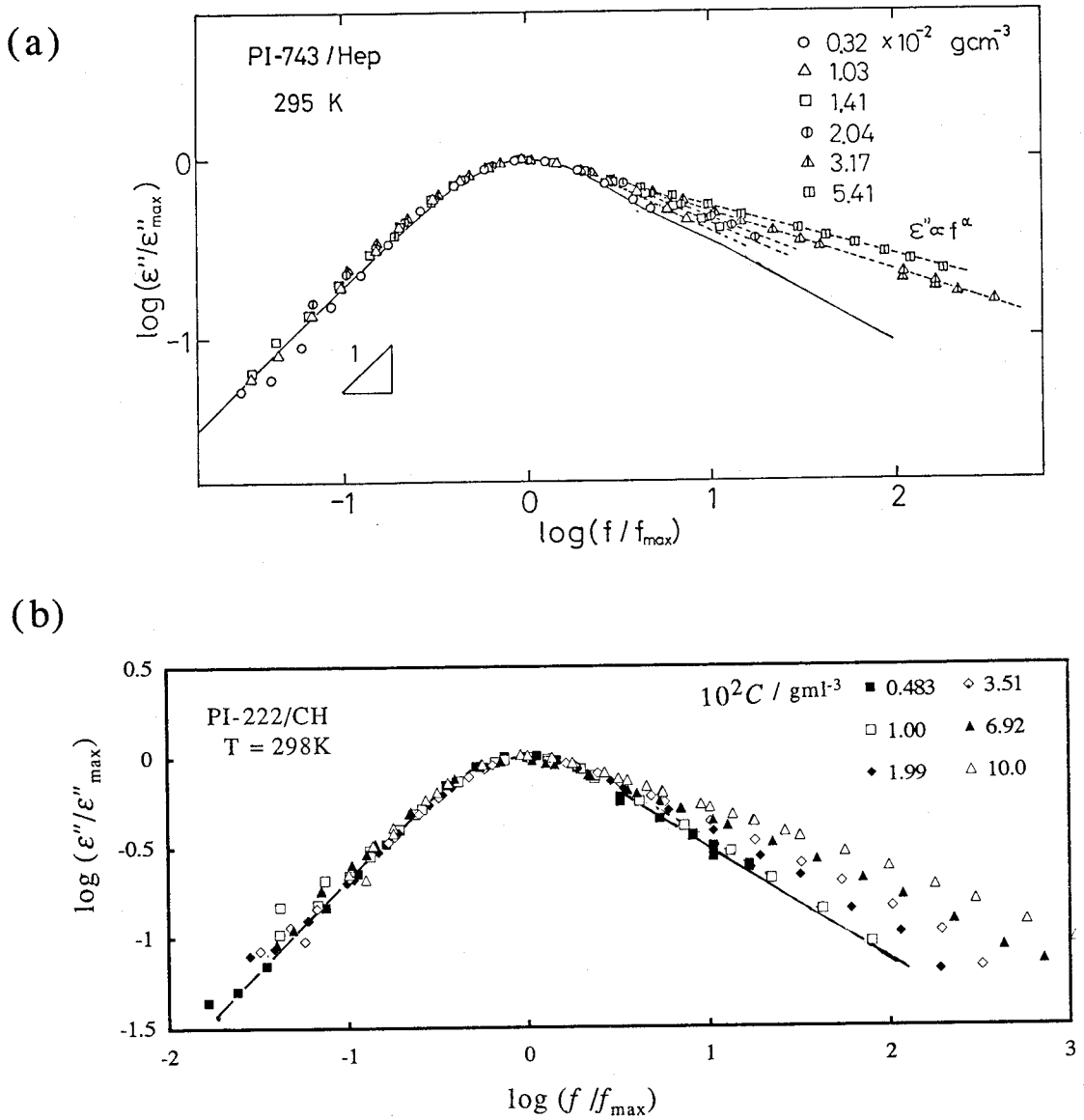

Figure V-15. Reduced ε'' curves for (a) PI-743/heptane and (b) PI-222/cyclohexane solutions of various concentrations. The solid line indicate the predicted curves by Zimm theory.

not be explained by any combinations of the Zimm, Rouse, and tube theories which predict slope of -1/3 and -1/2 and -1/2 respectively. New theory is required to explain the effect of inter-chain interactions on mode distribution.

Examining the ε'' curve carefully, we found that the α begins to increase around $C \cong C^*$ as shown in Figure V-16(a) for heptane and (b) cyclohexane solution. We also plotted α against $C[\eta]$ in Figure V-17, in which the α vs. $C[\eta]$ plots for various MW almost coincide. This result suggests that the mode distribution can be expressed by a universal function of $C[\eta]$.

The scaling theory predicts that the C dependence of properties in semidilute solutions can be expressed by a function of $C[\eta]$ as far as the frequency region is not too high. Our experimental result is consistent with the scaling theory. However, the change in dynamics with increasing C caused by complex inter-chain interactions have not been explained.

For the broadening of ε'', the entanglement effect must be taken into account. The onset of entanglement estimated in Figures V-9 and V-10 is indicated in Fig.V-17 by arrows. We see that the broadening occurs below the onset of entanglement.

Figure V-18 shows the C dependence of the shape of ε'' of PCL-158/benzene solutions. The broadening of ε'' curves with increasing C can be seen as observed above for PI solutions.

V-3-6. Comparison with the Result of Complex Modulus G^*

As shown in figure V-2, the Rouse and Zimm models predict the considerably different G' or G'' curves. Ferry and coworkers[1,14,15] reported that the shape of G^* in a semidilute solution of polystyrene of $C[\eta] \cong 2$ was perfectly described by the Zimm model and it changed from the Zimm-like to the Rouse-like shape with increasing C. In the high C regime the agreement with the Rouse model became perfect. This transition occurred at $C[\eta] \cong 3$ and even at C about $C[\eta] \cong 10$ the shapes of G' and G'' curve still showed Rouse-like behavior. These findings were interpreted by the screening of hydrodynamic interaction. Yamamoto and Tanaka[16]

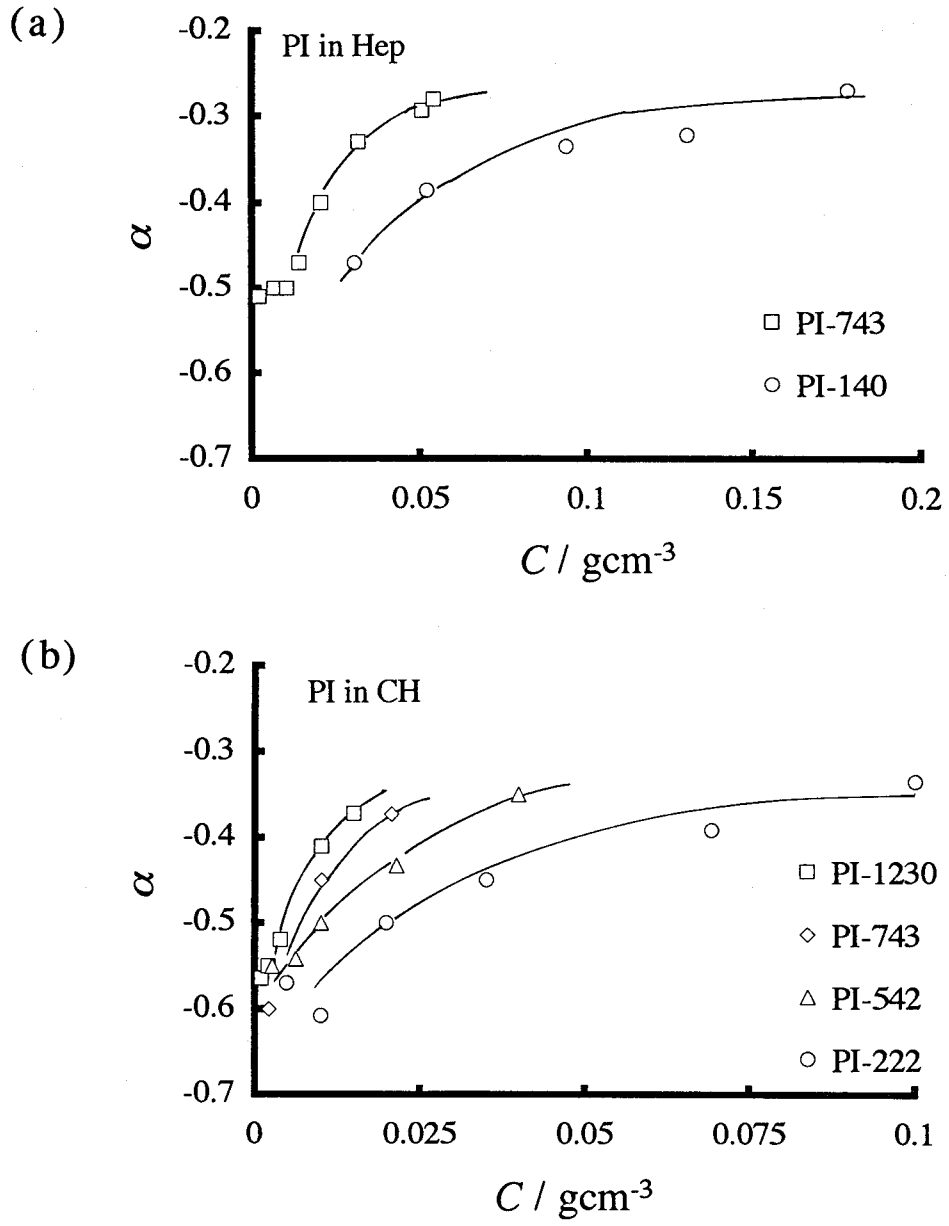

Figure V-16. C-dependence of the slope α of log ε'' vs. log f curve in the high frequency side for (a) PI/heptane and (b) PI/cyclohexane solutions.

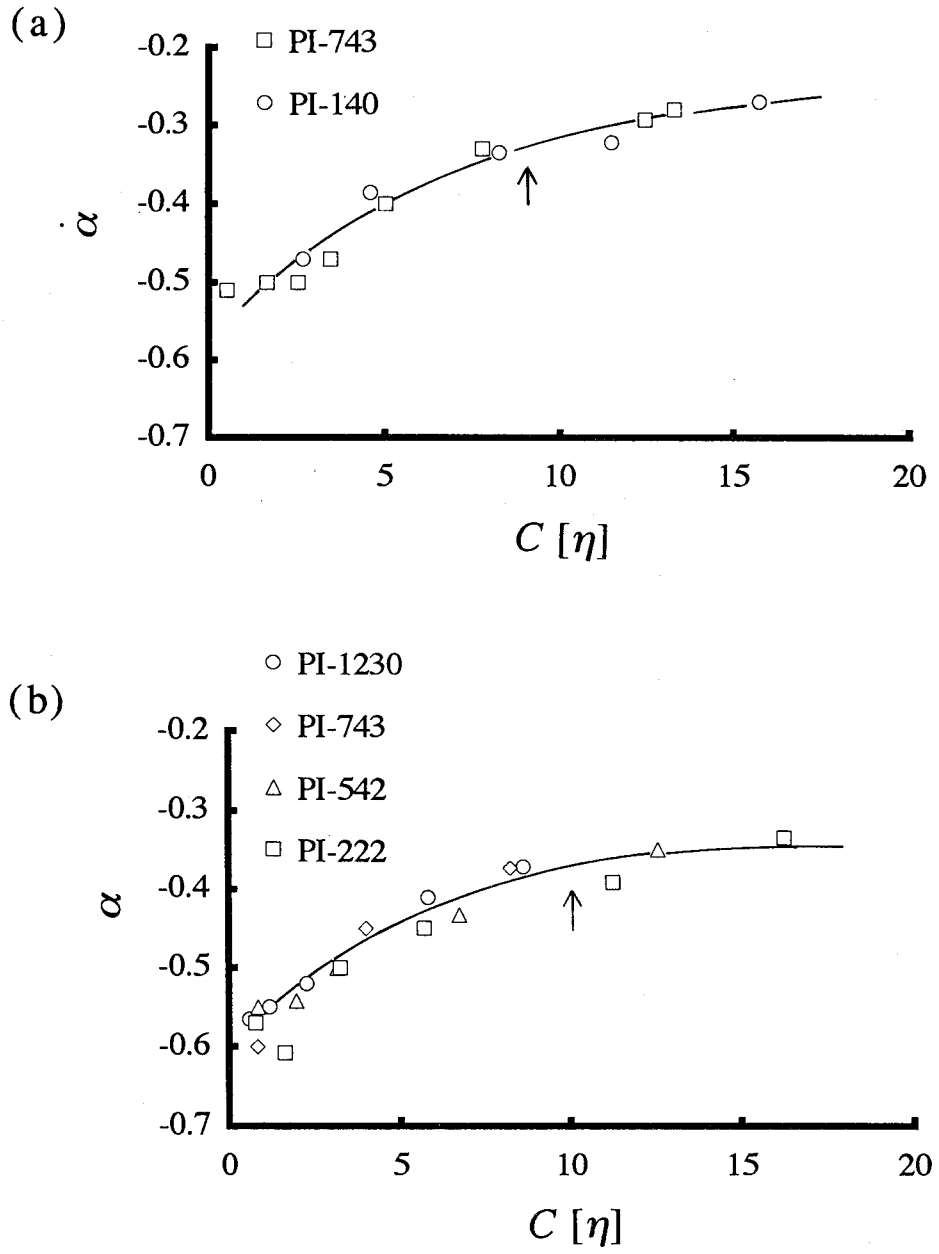

Figure V-17. $C[\eta]$ dependence of α for (a) PI/heptane and (b) PI/cyclohexane solutions.

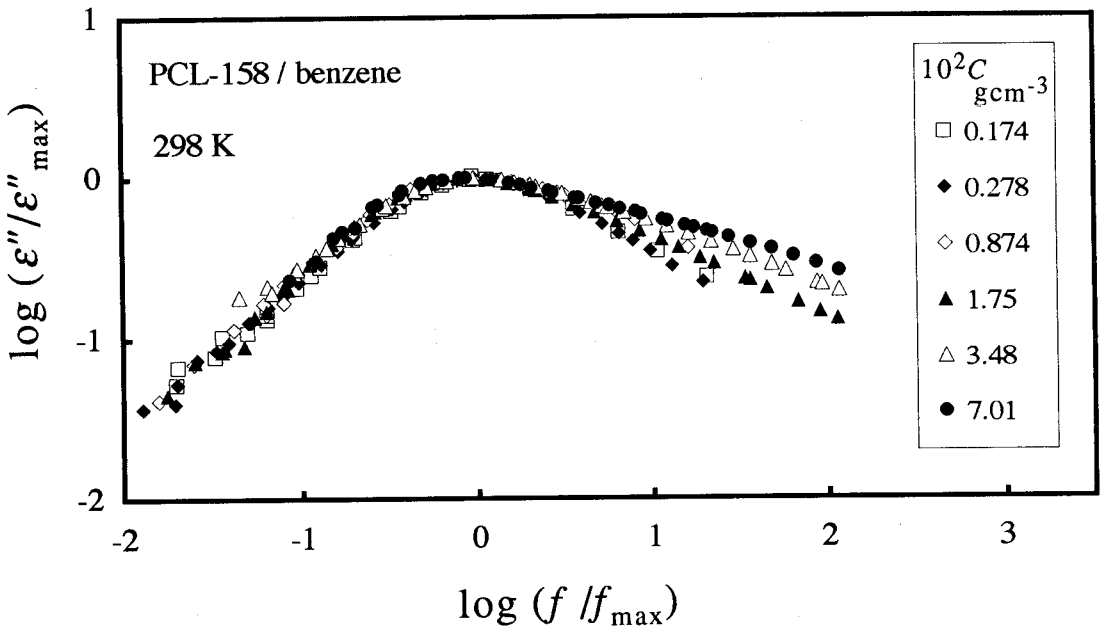

Figure V-18. Reduced ε'' curves for PCL-158/benzene solutions of various concentrations

opposed the view of Ferry *et al.* and explained the Rouse-like behavior by a combination of the hydrodynamic interaction and the entanglement coupling. They considered doubtful the applicability of the Rouse model to such a high concentration region as $C[\eta] \cong 10$.

The present study has clearly shown that our ε'' data do not agree with the Rouse model in semidilute solutions. Although the theoretical ε'' curves by the Rouse and Zimm theories exhibit a small difference, we can conclude that the data at $C[\eta] \cong 10$ differ considerably from the Rouse theory.

Here we list possible origins of the broadening of ε'' curve.

(1) Shielding of the hydrodynamic interaction.

(2) Shielding of excluded volume effect.

(3) Entanglement effect.

(4) The other inter-chain interactions.

At present we so not have evidences to conclude which interaction affects mainly the mode distribution. For this problem we will make further considerations in the following section of this chapter.

V-4. Dynamics of Polymers in Polymer/Polymer/Solvent Ternary Systems

V-4-1. τ of Tracer Polyisoprene Chain in Polybutadiene/Heptane Solutions

In this section the dynamic behavior in the PI/PB/heptane system are studied. It is noted that the PI concentration C_I was taken so that the PI chains do not overlap each other. The concentration C_B of PB was changed widely.

Figure V-19 shows the C_B dependence of τ for PI-140, PI-743, and PI-651 in PB semidilute solution. The values of τ in PI/heptane binary solutions are also plotted against C_I with filled symbols. It is seen that at fixed molecular weight M_B of PB, τ of PI increases with C_B and at fixed C_B, τ increases with M_B. Since C_I is kept less than C^*, the increase in τ is caused by overlapping or entanglement between the PI and PB chains.

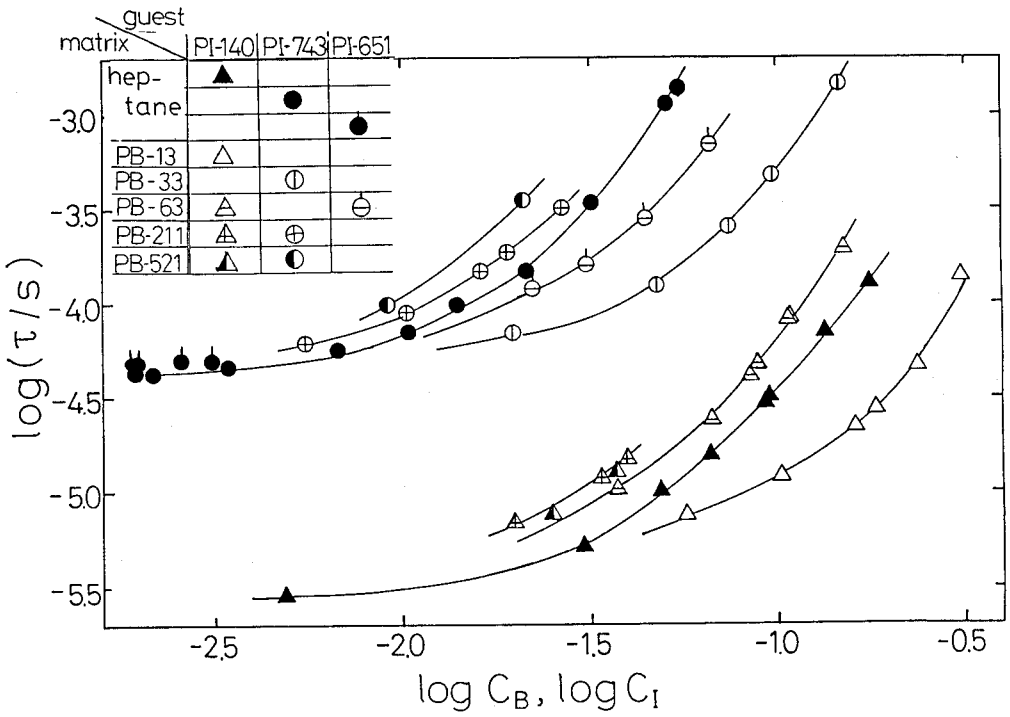

Figure V-19. Dependence of τ of PI on PB concentration C_B in ternary solutions at 295 K. The data of binary PI/heptane systems are plotted against PI concentration C_I with filled symbols.

V-4-2. Expression of τ by Scaling Theory

The C_B and M_B dependence of τ were analyzed in terms of the blob model for two extreme cases: $M_I >> M_B$ and $M_I << M_B$.

(1) $M_I >> M_B$

For dilute solutions of the PI chain, the relaxation time τ_0 is given by the Zimm theory (cf. eq V-3):

$$\tau_0 \cong \eta_s <r_0^2>^{3/2} / (k_B T) \qquad \text{(V-13)}$$

where $<r_0^2>^{1/2}$ is the end-to-end distance at infinite dilution. For the ternary solutions, this equation may be correct when C_B is smaller than C_B^*. As was demonstrated in the study of diffusion, we expect that even in the range of $C_B > C_B^*$, eq V-13 may hold if $M_I >> M_B$. Under such a condition, the PB chains move much faster than the PI chain and act as solvents:

$$\tau \cong \eta_B <r^2>^{3/2} / (k_B T) \qquad \text{(V-14)}$$

where η_B is the viscosity of a PB solution and $<r^2>^{1/2}$ the end-to-end distance of the PI chain in the PB solution. assuming that the front factor of eqs V-13 and V-14 are the same, we can derive

$$\tau / \tau_0 = (\eta_B / \eta_s) (<r^2> / <r_0^2>)^{3/2} \qquad \text{(V-15)}$$

The ratio $<r^2>/<r^2>_0$ determined in section IV-4 and was represented approximately by a universal function f of $C_B[\eta]_B$ ($=C_B/C_B^*$) in the case of $M_I > M_B$:

$$<r^2>/<r^2>_0 \cong f(C_B[\eta]_B) \qquad \text{(V-16)}$$

It is well known that η_B/η_s in semidilute solution is expressed approximately by a

universal function g of $C_B[\eta]_B$:[17]

$$\eta_B/\eta_s \cong g(C_B[\eta]_B) \tag{V-17}$$

Combining eqs V-15, 16, and 17, we obtain

$$\tau/\tau_0 \cong F_1(C_B[\eta]_B) \tag{V-18}$$

where F_1 is a function. This equation predicts that τ of the single PI chain in various MW matrices of PB is expressed by a universal function of $C_B[\eta]_B$.

(2) $M_I << M_B$.

Next we consider the opposite case of $M_I << M_B$. In this case the matrix PB chain is regarded as a fixed network and the PI chains move under constraints of the network. The tube model predicts that τ of PI may be determined by the tube diameter a which is equal to the distance between entanglements of PB chains and the friction coefficient ζ_{blob} per blob. According to de Gennes[10,18-21] and recent experimental data,[21,22] a is proportional to the blob size ξ_B of the PB matrix solution and ζ_{blob} is also proportional to the blob size as is given by the Stokes law for a non-draining sphere. We assume that the size of the blob of PI is equal to that of PB. Then τ is given by

$$\tau \cong \tau_{blob} f'(N_I/g_B) \tag{V-19}$$

where f' represents a function and τ_{blob} ($\propto \xi_B^2 \cdot \zeta_{blob}$) is the relaxation time for the single free blob; N_I, the degree of polymerization of the PI; and g_B, the number of the monomeric unit of PB in the single blob. τ_0 in eq V-13 is scaled by the blob and is rewritten as

$$\tau_0 \cong \tau_{blob}(N_I/g_B)^{3\nu} \tag{V-20}$$

From eqs V-19 and V-20, τ is written in the form:

$$\tau \equiv \tau_0 F_2(C_B[\eta]_I) \qquad \text{(V-21)}$$

where F2 is a function of $C_B[\eta]_I$.

V-4-3. Analysis of Experimental Dielectric Relaxation Time τ

In order to test eqs V-15, 17, and 18 we measured the relative viscosity η_B/η_s and plotted in Figure V-20(a). These data were then plotted against $C_B[\eta]_B$ in Figure V-20(b). We see that η_B/η_s is expressed approximately by a universal function in accordance with the result reported by many authors,[17,23-25] though the curves slightly shift downward with decreasing M_B. The weak M_B dependence of η_B/η_s may be considered to be caused by the poor solvent quality.[26-28] However we ignore the effect here.

In Figure V-21 eq. V-18 is tested by plotting τ/τ_0 double logarithmically against $C_B[\eta]_B$. The data points for $M_I/M_B > 3.52$ fall on a single curve. Thus we conclude that there is a regime in which eq V-18 holds.

Obviously this does not necessarily mean that the PI chain behaves Zimm-like. Thus we checked eq V-15 directly. Figure V-22 shows the C_B dependence of $(\tau/\tau_0)(<r_0^2>/<r^2>)^{3/2}$ and η_B/η_s. If eq V-15 is valid, the $(\tau/\tau_0)(<r_0^2>/<r^2>)^{3/2}$ and η_B/η_s curves should coincide. As is seen in the figure, the relative viscosity is slightly larger than the $(\tau/\tau_0)(<r_0^2>/<r^2>)^{3/2}$ for all systems. The discrepancy may be attributed to the following two origins: (1) the PI chains are not Zimm like depending on C_B and (2) the macroscopic viscosity differs from the local viscosity for the PI chain.

Figure V-23 shows the test of eq V-21 made by double logarithmic plots of τ vs. $C_B[\eta]_I$. The data points for $M_I/M_B < 1.43$ are represented by a single curve, indicating that there exists a regime where eq V-21 holds.

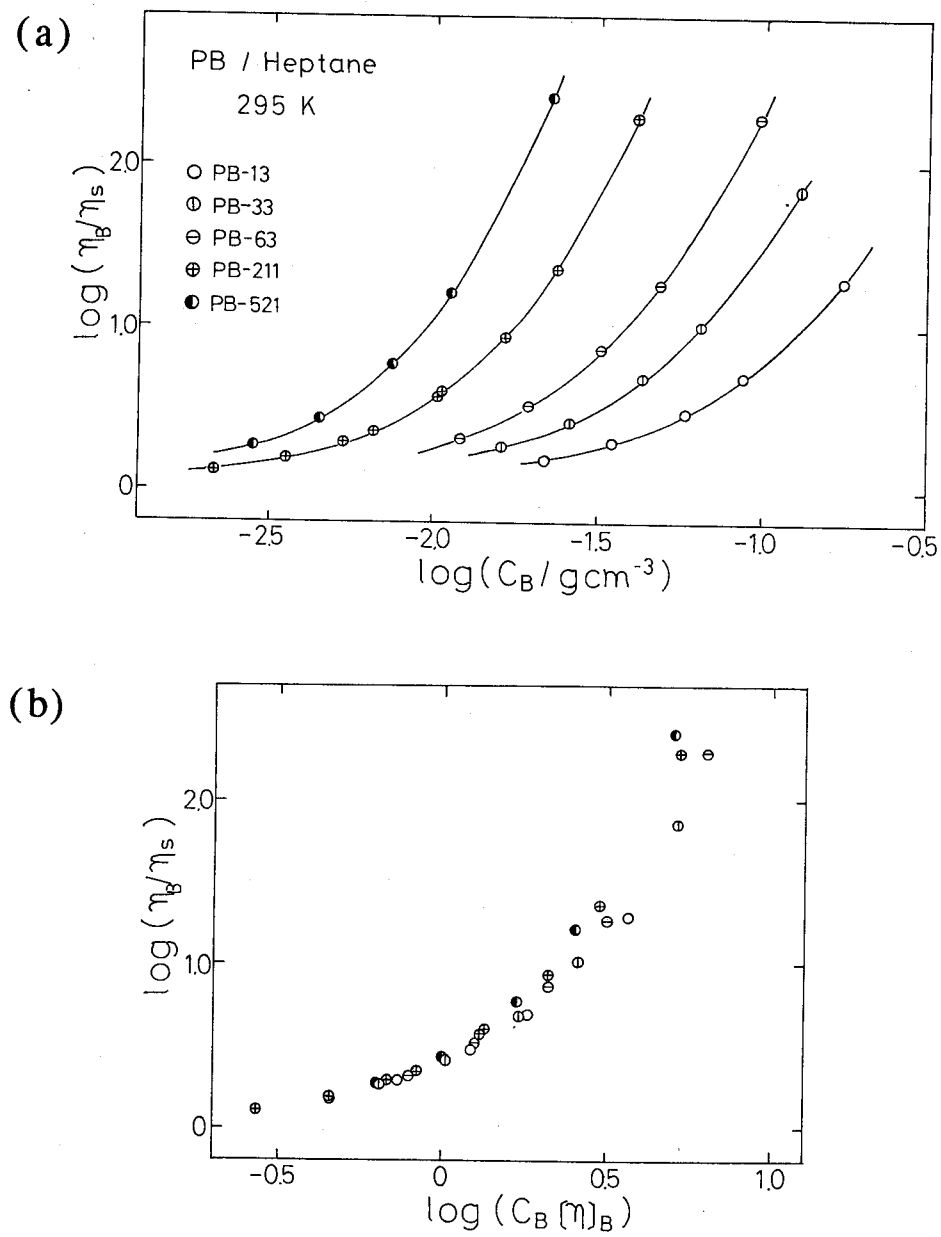

Figure V-20. (a) Double-logarithmic plots of relative viscosity η_B/η_s vs. PB concentration C_B for PB/heptane solutions at 295K. (b) Same data plotted against $C_B[\eta]_B$.

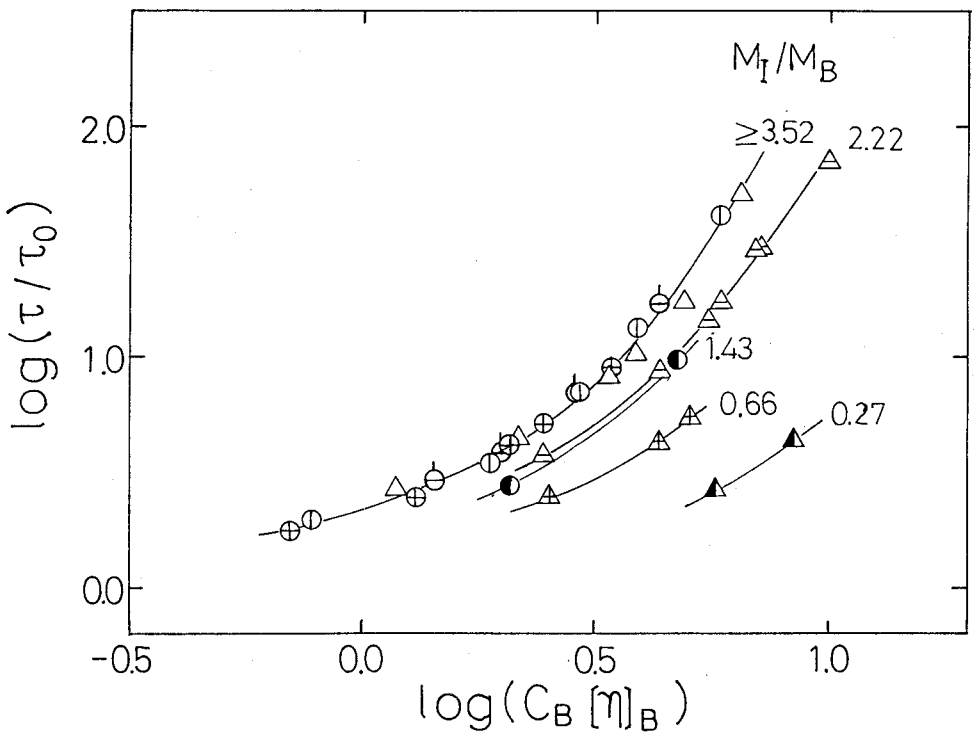

Figure V-21. Double-logarithmic plots of τ/τ_0 vs. $C_B[\eta]_B$. The ratio M_I/M_B is indicated in the curve. The symbols are the same as in Figure V-19.

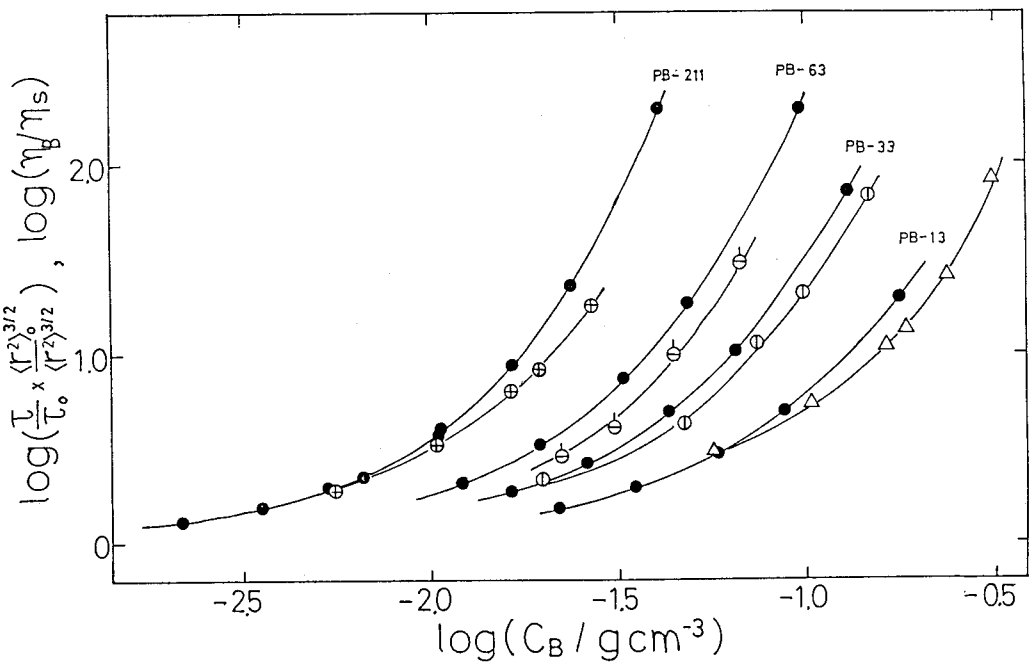

Figure V-22. Comparison of the viscosity of PB matrix solutions with the relaxation times of PI reduced by the chain dimension. The symbols are the same as in Figure V-19

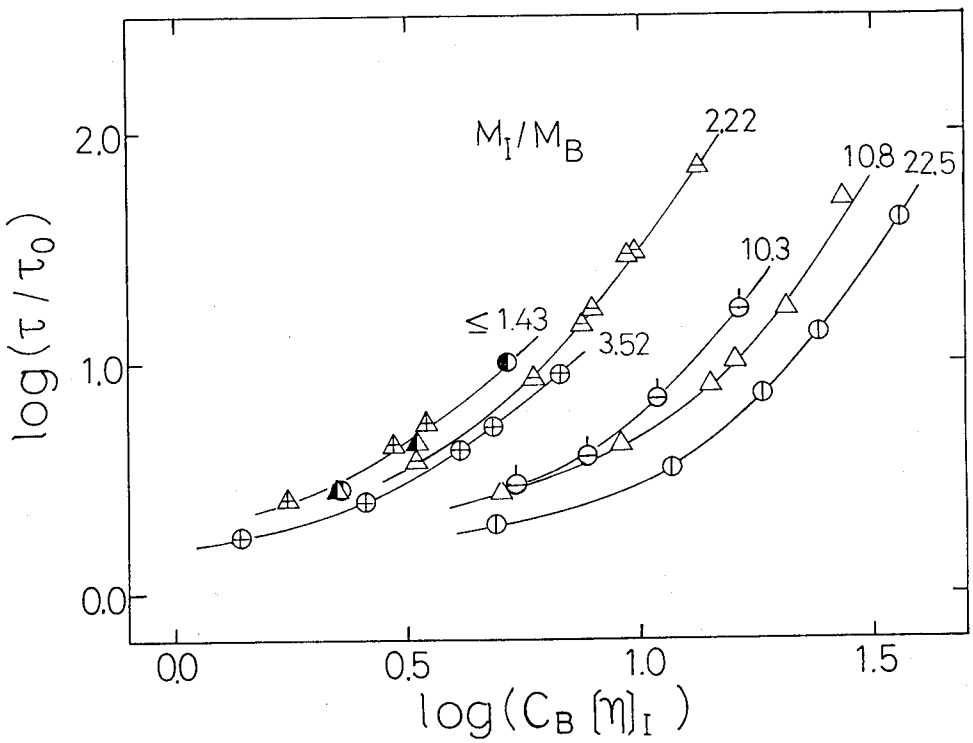

Figure V-23. Double-logarithmic plots of τ/τ_0 vs. $C_B[\eta]_B$. The symbols are the same as in Figure V-19.

Nemoto *et al.*[29] showed that the sedimentation coefficient S of PMMA in high MW PS solutions was expressed as

$$S / S(0.1M_e(\mathrm{PS})) \approx H(M / M_e(\mathrm{PS})) \qquad \text{(V-22)}$$

where $S(0.1M_e(\mathrm{PS}))$ indicates the sedimentation coefficient of PMMA with MW equal to $0.1M_e(\mathrm{PS})$ and H is a function. We see that this equation has the same functional form as eq (V-20) because $S(0.1M_e(\mathrm{PS}))$ and $M/M_e(\mathrm{PS})$ correspond to τ_{blob} and N_I/g_B, respectively.

To summarize, eqs V-18 and V-21 are valid for the cases $M_I/M_B > 3.52$ and $M_I/M_B < 1.43$, respectively. The data of τ for PI-140/PB-63 system (M_I/M_B = 2.22) are expressed by neither eq. V-18 nor eq. V-21. In this case the motion of PI chains is in the crossover region between the Zimm-like and reptation regimes, which are discussed in the following sections. The existence of the Zimm-like regime in condensed systems was reported by measurements of diffusion coefficients.[21,30,31]

V-4-4. General Representation of τ for Ternary Systems

In this section we attempt to express τ more generally including the case of $M_I \cong M_B$. In the previous section we indicated that τ is expressed by a universal function of $C_B[\eta]_B$ and $C_B[\eta]_I$. In the ternary system examined here, τ should be a function of N_I, N_B and C_B. If the elementary process of the dynamics is the motion of the blobs, τ may be scaled by a form

$$\begin{aligned} \tau &\cong \tau_{blob} \Psi'(N_I/g_B,\ N_B/g_B) \\ &\cong \tau_0\ \Psi(C_B[\eta]_I,\ C_B[\eta]_B) \end{aligned} \qquad \text{(V-23)}$$

where Ψ and Ψ' represent functions. If this equation holds, the observed data points of τ for various M_I, M_B, and C_B should fall on a smooth universal surface in the three dimensional space of τ vs. $C_B[\eta]_I$ vs. $C_B[\eta]_B$. Figure V-24 shows a

contour diagram in which the iso-τ/τ_0 lines are plotted on the plane of $C_B[\eta]_I$ vs. $C_B[\eta]_B$. The plotted points on the figure represent the interpolated values. We see that the contour line is smooth and monotonous over wide ranges of M_I, M_B, and C_B. This fact indicates that eq V-23 holds at least in the C_B range examined here.

$C_B[\eta]_I$ Dependence of τ

Figure V-25 shows the cross-sectional view of Figure V-24 at $C_B[\eta]_B$ = constant. Here we recall that the parameters of $C_B[\eta]_I$ and $C_B[\eta]_B$ correspond to the number of blobs in the PI chain and that in the PB chain, respectively: $C_B[\eta]_I \propto (N_I/g_B)^{3\nu-1}$ and $C_B[\eta]_B \propto (N_B/g_B)^{3\nu-1}$. The number of blobs corresponds to either the number of beads in the bead-spring model or the number of entanglement of the tube model depending whether the test chain is entangled with the matrix chains. Thus, Figure V-25 is equivalent to the M_I dependence of τ/τ_0 at fixed M_B. The N_I/g_B dependence of τ is generally expressed as

$$\tau \propto \tau_{blob}(N_I/g_B)^x \qquad \text{(V-24)}$$

where $x = 3\nu$, 2, and 3, for the Zimm, Rouse and tube theories, respectively. Here we neglected the difference of front factors of eq. V-24 for these theories. Then the $C_B[\eta]_I$ dependence of τ/τ_0 is given by

$$\tau/\tau_0 \propto (C_B[\eta]_I)^{(x-3\nu)/(3\nu-1)} \qquad \text{(V-25)}$$

where we have used the relation $\tau_{blob} \propto \xi^3$ (eq. V-11). With $\nu = 0.55$ determined in the previous section, the slopes of the $\log(\tau/\tau_0)$ vs. $\log(C_B[\eta]_I)$ plot for $x = 3\nu$, 2, and 3 were calculated and indicated in Figure V-25 with the notations of Zimm, Rouse, and Reptation, respectively.

When $\log(C_B[\eta]_B)=0.3$, the matrix PB chains are not entangled. In this case the slope in the range of $\log(C_B[\eta]_I) < 0.7$ agrees with the Rouse theory, but in the higher $C_B[\eta]_I$ range the slope becomes zero, corresponding to the Zimm theory.

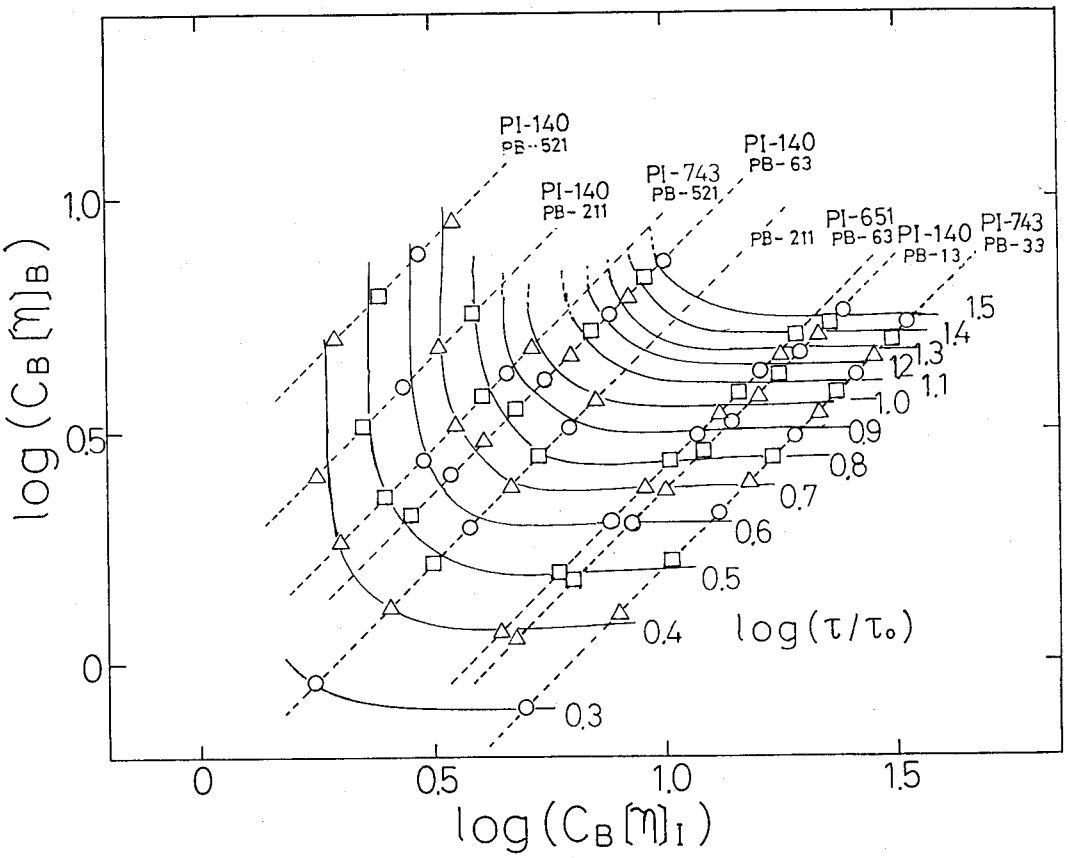

Figure V-24. Iso-τ/τ_0 lines on the plane of $C_B[\eta]_B$ vs. $C_B[\eta]_I$.

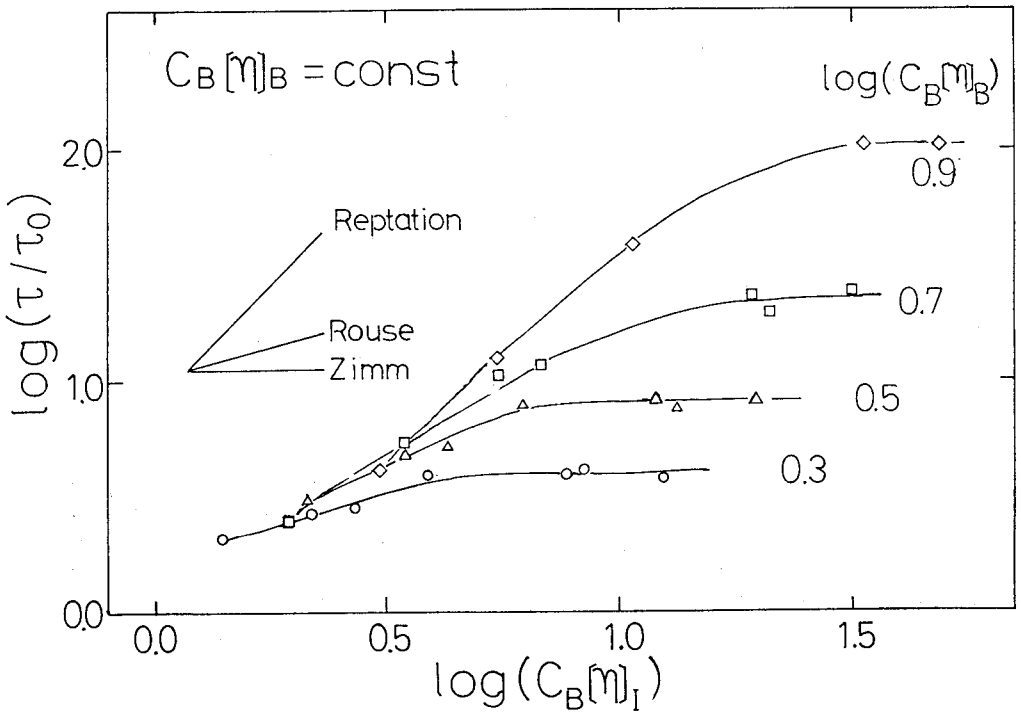

Figure V-25. Double-logarithmic plots of τ/τ_0 against $C_B[\eta]_I$ at constant $C_B[\eta]_B$.

Obviously the slope must become zero at sufficiently low C_B. Thus there exist two regimes in which τ conforms to the Zimm theory. The regime where the slope agreed with the Rouse model is considered to appear as a result of the transition between two Zimm-like regimes where chains are in pure solvent and polymeric viscous media.

In the case of $\log(C_B[\eta]_B)=0.9$ where the matrix PB chains are entangled, the slope in the range of $0.5 < \log(C_B[\eta]_I) < 1.0$ is close to that for the reptation model. However, with increasing $C_B[\eta]_I$ the slope decreases and appears to flat. These facts indicate that if the dilute guest chain is much longer than the matrix chain, it behaves like a Zimm chain whatever the matrix is entangled or not.[21]

$C_B[\eta]_B$ Dependence of τ/τ_0

Figure V-26 shows the cross sectional view of Figure V-24 at $\log(C_B[\eta]_I)$=constant, namely the M_B dependence of τ/τ_0 at fixed M_I. The data of matrix viscosity η_B/η_s are compared with the τ/τ_0 data in this figure. With increasing $C_B[\eta]_B$ the matrix viscosity increases exponentially but τ/τ_0 becomes independent of $C_B[\eta]_B$ eventually. In this high $C_B[\eta]_B$ region the PB chains form a temporary network and the PI chain moves by the reptation mechanism irrespective of the macroscopic matrix viscosity. But in low $C_B[\eta]_B$ the τ/τ_0 of PI becomes proportional to the matrix viscosity.

V-4-5 M_I Dependence of τ

In this section we discuss the M_I dependence of τ at fixed C_B and M_B specifically at $C_B = 4.84\times10^{-2}$ gcm^{-3} and $M_B = 3.3\times10^4$. From the C_B dependence of η_B/η_s shown in Figure V-20a, we see that the PB chains are not entangled in this conditions. Figure V-27 compares the M_W dependence of τ of the PI molecules dissolved in heptane and that in a PB/heptane semidilute solution. The plot for dilute heptane solutions is linear with slope 1.68. This behavior can be explained by the modified Zimm theory (eq. V-13) in which the excluded-volume effect is taken into account ($\nu = 0.55$). The slope for the ternary systems in high M_I region

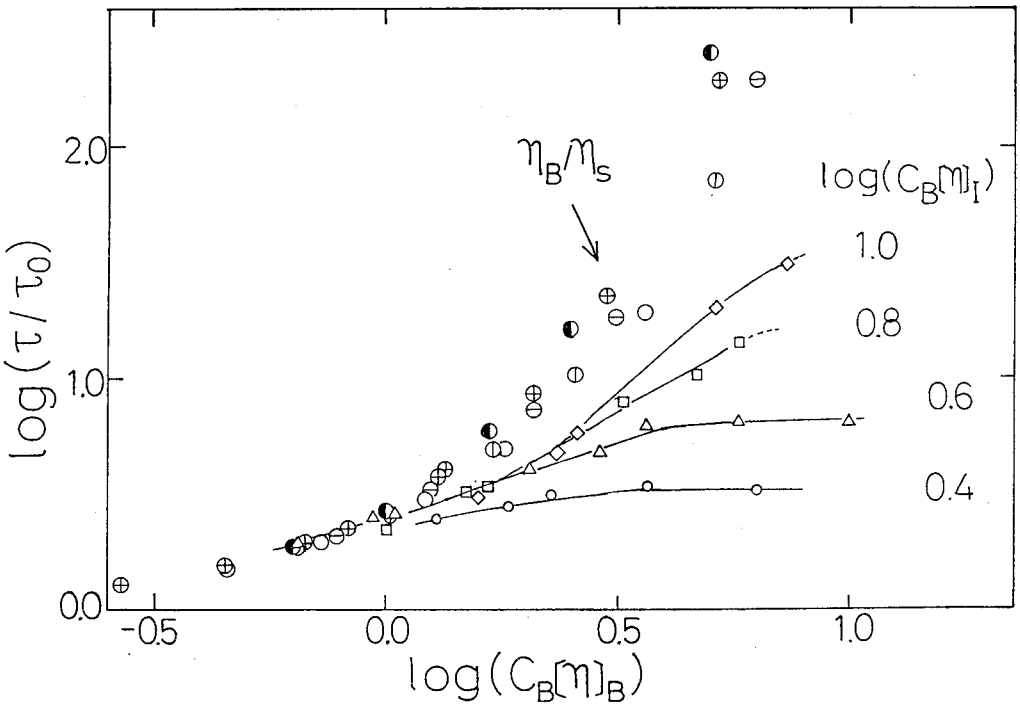

Figure V-26. Double logarithmic plot of τ/τ_0 against $C_B[\eta]_B$ at $C_B[\eta]_I$ = constant. For comparison, log η_B/η_s is also plotted.

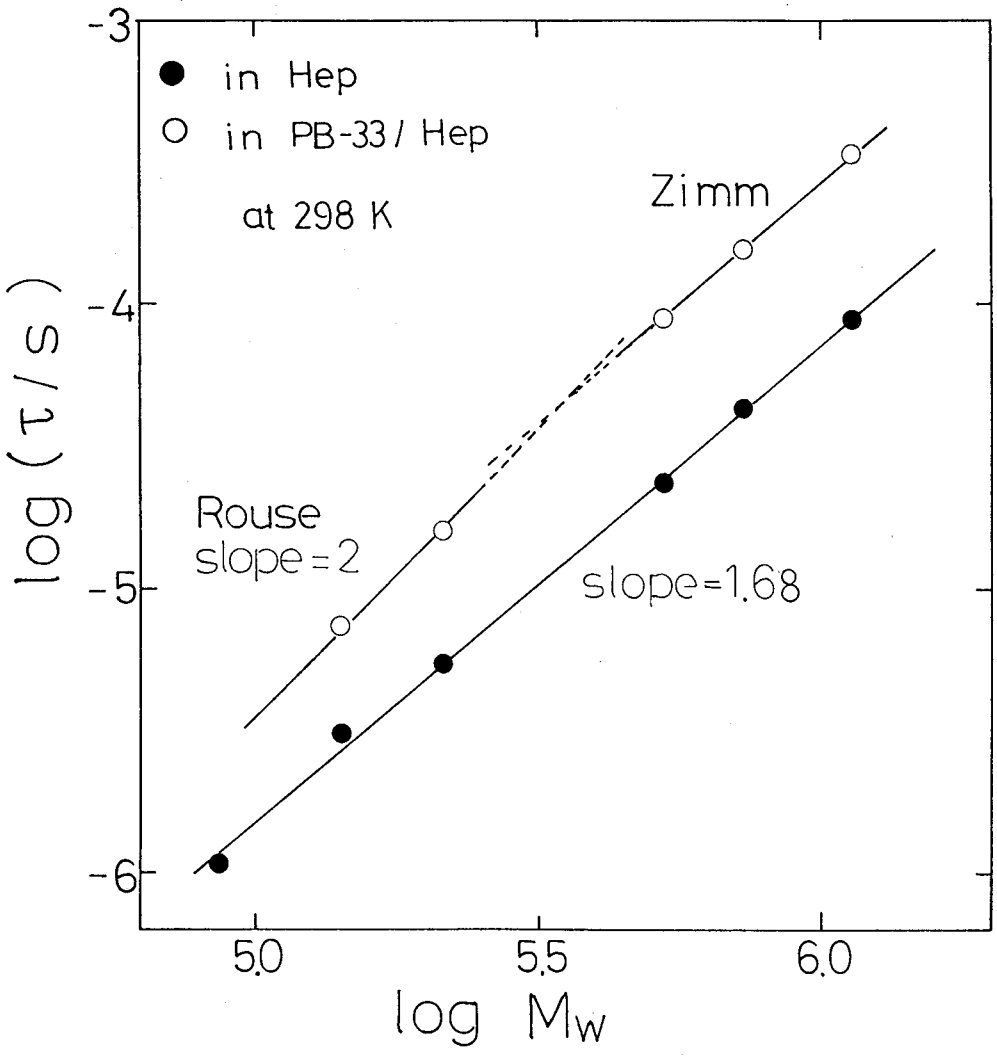

Figure V-27. Double-logarithmic plot of τ vs. M_I for binary solutions of PI/heptane (filled circles) and that for PI dissolved in a PB-33/heptane solution of C_B=4.84×10^{-2} gcm^{-3} (open circles).

is the same as that for the binary systems. However in the low M_I region, the slope is about 2 as predicted by the Rouse theory (eq. V-2). These findings may be interpreted as follows: when M_I is much higher than M_B, the PI chain behaves like a Zimm chain, but when M_I is comparable to M_B, the hydrodynamic interaction is screened and the PI chain behaves like a Rouse chain.

Figure V-28 shows the double logarithmic plot of τ/τ_0 vs. M_I. This figure corresponds to Figure V-25. The value of (η_B/η_s) $(<r^2>/<r_0^2>)^{3/2}$ are indicated in this figure to check eq. V-15. As seen in the figure, these value are seen to be larger than the relaxation time of PI.

V-4-6. Classification of the Motion of PI Chain

Here we classify the dynamical states in the ternary system studied in this section. The crossover points between the regimes in which the behavior of τ conforms to the Zimm, Rouse, and the tube theories are determined by using Figures V-25 and 26 and plotted on the log $C_B[\eta]_I$ vs. log $C_B[\eta]_B$ plane (Figure V-29). The concentration at which PB chains begin to entangle each other (dashed line in Fig. V-29) is roughly estimated from the curves shown in Figure V-20(b). The crossover is given by log $C_B[\eta]_B \cong 0.4$; above which the slope of the plot in Figure V-20(b) becomes $3.5/(3\nu\text{-}1)$. For $C_B[\eta]_I$ smaller than unity, the dimension of the PI chain is smaller than the screening length of PB solutions. Thus the PI chain may behave like a Zimm chain. When $C_B[\eta]_I >> C_B[\eta]_B$ the PI chain moves like a Zimm chain, but in the opposite case of $C_B[\eta]_I << C_B[\eta]_B$, it moves by the reptation mechanism.

V-4-7. Shape of ε'' Curves

In section V-3 we demonstrated that the shapes of ε'' curves for PI (binary) solutions change with the concentration (see Fig. V-15). For ternary solutions the C_B dependence of the shape of ε'' curves is shown in Figure V-30 (a) and (b). We see that the shape in PI-743/PB-521 (b) changes with C_B but that of PI-743/PB-211 (a) does not in the similar C_B range.

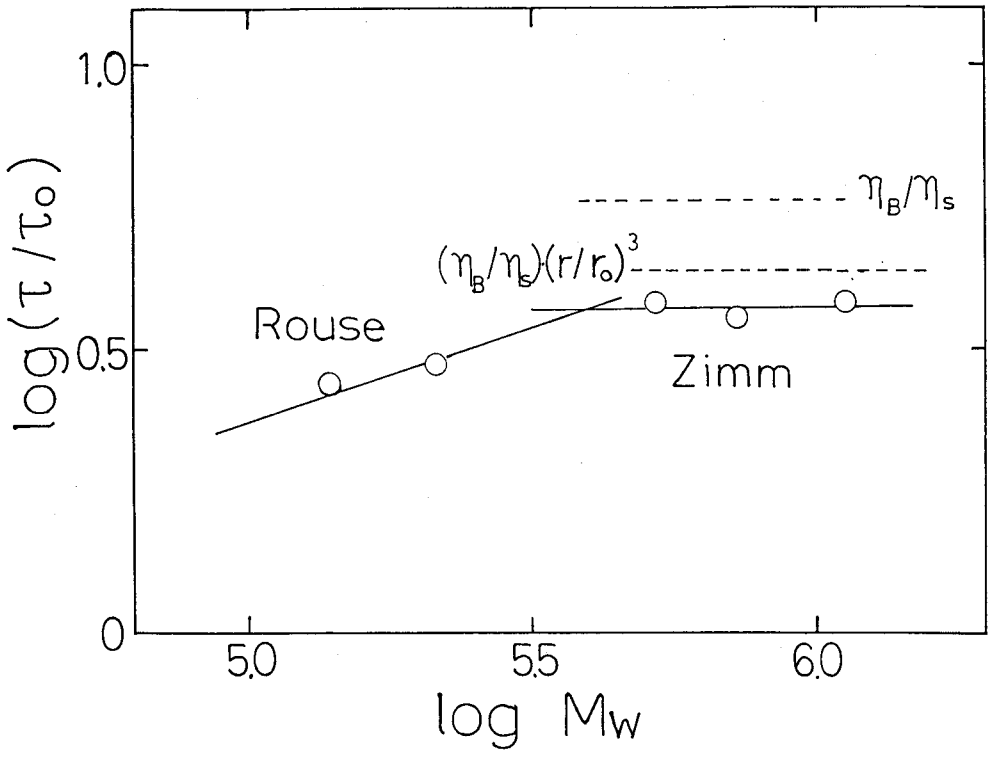

Figure V-28. Double logarithmic plot of τ/τ_0 for PI dissolved in a PB-33/heptane solution of C_B=4.83×10^{-3}gcm^{-3}. The values of η_B/η_s and $(\eta_B/\eta_s)(<r^2>/<r_0^2>)^{3/2}$ are indicated for comparison.

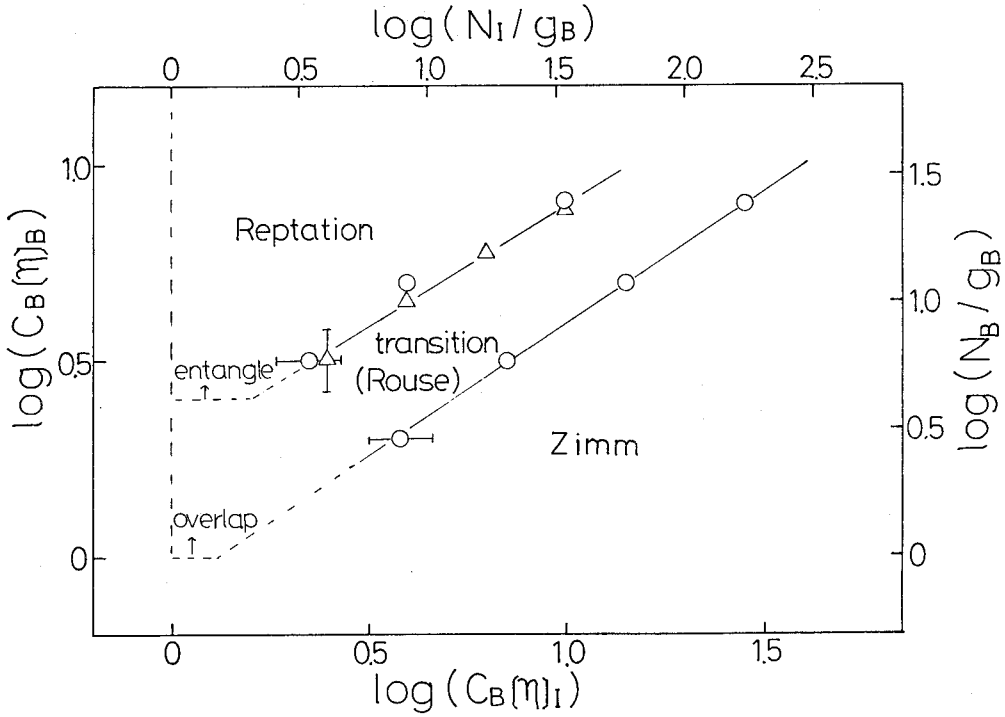

Figure V-29. Dynamic state diagram indicating the crossover points between the regimes in which the dynamics of PI chains in semidilute PB solutions is described by the Zimm theory and the tube theory. The intermediate region is assigned to the transition regime.

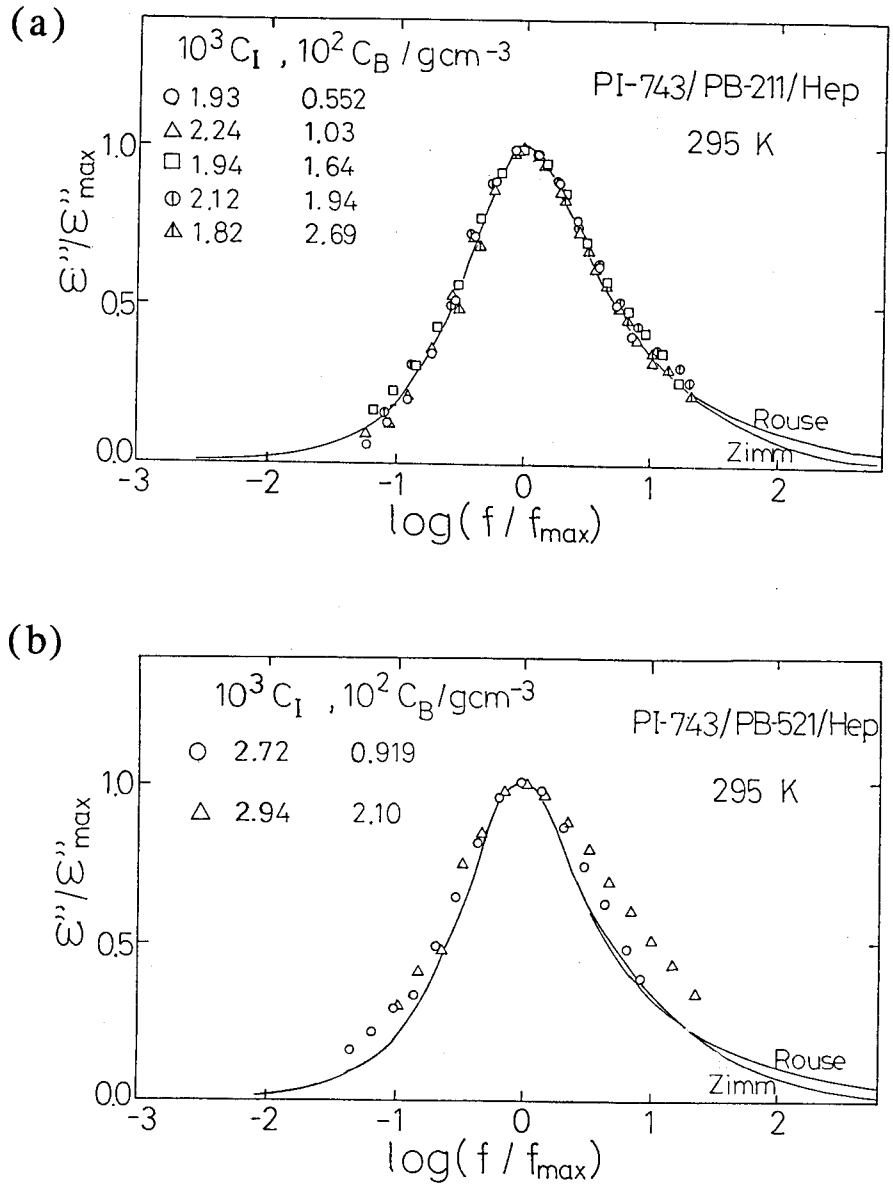

Figure V-30. Normalized ε'' curves for (a) PI-743/PB-211/heptane, (b) PI-743/PB-521/heptane.

In the previous section we have classified the PI chain motion by using two parameters $C_B[\eta]_I$ and $C_B[\eta]_B$. This sets of two parameters (log $C_B[\eta]_I$, log $C_B[\eta]_B$) for the PI-743/PB-211 system in Figure V-30(a) changes from (0.14, -0.15) to (0.83, 0.53) but that for the PI-743/PB-521 system in Figure V-30(b) from (0.36, 0.31) to (0.72, 0.67). By plotting these coordinates on the plane of Fig. V-29, we see that the former system is in the Zimm and transition region, but the latter system in the region where the entanglement starts. Thus the change in the relaxation spectrum occurs at the transition regime. For the binary systems we observed that the broadening of ε'' started at $C \cong C^*$ and completed at $C \cong C_e$. The regime of $C^* < C < C_e$ corresponds to the transition regime of polymer chain dynamics from the Zimm-like behavior to the reptation mechanism. Thus, the observed change of the relaxation spectrum in ternary system is consistent with that in the binary system.

V-5. Dynamics of Polymers in Condensed Systems

V-5-1. Dielectric Relaxation of Dilute Polyisoprene in Undiluted Polybutadiene Matrices

In the above section, we examined the C dependence of the shape of the ε'' curves. In order to understand the broadening phenomenon from another aspect, the dielectric behavior of blends consisting of a trace amount of PI and undiluted polybutadiene (PB) was also examined. We expect that if the MW of matrix PB is sufficiently low, the dynamics of PI will correspond to that in dilute solution examined in section V-2. But in the case of PB having an MW comparable to that of PI, it will be equivalent to that in concentrated solution. Our interest is to detect at what MW of PB such a transition occurs.

We investigated the dielectric normal mode process for two series of systems: (a) and (b). The series (a) is composed of PI-49 (5wt%) in various PBs with M_w from 7.1×10^2 to 8.9×10^4, covering the non-entangled to entangled regime; the

characteristic MW of PB (M_C^B) reported by Colby *et al.*[32] is 6.38×10^3. Another series (b) is all non-entangled systems which are blends of 10wt% PI-6 dissolved in PB-0.7 or PB-6. By using $[\eta]$ data in dioxane (θ condition)[33], we roughly estimated the $C[\eta]$ to be 1.3 for PI-49(5wt%)/PB systems and 0.9 for PI-6(10wt%) /PB systems. Since in section V-3 we showed that the broadening of ε'' curves began at $C[\eta] \cong 1\sim2$, the systems can be regarded as dilute solutions in PB.

In Figure V-31(a) and (b), the master curves of ε'' at 40°C for PI-49/PB and PI-6/PB systems are shown. Here it is reminded that PI possesses both the type-A and B dipole components. In undiluted high MW PI, the ε'' peaks due to these components were observed in well separated frequency ranges.[34] In the present system, the observed loss peaks are attributed to the normal mode process. In Fig. V-31 (b) we see the contribution of the segmental mode of PI and PB in the high frequency range. For the comparison of the shapes of ε'' curves of low MW PI it must be necessary to take into account the high frequency dispersion contribution.

The reference temperature T_r was 40°C and ε'' data from 80 to -30°C were superposed. In this temperature range the time-temperature superposition worked well. Figure V-32 shows the temperature dependence of the shift factor a_T (for T_r = 313 K). Colby *et al.*[32] reported that a_T for the viscoelastic data of bulk PB conformed well to the WLF equation. Our data come very close to theirs shown by a solid line in the figure, indicating that for our PI/PB blends the phase separation did not occur in this temperature and MW range. The a_T value for PI/PB-0.7 at the lowest temperature deviates to the downwards slightly from the line. This indicates that the reference temperature of this blend changes with MW of PB. However, no correction to the iso-free-volume state was made since a_T data over a wide range of temperature are unavailable.

V-5-2. Comparison of the Shape of ε'' Curves for PI/PB Blend Systems

The comparison of the shapes of ε'' curves is shown in Figure V-33(a) for PI-49/PB blends and (b) for PI-6/PB blends. We see that the ε'' curve becomes

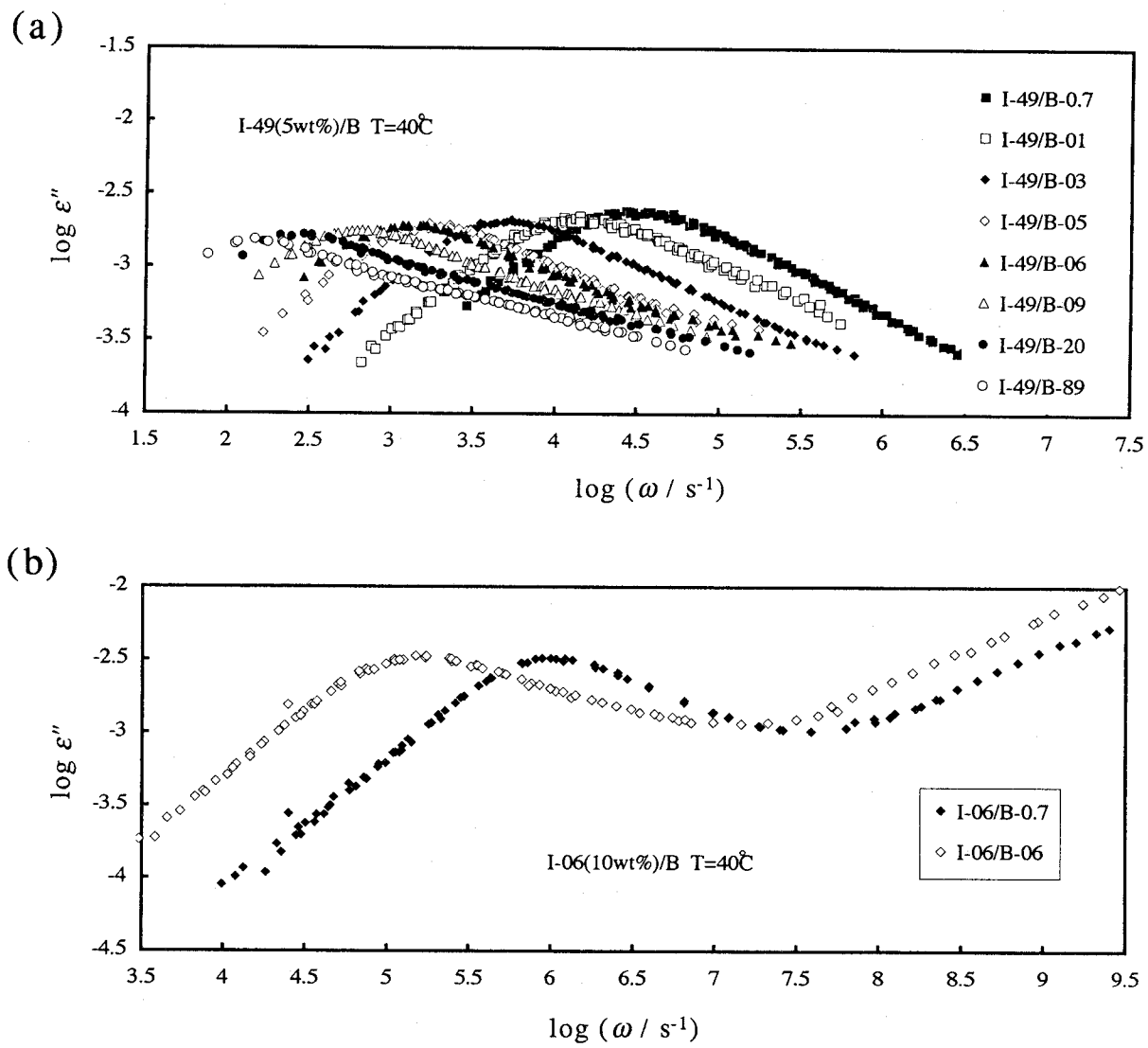

Figure V-31. Master curves of ε'' for blends of (a) PI-49(5wt%)/PB and (b) PI-6(10wt%)/PB at 40°C.

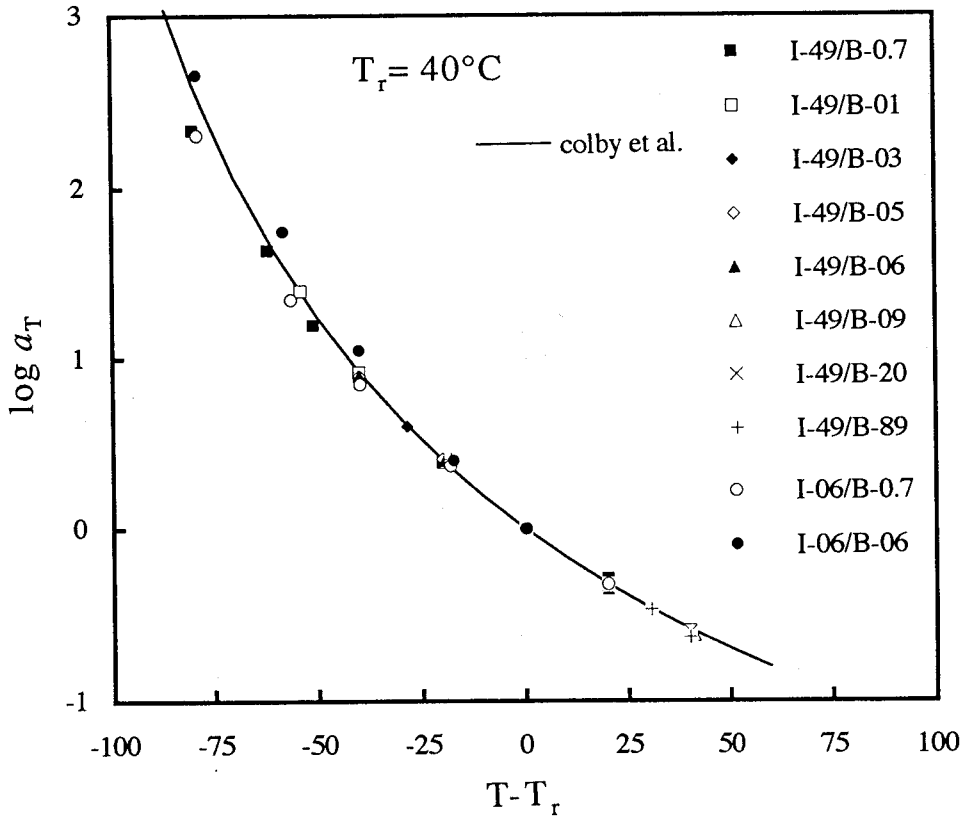

Figure V-32. Temperature dependence of the shift factor a_T for the PI/PB blends. The solid line represents the a_T determined from viscoelastic measurements for bulk PB by Colby *et al.*[32]

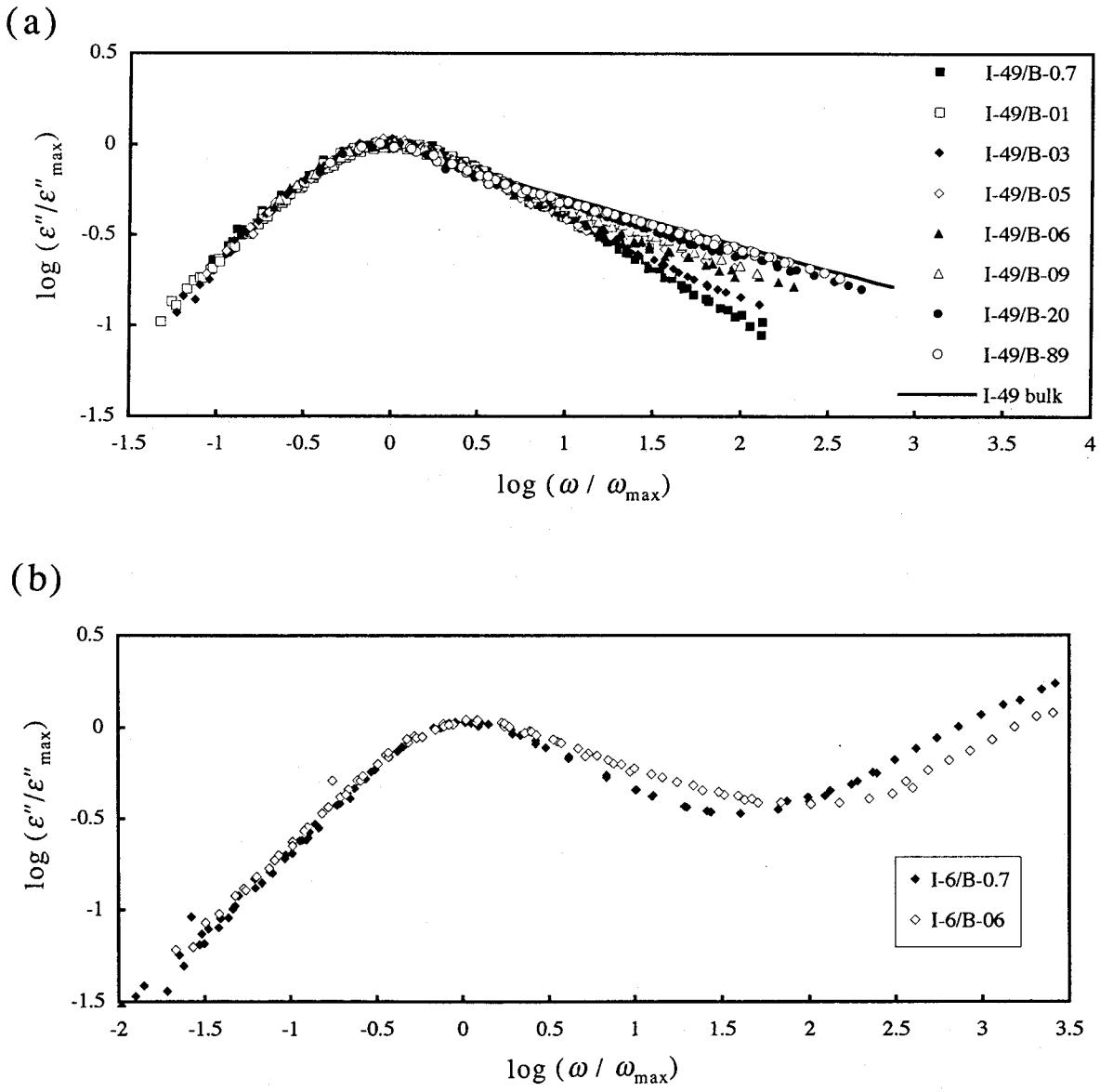

Figure V-33. Comparison of the shapes of ε'' curves for blends of (a) PI-49(5wt%)/PB and (b) PI-6(10wt%)/PB.

broader with increasing M_B as seen for PI solutions in section V-3. It is noted that for such non-entangled systems as shown in Figure V-33(b) similar behavior is also observed. The contribution of the segmental mode process in PB-0.7 system must be larger than that in PB-6 system, since the separation between the peak frequencies for the normal mode and segmental mode processes in the former is smaller than that in the latter. Thus without correction for subtracting the high frequency contribution we can conclude that the peak for the normal mode becomes narrower with decreasing MW of PB even in the non-entangled system and hence the broadening is not due to the entanglement effect. Another important point is that the excluded volume effect should be weak in such low MW PI-6. Thus we can also rule out the excluded volume effect from the origins of broadening In Figure V-33(a) we also showed the data of bulk PI-49. The shape of ε'' of blends converges to that of bulk system with increasing M_B.

Comparing with the behavior of PI solutions (see Fig. V-15 and V-16) we see that M_B affects the mode distribution as C does. The broadening of the ε'' curves for PI-49 starts at $M_B \cong 3\sim6$K.

V-5-3. Comparison of the Shape of ε'' Curves for Bulk Systems

Figure V-34 compares the shapes of ε'' curves for bulk PI of M_w=3.5×10^3, 9.49×10^3 and 20.7×10^3 which are the reported data of Yoshida et al.[35] The characteristic molecular weight M_C of PI was reported to be 10K [36] and hence PI-21 is entangled but PI-04 and PI-09 are not. The shape of the ε'' curve does not change with MW for $\log(\omega/\omega_{max})$ below 1.5. It is noted that the data of PI-4 contain the contribution of the segmental mode process in the high frequency regime. By subtracting the contribution from the normal mode dispersion curves, its shape may become slightly sharp. Imanishi *et al.* reported that if the contribution of the segmental mode is subtracted, the ε'' curve of the normal mode narrows with decreasing MW.[37] According to the Rouse and Zimm models, as the number of beads decreases, the theoretical ε'' curve becomes narrower than those

for the chains consisting of many beads. Due to this effect, it is difficult to discuss about the shape of ε'' for low MW PI in the bulk system. However if we ignore the slight effect of the segmental mode, we may conclude that the entanglement effect is not the direct origin of the change of ε'' curves. This conclusion agrees with the result obtained in the previous section.

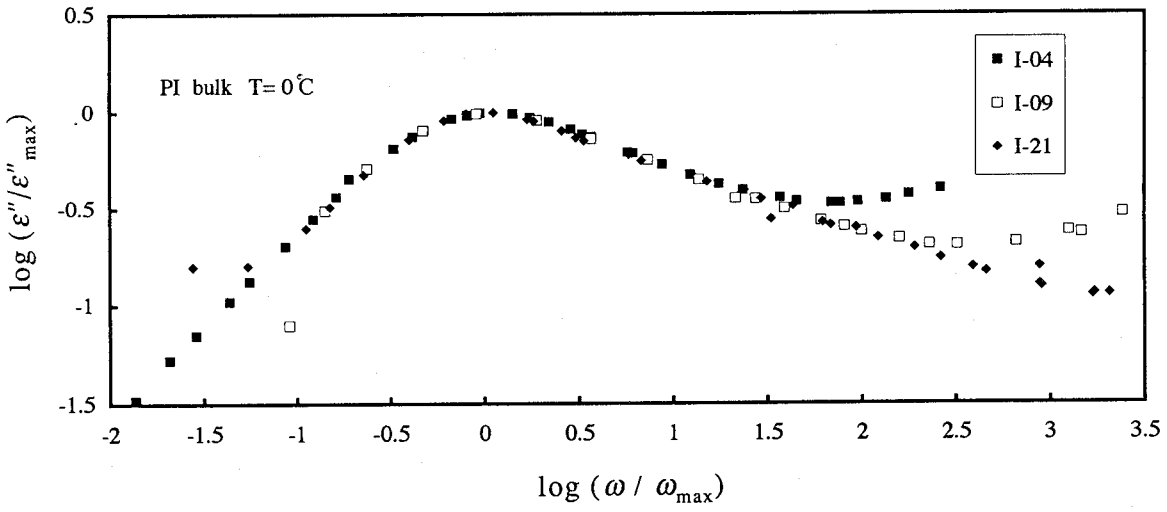

Figure V-34. Comparison of the shape of ε'' curves for bulk PI with M_w=3.5×10^3, 9.49×10^3 and 20.7×10^3 reported by Yoshida *et at.*[35]

V-6 Summary of the Results for the Shape of ε''

V-6-1. Relation between the Results of Bulk, Blend and Solution Systems

The behavior of the loss curves in various systems examined in the present experiments is summarized below.

In dilute solution systems the shape of the ε'' curve agreed well with the Zimm model as reported by Ferry *et al.*[1,14,15] for the viscoelastic behavior of PS solution. In semidilute solutions we observed that the ε'' curve broadens with increasing C. The onset of the broadening occurred in the C range below the entanglement concentration C_e that is defined as C above which the C dependence of τ conforms to the 3.5 power low (eq V-6).

In the PI/PB/heptane ternary solutions, the broadening is observed when the system is in the region of transition from the Zimm-like to the entangled regime.

In the PI/PB blend systems the onset of the broadening is observed at the critical value of MW of PB. Especially in the non-entangled systems of PI-06/PB blend, the broadening is also observed. From this result we conclude that neither entanglement nor excluded volume effect contributes to the broadening of the ε'' curve.

V-6-2. Discussion

In this section origins of the broadening of ε'' curves are discussed. We have already ruled out the entanglement effect and the excluded volume effect from the possible origins. Another possibility is the shielding effect of hydrodynamic interactions. In dilute solutions, it is concluded that the shape of ε'' (including G', G'') well conforms to the theoretical curves given by the Zimm model and the τ_1/τ_2 ratio is also close to the value predicted by the same model. Thus the hydrodynamic interactions are prevailing in dilute solutions.

In the semidilute regime where the hydrodynamic interaction is shielded and especially in the case that chains are not entangled yet, the shape of relaxation spectrum is expected to agree with the prediction by the Rouse model. Ferry *et al.*

reported that the viscoelastic spectrum for chlorinated diphenyl solutions of PS in the semidilute regime agreed with that of Rouse model. However, in the present study the ε'' curve in the range of $C^* < C < C_e$ was broader than the theoretical curve predicted by the Rouse theory, indicating that the change is not caused by the shielding effect of hydrodynamic interaction.

From the results mentioned above, we consider that the broadening of the ε'' curve occurs as a result of the restriction of the Rouse like motion by interactions with surrounding chains. For solution systems we have concluded that $C[\eta]$ is a major parameter affecting the change of spectrum. Since $C[\eta]$ represents the degree of chain overlapping, the restriction of the free motion can be described by this parameter. In addition, the result for the PI/PB blend system in which the ε'' broadens with increasing M_B supports our speculation because the increase in the MW of the matrix PB causes the restriction of a free motion of PI chains.

What kind of inter-molecular force causes the broadening? We speculate the restriction is caused by the viscoelasticity of the matrix medium. When the medium is a simple viscous fluid a chain in such a solution is only damped by the viscosity and behaves as a Zimm like chain. In the case that the matrix is composed of polymer chains exhibiting viscoelasticity, the motion of the probe chain will be restricted by the elastic force due to the matrix molecules. The elasticity of media may occur not only by the topological interactions but by the thermodynamic osmotic pressure to minimize concentration fluctuation. In fact Yao et al.[38] reported a broad ε'' curve for styrene-isoprene block copolymers in which the normal modes of the PI block are heavily restricted by both topological interactions and thermodynamic osmotic pressure. We expect that the elastic force between the test chain and medium is the origin of the broadening of the ε'' curve. A theoretical approach based on this picture is described in Chapter VI.

References and Notes.

1. Ferry, J. D. "Viscoelastic Properties of Polymers", 3rd ed.; Wiley: New York, 1980.
2. Zimm, B. H. *J. Chem. Phys.* **1956**, *24*, 269.; Zimm, B. H.; Roe, G. L.;Epstein, L. F. *J. Chem. Phys.* **1956**, *24*, 279.
3. Rouse, P. E. *J. Chem. Phys.* 1953, 21, 1272.
4. Doi, M.; Edwards, S. F. "The Theory of Polymer Dynamics" Clarendon: Oxford, 1986.
5. Klein, J. *Macromolecules*, **1978**, *11*, 852.
6. Graessley, W. W. *Adv. Polym. Sci.* **1982**, *47*, 67.
7. Watanabe, H.; Tirrel, M. *Macromolecules*, **1989**, *22*, 927.
8. Adachi, K.; Fukui, F.; Yoshida, H.; Kotaka, T. *Macromolecules*, **1990**, *23*, 3138.
9. Watanabe, H.; Yamazaki, M.; Yoshida, H.; Kotaka, T. *Macromolecules*, **1991**, *24*, 5573.
10. de Gennes, P. G., Scaling Concept in Polymer Physics. (Cornell University Press, Ithaca N.Y.), **1979**.
11. Jones, A. A.; Stockmayer, W. H.; Molinari, R. J. *J. Polym. Sci. Polym. Symp.* **1976**, *54*, 227.
12. Muthukumar, M.; Freed, K. F. *Macromolecules* **1978**, 11, 843.
13. Muthukumar, M. *Macromolecules* **1984**, 17, 971.
14. Holmes, L. A.; Ferry, J. D. *J. Polymer Sci.*, **1968**, *C23*, 291.
15. Holmes, L. A.; Kusamizu, S.; Osaki, K. Ferry, J. D. *J. Polymer Sci. Part A-2*, **1971**, *9*, 2009.
16. Yamamoto, M.; Tanaka, H. *J. Macromol. Sci.*, **1967**, *B1*, 199.
17. Takahashi, Y.; Isono, Y.; Noda, I.; Nagasawa, M. *Macromolecules* **1985**, *18*, 1002.
18. de Gennes, P.-G. *J. Chem. Phys.* **1971**, *55*, 572.
19. Doi, M.; Edwards, S. F. *J. Chem. Soc., Faraday Trans. 2* **1978**, *74*, 1789.
20. de Gennes, P.-G. *J. Macromolecules.* **1976**, *9*, 587.
21. Numasawa, N.; Kuwamoto, K.; Nose, T. **1986**, *19*, 2593.
22. Osaki, K.; Nishimura, Y.; Kurata, M. *Macromolecules* **1985**, *18*, 1153.
23. Adam, M.; Delsanti, M. *J. Phys.* (*Paris*) **1982**, *43*, 549.
24. Adam, M.; Delsanti, M. *J. Phys.* (*Paris*) **1983**, *44*, 1185.
25. Jamieson, A. M.; Telford, D. *Macromolecules* **1982**, *15*, 1329.
26. Adam, M.; Delsanti, M. *J. Phys.* (*Paris*) **1984**, *45*, 1513.
27. Roy-Chowdhury, P.; Deuskar, V. D. *J. Appl. Polym. Sci.* **1986**, *31*, 145.

28. Colby, R. H.; Rubinstein, M.; *Macromolecules* **1990**, *23*, 2753.
29. Nemoto, N.; Okada, T.; Kurata, M. *Macromolecules* **1988**, *21*, 1502.
30. Antonietti, M.; Coutandin, J.; Sillescu, H. *Macromolecules* **1986**, *19*, 793.
31. Green, P. F.; Kramer, E. J. *Macromolecules* **1986**, *19*, 1108.
32. Colby, R. H.; Fetters, L. J.; Graessley, W. W. *Macromolecules* **1987**, *20*, 2226.
33. Tunashima, Y.; Hirata, N.; Nemoto, N.; Kurata, M. *Macromolecules* **1988**, *21*, 1107
34. Adachi, K.; Imanishi, Y.; Kotaka, T. *J. Chem. Soc., Faraday Trans. 1*, **1989**, *85* (5), 1065, 1075, 1083.
35. Yoshida, H.; Adachi, K.; Watanabe, H.; Kotaka, T. *Polym. J.*, **1989**, *21*, 863.
36. Gotro, J.; Graessley, W. W. *Macromolecules* **1984**, *17*, 2767.
37. Imanishi, Y.; Adachi, K.; Kotaka, T. *J. Chem. Phys.* **1988**, *89* (12), 7585.
38. Yao, M. L.; Watanabe, H.; Adachi, K; Kotaka, T. *Macromolecules* **1991**, *24*, 2955.

VI. Investigation of Polymer Chain Dynamics by Using Dipole-Inverted PI Chains

VI-1. Introduction

In the previous chapter we discussed the change of dielectric relaxation spectrum for the fluctuation of the end-to-end vector in various surroundings which cause changes of inter-chain interactions. However, for the origin of such a change, our understanding was based on the speculations. For investigation of details of the chain dynamics, it is most efficient to use some labeling techniques and examine various dynamic quantities for a particular segment and/or a chain involved in the system. *Dielectric labeling* can be attained for a special sort of chains possessing type-A dipoles inverted once at a particular point in the chain contour[1-4] (cf., Figure VI-1). The dielectric relaxation process of those chains reflects fluctuation of a vector $\Delta \boldsymbol{r} = \boldsymbol{r}_1 - \boldsymbol{r}_2$, with $\boldsymbol{r}_1$ and $\boldsymbol{r}_2$ being the vectors that connect the dipole-inversion point and the two chain-ends. Namely, the chains having differently located dipole-inversion points should exhibit different relaxation processes even if the molecular motion itself is the same. In this sense, the dipole-inversion works as the dielectric labeling.

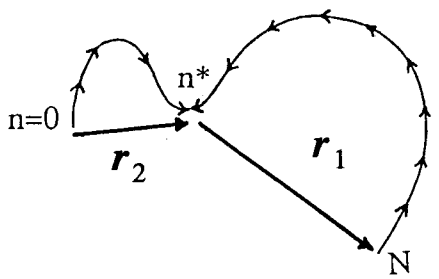

Figure VI-1. Schematic representation of a PI chain having asymmetrically inverted dipoles.

On the basis of the above ideas, we have anionically synthesized an unique series of linear *cis*-polyisoprene (PI) chains having almost the same M but dipole-inversion at different locations and examined their dielectric relaxation processes. Specifically, analyses for these processes enabled us to obtain an entirely new and interesting information on the eigenfunctions which describe the displacement of the backbone atoms for each mode.[4] In this chapter we describe the dielectric data for such dipole inverted PIs in the bulk and dilute solution systems, and the resulting information for the eigenfunctions.

VI-2. Theory of Dielectric Relaxation of Dipole-Inverted Chains

We here consider a linear Gaussian chain composed of N segments in which the type-A dipoles are inverted once at the n*th segment (Figure VI-1). We can extract some detailed information on the motion of this chain from its dielectric data, as explained below.

The total polarization of the dipole-inverted chain at a time t is proportional to a vector $\Delta \boldsymbol{r}(t) = \boldsymbol{r}_1(t) - \boldsymbol{r}_2(t)$, with $\boldsymbol{r}_1(t)$ and $\boldsymbol{r}_2(t)$ being the vectors connecting the n*th segment and the two chain-ends. Thus, its dielectric relaxation function $\Phi(t)$ normalized to unity at t = 0 is written in terms of $\Delta \boldsymbol{r}$ and the end-to-end vector $\boldsymbol{r}$ as[1-3]

$$\Phi(t) = \frac{<\Delta \boldsymbol{r}(t) \cdot \Delta \boldsymbol{r}(0)>}{<\Delta r^2>} \qquad \text{(VI-1)}$$

(Here, we have used a relation $<\Delta r^2> = <r^2>$ valid for a Gaussian chain.) The dielectric loss factor ε'' is written in terms of Φ as[5]

$$\varepsilon''(\omega) = -\Delta\varepsilon \int_0^\infty \frac{d\Phi(t)}{dt} \sin \omega t \, dt \qquad \text{(VI-2)}$$

Here, ω and $\Delta\varepsilon$ are the angular frequency and the dielectric relaxation intensity,

respectively.

As can be seen from eqs VI-1 and VI-2, the dielectric normal mode process of the dipole-inverted chain reflects fluctuation of $\Delta \boldsymbol{r}$. We here introduce a local correlation function[2,3,6]

$$C(n,t;\, m) = (1/b^2) \langle \boldsymbol{u}(n,t) \cdot \boldsymbol{u}(m,0) \rangle \qquad \text{(VI-3)}$$

with $\boldsymbol{u}(n,t)$ being a bond vector for the n-th segment at time t and $b^2 = \langle \boldsymbol{u}^2 \rangle$ (the mean-square segment size). This function represents an orientation correlation of n and m-th bond vectors at two separate times, so that it contains detailed information for the global chain motion. Assuming a very rapid orientation-randomization for two bond vectors at the chain-ends, we have a boundary condition for $C(n,t;m)$,

$$C(n,t;\, m) = 0 \quad \text{for } n,\ m = 0,\ N \qquad \text{(VI-4)}$$

For a Gaussian chain having no isochronal orientation-correlation for different bond vectors, we may write the initial condition as[2-4,7]

$$C(n,0;\, m) = \delta_{nm} = \frac{2}{N} \sum_{p=1}^{N} sin \frac{p\pi n}{N} \sin \frac{p\pi m}{N} \qquad \text{(VI-5)}$$

From eqs VI-1 and VI-3, the relaxation function Φ is related to the local correlation function as

$$\Phi(t;\, n^*) = \frac{1}{N} \left[\int_0^{n^*} dn - \int_{n^*}^{N} dn \right] \left[\int_0^{n^*} dm - \int_{n^*}^{N} dm \right] C(n,t;\, m) \qquad \text{(VI-6)}$$

This relation clearly indicates that Φ and thus ε'' (cf., eq VI-2) change with n^* even if the molecular motion described by $C(n,t;\, m)$ is the same. In other words, using

eq VI-6 to analyze the n^*-dependent ε'' data of the dipole-inverted PI chains, we can find features of $C(n,t;\, m)$, i.e., how the orientation-correlation of two particular bond vectors changes with time.

For convenience of the above analysis, we expand $C(n,t;\, m)$ at long time scales with respect to its *eigenfunctions* $f_p(n)$ with the mode number p = 1, 2,.., N. The functional form of $f_p(n)$ is determined by a time evolution equation for $C(n,t;\, m)$, i.e., by a nature of the global chain motion. As discussed in Appendix A, we may use f_p and generally write $C(n,t;\, m)$ in a form

$$C(n,t;\, m) = \frac{2}{N} \sum_{p=1}^{N} f_p(n)\, f_p(m) \exp(-t/\tau_p) \qquad \text{(VI-7)}$$

Here, τ_p is the p-*th* relaxation time being the reciprocal of the p-*th* eigenvalue. The f_p's involved in eq VI-7 satisfy a boundary condition (cf., eq VI-4)

$$f_p(0) = f_p(N) = 0 \qquad \text{(VI-8)}$$

and the normalization condition given by eq VI-5.

$$\frac{2}{N} \sum_{p=1}^{N} f_p(n)\, f_p(m) = \delta nm \qquad \text{(VI-9)}$$

From eqs VI-1, VI-2, VI-6, and VI-7, we find

$$\varepsilon''(\omega;\, n^*) = \sum_{p=1}^{N} g_p(n^*) \frac{\omega\tau_p}{1 + \omega^2\tau_p^2} \qquad \text{(VI-10)}$$

Here, g_p is the intensity of the p-*th* dielectric mode,

$$g_p(n^*) = \frac{2\Delta\varepsilon}{N^2} \left[\int_0^{n^*} f_p(n)\, dn - \int_{n^*}^{N} f_p(n)\, dn \right]^2 \qquad \text{(VI-11)}$$

Equation VI-11 indicates that the integral of the *p-th* eigenfunction f_p is evaluated from experimentally determined g_p. For convenience of this evaluation, we classify f_p in two categories: Two ends of a linear chain should move in an equivalent fashion, so that f_p should be either symmetrical ($f_p(n) = f_p(N-n)$) or anti-symmetrical ($f_p(n) = -f_p(N-n)$) with respect to the chain center ($n = N/2$). The symmetrical f_p are classified as odd f_p (with p = 1, 3,..), and the anti-symmetrical f_p, as even f_p (p = 2, 4,..). Then, as seen from eq VI-11, an integral of f_p defined by

$$F_p(n^*) = \frac{\sqrt{2}}{N} \int_0^{n^*} f_p(n)\, dn \qquad (= 0 \text{ for } n^* = 0) \qquad \text{(VI-12)}$$

is evaluated as

$$F_p(N/2) - F_p(n^*) = \pm [g_p(n^*)/4\Delta\varepsilon]^{1/2} \quad (= 0 \text{ for } n^* = N/2);\ p = odd \qquad \text{(VI-13a)}$$

and

$$F_p(n^*) = \pm [g_p(n^*)/4\Delta\varepsilon]^{1/2} \quad (= 0 \text{ for } n^* = 0);\ p = even \qquad \text{(VI-13b)}$$

When $g_p(n^*)$ is obtained for dipole-inverted PI chains with various n^* values = 0, n_1^*, n_2^*,..., $N/2$ increasing in this order, we can choose either $+[g_p/4\Delta\varepsilon]^{1/2}$ or $-[g_p/4\Delta\varepsilon]^{1/2}$ for $n^* = 0$ in eq VI-13a and for $n^* = n_1^*$ in eq VI-13b, because $f_p(n)$ and $-f_p(n)$ are equivalent eigenfunctions and thus either $F_p(n^*)$ or $-F_p(n^*)$ can be used as the integral. For definiteness, we choose $+[g_p/4\Delta\varepsilon]^{1/2}$ here. With this constraint, a requirement of smooth and continuous n^* dependence of $F_p(n^*)$ unequivocally determines the signs of the terms $[g_p(n^*)/4\Delta\varepsilon]^{1/2}$ in eq VI-13 for any other n^* values, if the intervals between the neighboring n^* values are sufficiently small. This was the case for the determination of $F_p(n^*)$ ($p = 1 \sim 3$) made here for

seven n^* values in a range $0 \leq n^* \leq N/2$ (cf., Table III). For $n^* > N/2$, eigenfunction symmetries lead to relations, $F_p(n^*) = -F_p(N-n^*) + 2F_p(N/2)$ for p = odd and $F_p(n^*) = F_p(N-n^*)$ for p = even. Thus, from g_p (p = 1 - 3) obtained for $0 \leq n^* \leq N/2$, we unequivocally evaluated $F_p(n^*)$ in an entire range $0 \leq n^* \leq N$ through eq VI-13.

VI-3. Dipole Inverted Chain in Bulk Systems

VI-3-1. ε'' Curves in Bulk Systems

Figure VI-2 shows the frequency (ω) dependence of ε'' at 40°C for PI chains with various locations of the dipole-inversion points.[8] The time-temperature superposition worked very well, and the ε'' data were reduced at T_r = 40°C. The shift factors a_T for the dipole-inverted PI chains were identical to those for regular PI chains without inversion, suggesting that the small coupler units involved in the former did not affect the chain motion. In the temperature range examined, the amount of the shift was less than one decade and ambiguities due to the shift were negligibly small.

Those PI chains having $M \cong 10Me$ ($Me \cong 5000$ for bulk PI[1,2]) are rather heavily entangled in their monodisperse bulk systems. In Figure VI-2, the respective ε'' curves are shifted vertically to avoid heavy overlapping of the data points. Details for differences of the curves are more clearly examined in Figure VI-3, where the data points are not shown and no vertical shifts are made.

As seen in Table III, the molecular weights are close but not exactly the same for the PI chains examined. Correspondingly, the longest relaxation time τ_1 for the local correlation function is slightly different for those PI chains. Throughout this section including Figures VI-2 and VI-3, we use the I-I 24-24 sample with M = 47.7×10^3 as a reference and shift the ε'' curve of each PI sample along the ω axis by a factor $a_M = (M/47.7 \times 10^3)^{3.5}$ to correct the difference of τ_1. Here $\tau_1 \propto M^{3.5}$ for monodisperse chains.[10] The log a_M values are summarized in Table VIII (a).

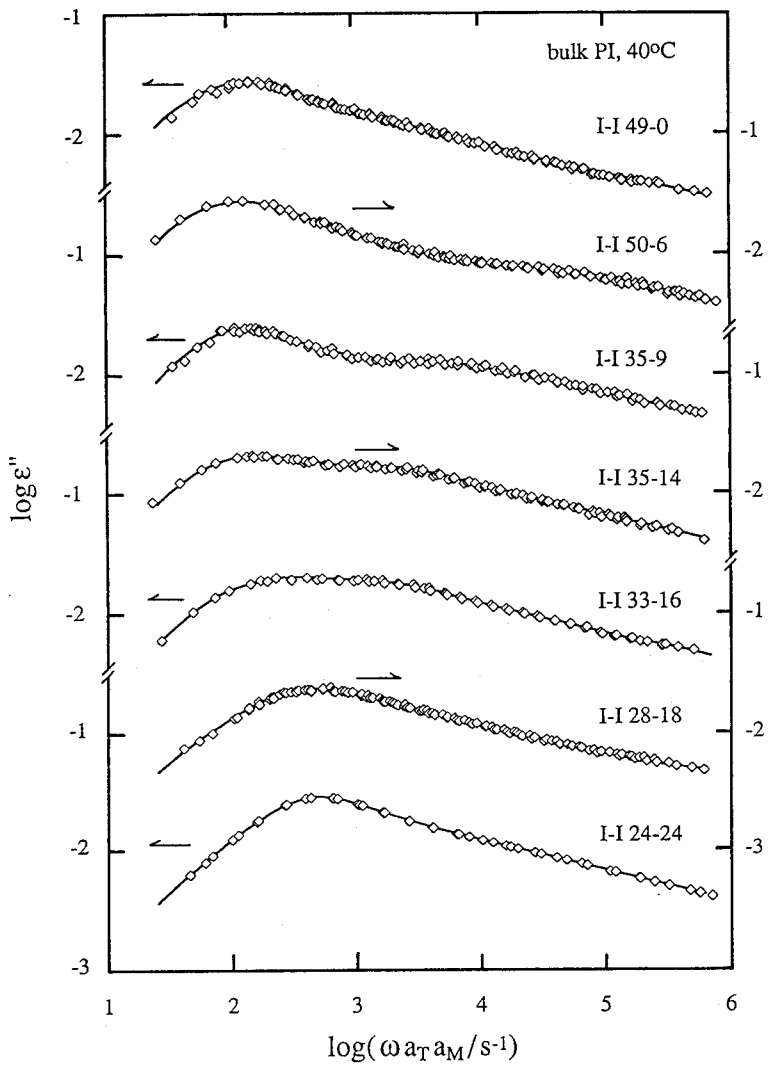

Figure VI-2 Frequency (ω) dependence of the dielectric loss factors ε'' at 40°C for dipole-inverted PI chains. Small differences of the longest relaxation times τ_1 of the PI chains are corrected by shifts of the ε'' curves along the ω axis by factors $a_M = (M/47.7 \times 10^3)^{3.5}$. (The I-I 24-24 chain with M = 47.7 x 10^3 was used as a reference for this shift.) Respective curves are further shifted vertically to avoid heavy overlapping of the data points.

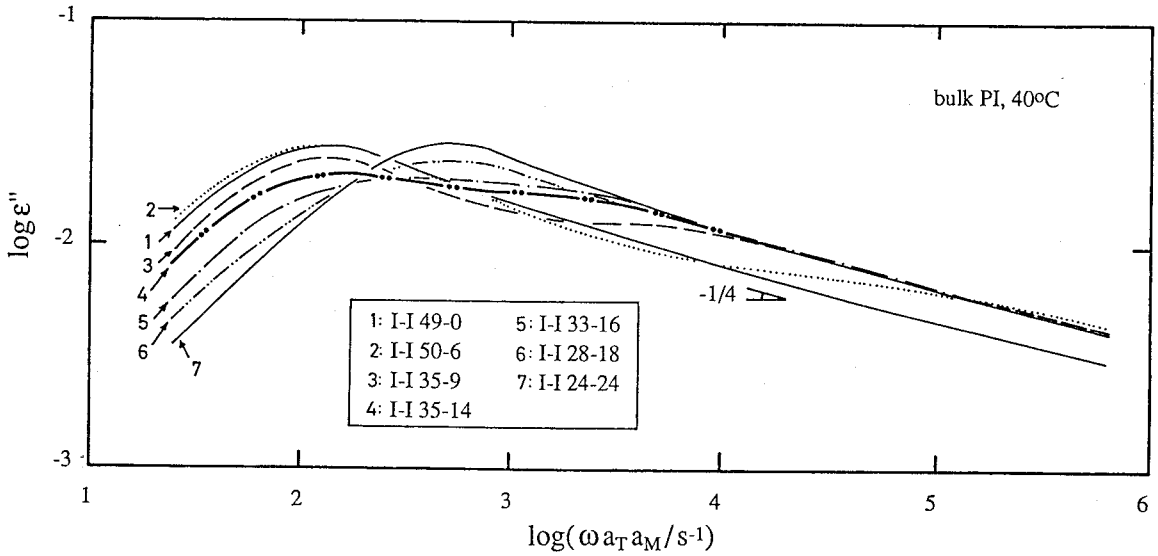

Figure VI-3 Comparison of the ε'' curves at 40°C for the dipole-inverted PI chains. Only the curves smoothly connecting the data points are shown, and no vertical shifts are made. As done in Figure VI-2, horizontal shifts by factors $a_M = (M/47.7\times10^3)^{3.5}$ are made to correct small differences of τ_1.

The small coupler units involved in the long PI chains should have no effect on the global motion. Thus, after the small correction for τ_1 (with $|\log a_M| \leq 0.1$ except for I-I 50-6 with $\log a_M \cong 0.2$), we can consider the motion of the PI chains to be exactly the same. Nevertheless, large differences of the ε'' curves are observed in Figures VI-2 and VI-3, because of the dielectric labeling due to dipole-inversion: As the dipole-inversion point moves from the chain end (I-I 49-0) to the center (I-I 24-24), the ε'' peak intensity decreases at $\log \omega \cong 2.1$ and increases at $\log \omega \cong 2.7$, and the shape of the ε'' curve first becomes broad and bimodal and then becomes narrow again. These changes correspond to those in the dielectric relaxation mode distribution, and provide us with information for the chain motion through eqs VI-10, VI-12, and VI-13.

Table VIII Correction Factors for Small Differences of the Longest Relaxation Times τ_1 for (a) bulk system and (b) I-I / PB-0.7 system.

Sample	$\log a_M$	
	(a) bulk	(b) I-I /PB-0.7
I-I 49-0	0.035	0.017
I-I 50-6	0.227	0.112
I-I 35-9	-0.109	-0.054
I-I 35-14	-0.003	-0.002
I-I 33-16	0.038	0.019
I-I 28-18	-0.010	-0.005
I-I 24-24	0	0

In Figure VI-4, the ε'' curve for I-I 49-0 (after the correction for τ_1) is shifted along the ω-axis by a factor $\Delta_M = 3.9$ and compared with the curve for I-I 24-24. The two curves are indistinguishable, meaning that the relaxation mode distribution is the same for the I-I 49-0 and 24-24 chains but the *dielectrically observed* relaxation time is 3.9 times shorter for the latter.[10,14] As seen from

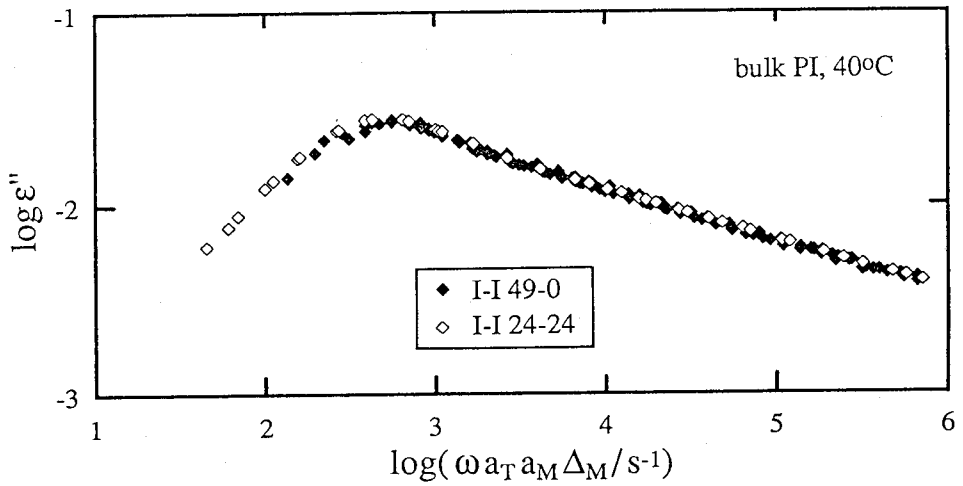

Figure VI-4 Comparison of the ε'' curves at 40°C for the I-I 49-0 and I-I 24-24 chains. The curve for the former is shifted along the ω-axis first by a factor $a_M = (48.8/47.7)^{3.5} = 1.083$ (a correction for difference of τ_1) and further by a factor $\Delta_M = 3.9$.

eq VI-13, only odd eigenmodes of the chain motion contribute to ε'' of the I-I 49-0 chain (with $n^* = 0$), while only even modes contribute to ε'' of the I-I 24-24 chain (with $n^* = N/2$). Thus, the sharp ε'' peaks for these PI chains correspond to the first and second modes with the relaxation times τ_1 and τ_2 (= $\tau_1/3.9$; cf., Figure VI-4). Specifically, the τ_1 and τ_2 values are evaluated from the peak frequencies as

$$\tau_1 = 8.13 \times 10^{-3} \text{ s}, \quad \tau_2 = 2.09 \times 10^{-3} \text{ s} \tag{VI-14}$$

VI-3-2. Experimental Determination of Eigenfunctions in Bulk Systems

For evaluation of the integrals F_p of the eigenfunctions f_p, we have to decompose the ε'' curves of the dipole-inverted PI chains into the contributions from the eigenmodes (cf., eqs VI-10, VI-12, and VI-13). Although we may do this with various methods, we here use a linear-least-square-fitting method that enables us to analyze the ε'' data with the highest accuracy attainable.

F_1 and F_2 are evaluated from the ε'' data at low ω where the contribution from all higher *p-th* modes with $p \geq 3$, $\Sigma_{p\geq 3}\, g_p(n^*)\, D_p(\omega)$ with $D_p(\omega) = \omega\tau_p/(1+\omega^2\tau_p^2)$ (cf., eq VI-10), is practically identical to its low-ω asymptote,

$$G_3\, \omega = \Big[\sum_{p\geq 3} g_p \tau_p \Big]\, \omega \tag{VI-15}.$$

At those low ω, eq VI-10 becomes a *linear* function of three variables g_1, g_2, and G_3, yielding

$$\varepsilon''(\omega; n^*) = g_1(n^*)\, D_1(\omega) + g_2(n^*)\, D_2(\omega) + G_3(n^*)\, \omega \tag{VI-16}$$

Note that the locations of the two single-relaxation functions $D_1(\omega)$ and $D_2(\omega)$ are determined by τ_1 and τ_2 given in eq VI-14. Thus, as explained in Appendix B, we made a standard linear-least-square-fit with eq VI-16 to determine g_1, g_2, and G_3.

Figure VI-5 demonstrates the results of the mode-decomposition. The

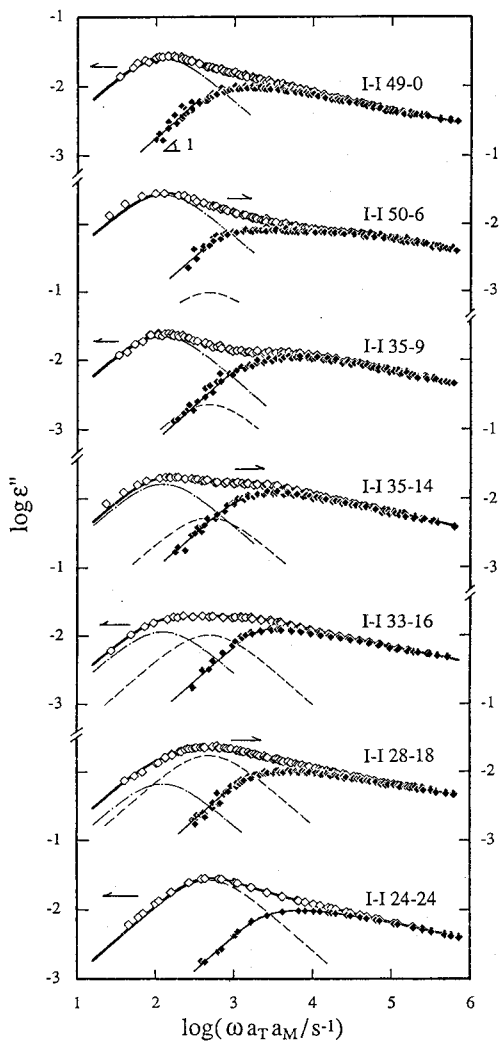

Figure VI-5. Results of the mode-decomposition of the ε'' data (unfilled symbols) for the dipole-inverted PI chains at 40°C. Linear-least-square-fit with eq VI-16 was made for the decomposition. The dash-dot and dashed curves indicate the contributions from the first and second eigenmodes $g_1D_1(\omega)$ and $g_2D_2(\omega)$, respectively. ($D_p(\omega) = \omega\tau_p/(1+ \omega^2\tau_p^2)$.) The contributions from all higher p-th eigenmodes with $p \geq 3$, $\varepsilon_{p\geq 3}''(\omega)$, is shown with the filled symbols. The thick solid curves indicate the re-calculated $\varepsilon'' = g_1D_1 + g_2D_2 + \varepsilon_{p\geq 3}''$, with $\varepsilon_{p\geq 3}''$ being evaluated for the thin solid curves that smoothly connect the filled symbols.

unfilled symbols indicate the ε'' data, and the dash-dot and dashed curves, the contributions from the first and second modes g_1D_1 and g_2D_2, respectively. The contribution from all higher *p-th* modes with $p \geq 3$, $\varepsilon''_{p\geq 3} = \varepsilon'' - g_1D_1 - g_2D_2$, is shown with the filled symbols. We see that the prerequisite of the fit, $\varepsilon''_{p\geq 3} \propto \omega$, is well satisfied at low ω. This result indicates that the mode-decomposition was well achieved and g_1 and g_2 were determined with little ambiguities. From these g_1 and g_2 together with the total relaxation intensity $\Delta\varepsilon$ determined by integration of ε'' curves with respect to $ln\ \omega$, we evaluated F_1 and F_2 through eq VI-13. As explained earlier, the requirement of smooth and continuous n^* dependence of F_1 and F_2 was successfully used in this evaluation. F_1 and F_2 monotonously increase with n^* for $0 \leq n^* \leq N/2$, as shown later in Figure VI-6.

It is desired to evaluate F_p also for higher modes ($p \geq 3$) from the linear-least-square-fit for the ε'' data. We can accurately do this *if we know the* τ_p *values for* $p \geq 3$ *and those values are sufficiently separated.* The τ_p values would be experimentally determined from ε'' peak frequencies for a special sort of PI chains with *multi-inversion* of dipoles, e.g., a PI chain with inversions at $n^* = N/3$ and $2N/3$ that would exhibit a peak corresponding to τ_3. However, such PI chains are not yet available. Thus, we *tentatively* estimated $\tau_3 = 1.1 \times 10^{-3}$ s from the ε'' data of the I-I 49-0 chain with a method explained in Appendix C. As did above, we used the τ_1 - τ_3 values and made a linear-least-square-fit for the ε'' data at low ω with an equation

$$\varepsilon''(\omega; n^*) = g_1(n^*)\, D_1(\omega) + g_2(n^*)\, D_2(\omega) + g_3(n^*)\, D_3(\omega) + \left[\sum_{p\geq 4} g_p\tau_p \right] \omega \qquad \text{(VI-17)}$$

From the resulting g_1 - g_3 values, we obtained F_3 together with the re-evaluated F_1 and F_2. Although not shown here, a prerequisite of this fit, $\varepsilon''-g_1D_1-g_2D_2-g_3D_3 \propto \omega$, was satisfied at low ω within a scatter similar to that seen in Figure VI-5. For

higher modes with $p \geq 4$, τ_p's were not estimated with acceptably high accuracy and the mode-decomposition was not made with good resolution. Thus, in this study we do not attempt to evaluate F_p for $p \geq 4$.

Figure VI-6 shows the plots of $\Delta F_p(n^*) = F_p(n^*) - F_p(N/2)$ $(p = 1, 2, 3)$ against n^*/N. For convenience of later comparison, we have shown ΔF_p, not F_p themselves. The unfilled and filled symbols indicate ΔF_p evaluated from the first and second least-square-fitting procedures using eqs VI-16 and VI-17, respectively. We may anticipate some ambiguity for the second procedure that involved the estimated τ_3 value. However, as seen in Figure VI-6, the two procedures gave almost identical ΔF_1 and ΔF_2. This result suggests an acceptably small ambiguity for the second procedure.

As explained later, some models have sinusoidal eigenfunctions, $f_p^\circ(n) = sin(p\pi n/N)$.[2,6,10-12] The integrals of these f_p° normalized according to eq VI-9 are given by

$$\Delta F_p^\circ(n^*) = \frac{\sqrt{2}}{p\pi}\left[\cos\frac{p\pi}{2} - \cos\frac{p\pi n^*}{N}\right] \qquad \text{(VI-18)}$$

These ΔF_p° are indicated by the dashed curves in Figure VI-6. As seen there, they are fairly close to the experimental ΔF_p for $n^* \cong N/2$ but systematically deviate from ΔF_p as n^* approaches 0 or N. The differences between ΔF_p and ΔF_p° seen for $n^* \cong 0$ and N are larger than the ambiguities in evaluation of ΔF_p. Because the eigenfunctions f_p and f_p° and thus their integrals ΔF_p and ΔF_p° are normalized (eq VI-9), those differences suggest some differences of the n^* dependence of f_p and f_p°. For a critical examination, only the eigenfunction $f_1(n) = [N/\sqrt{2}][d\Delta F_1(n)/dn]$ (cf., eq VI-12) was evaluated as an average gradient taken in an interval of $\Delta(n/N) = 0.1$ for the solid curve that smoothly connect the ΔF_p data points. The result for $f_1(n)$ is shown in Figure VI-7. This comparison most clearly demonstrates the *non-sinusoidal n* dependence of the experimental ΔF_1 and $f_1(n)$.

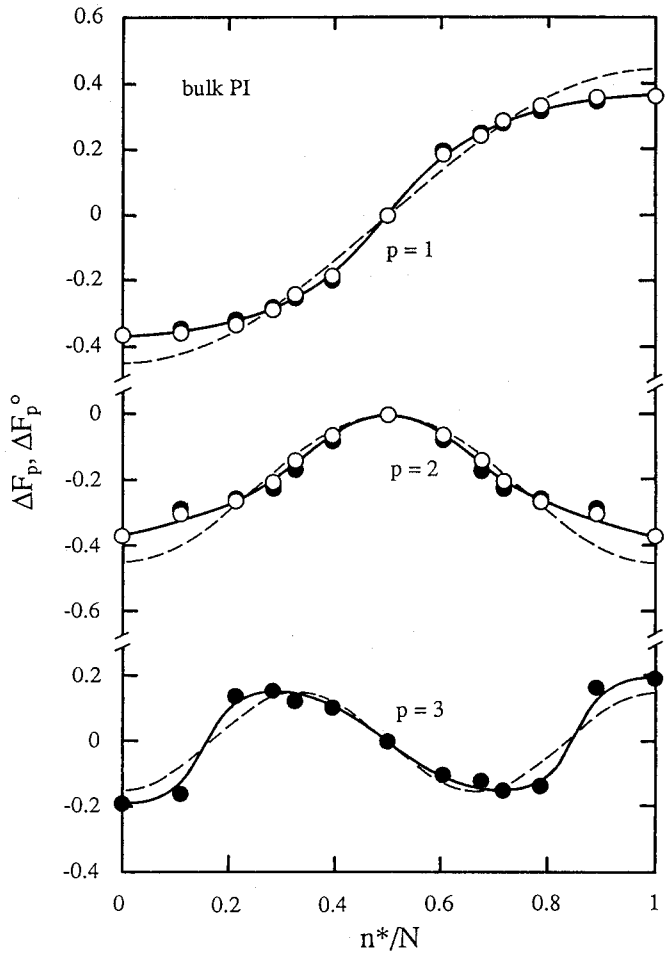

Figure VI-6. n^* dependence of the integrals of low order eigenfunctions for the PI chains,

$$\Delta F_p(n^*) = \frac{\sqrt{2}}{N} \int_{n^*}^{N/2} f_p(n)\, dn \quad (= F_p(n^*) - F_p(N/2);\ \text{cf., eq VI-18}).$$

The unfilled and filled symbols indicate the experimental ΔF_p obtained from the linear-least-square-fits for the ε'' data with eqs VI-16 and 17, respectively. The dashed curves indicate $\Delta F_p^\circ(n^*) = [\sqrt{2}/p\pi][cos(p\pi/2) - cos(p\pi n^*/N)]$ predicted from the reptation models. Note that $\Delta F_p^\circ(n^*)$ and $\Delta F_p^\circ(n^*)$ are normalized according to eq VI-9, so that their differences at $n^* \equiv 0, N$ suggest non-sinusoidal n dependence for the eigenfunctions $f_p(n) = [N/\sqrt{2}][d\Delta F_p(n)/dn]$ of actual PI chains.

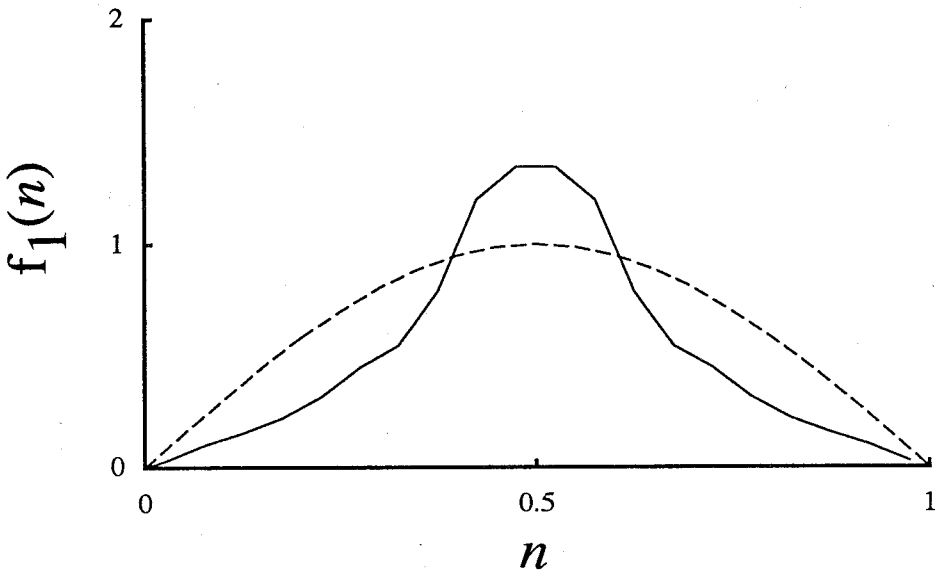

Figure VI-7. n dependence for the eigenfunction $f_1(n) = [N/\sqrt{2}][d\Delta F_1(n)/dn]$ for actual PI chains. The dashed curves indicate the $sin(\pi n/2)$ predicted from the reptation or Rouse models.

VI-4. Dipole Inverted Chain in Dilute Solution Systems

VI-4-1. ε'' Curves in Dilute Solution Systems

Figure VI-8 shows the ω dependence of ε'' at 40°C for I-I/PB-0.7 blend containing 5wt% PI chains with various locations of the dipole-inversion points.[19] The MW of PB is much lower than I-I and hence the matrix PB can be regarded as a solvent for the PI chains. The time-temperature superposition worked very well, and the ε'' data were reduced at T_r = 40°C. The shift factors a_T for the dipole-inverted PI chains were identical to that for regular PI chains in PB-0.7.

For the correction of $a_M = \tau_1/\tau_r$, with τ_r being τ_1 for the I-I 24-24/B-0.7 blend chosen as a reference for the shift, we interpolated the τ_1 data of I-I from those of three probe PI chains with M_w=35.0, 48.8, 59.9×10^3 in the B-0.7 matrix as is shown in Figure VI-9 (open circles). The log a_M values are summarized in Table VIII(b).

By shifting the ε'' curve for I-I 49-0 (after the correction of τ_1) along the ω-axis by a factor Δ_M = 3.4 and then comparing with the curve for I-I 24-24, we found that the shape of the two curves completely the same as was seen for the bulk system. As described previously, the ε'' peaks for I-I 49-0 and 24-24 chains correspond to the first and second modes with the relaxation times τ_1 and τ_2 (= τ_1/3.4), respectively. Specifically, the τ_1 and τ_2 values are evaluated from the peak frequencies as

$$\tau_1 = 8.13 \times 10^{-3} \text{ s}, \ \tau_2 = 2.09 \times 10^{-3} \text{ s} \qquad \text{(VI-19)}$$

According to the Zimm model, the ratio of τ_1/τ_2 becomes 3.17. On the other hand, the Rouse model or the Tube model predict the ratio as 4.0. Our experimental τ_1/τ_2 of 3.4 is close to the value predicted by the Zimm model.

The data of bulk I-I shown in Fig. VI-2 are also plotted in a reduced form, *i.e.*, $\varepsilon''/\Delta\varepsilon$ vs. $\omega\tau_1$, in Figure VI-8 . The difference between the two series of ε'' curves can be clearly seen: The strength of ε'' corresponding to the lower order

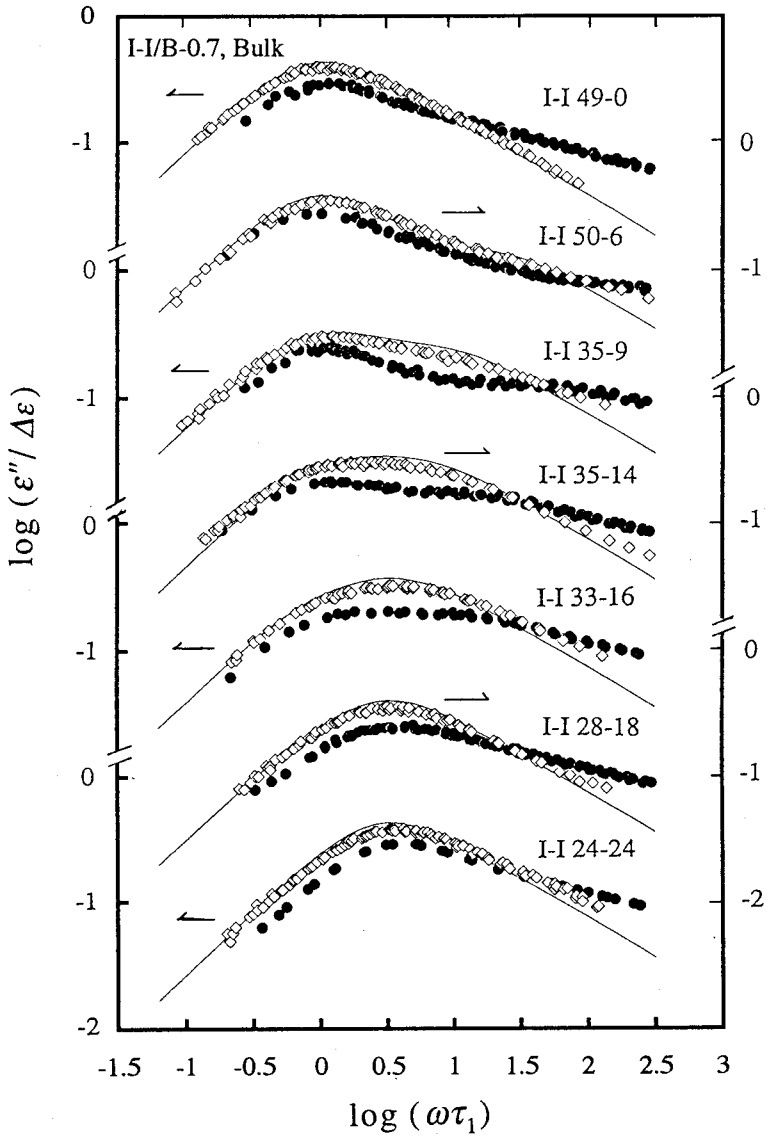

Figure VI-8 Reduced frequency ($\omega\tau_1$) dependence of the dielectric loss factors ε'' reduced by the relaxation strengths at 40°C for I-I (5wt%)/PB-0.7 systems (unfilled symbols). The solid circles represent the data of the bulk systems and the solid lines indicate the predicted curves from Zimm model.

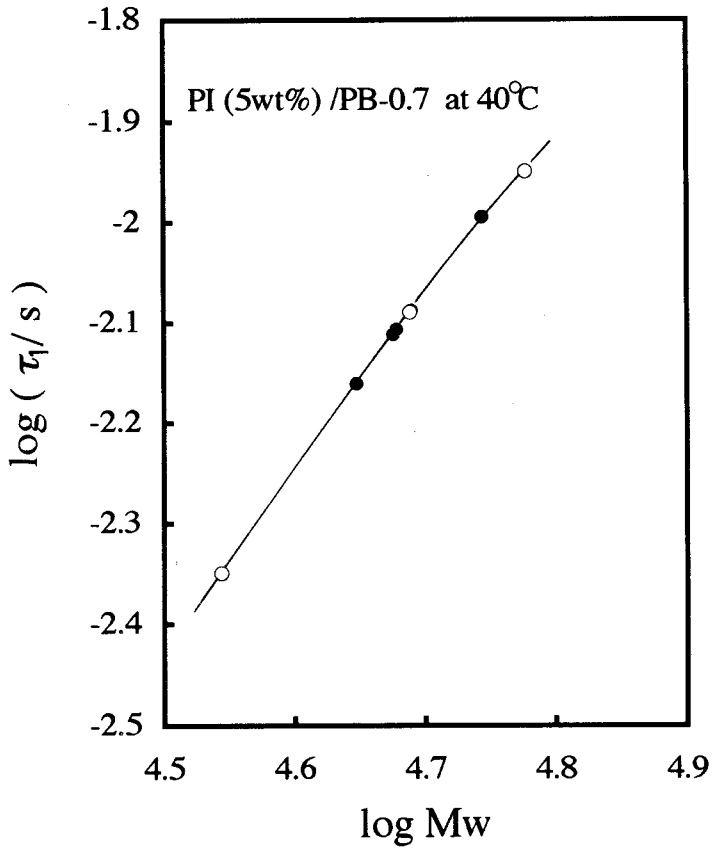

Figure VI-9. M_w dependence of τ_1 of dilute (5wt%) PI in PB-0.7 at 40°C. The open circles represent the data of standard PI (M_w=35.0, 48.8, 59.9×10^3) and the solid circles, the interpolated data for dipole inverted chains.

mode for the I-I/PB-0.7 system is larger than that for the bulk system. This behavior is similar to that observed in Figs. V-15 and V-33. In Figure VI-8, the theoretical curves for the Zimm model are also shown by the solid lines. Their agreement with experiment is good. In the previous chapter we mentioned that for regular type-A chains the difference between the ε'' curves predicted by the Zimm and Rouse models was hardly distinguishable. But for dipole inverted chains we can see the difference clearly. Figure VI-10 shows comparison of the ε'' curve of I-I 50-6 in PB-0.7 with the Zimm and Rouse models. We can see that the Zimm model agrees with experimental ε'' better than does the Rouse model.

VI-4-2. Eigenfunction in Dilute Solution Systems

Figure VI-11 shows the n^*/N dependence of experimental $\Delta F_p(n^*)$ for I-I/PB-0.7 system. The shape and the absolute value agree very well to the cosine functions represented by eq VI-18. This result is different from that for the bulk system shown in Figure VI-6.

According to the Zimm model the eigenfunction $f_p(n)$ is approximately given by $sin(p\pi n/N)$. Thus the integrated form $F_p(n)$ becomes $cos(p\pi n/N)$. This prediction is substantiated by our result for $\Delta F_p(n)$ in dilute solution. We have also found in Chapter V that the Zimm model is applicable to the PI/PB-0.7 system.

VI-5. Discussion

The non-sinusoidal eigenfunction is one of the key factors to explain the deviation of the shape of the ε'' curves from the bead-spring or tube models seen in Chapter V since these models predict the sinusoidal eigenfunction which is based on the following equation.

$$\frac{1}{\tau_p} f_p(n) = -\frac{1}{\tau_1^{\circ}} [N/\pi]^2 \frac{d^2}{dn^2} f_p(n) \qquad \text{(VI-20)}$$

where τ_1^{0} is the first mode relaxation time in the Rouse and tube models. In the

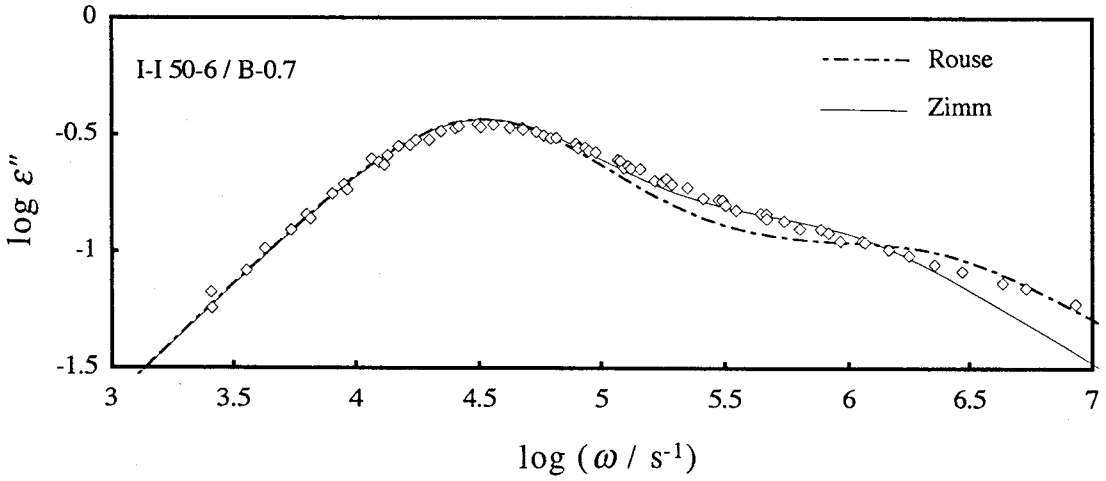

Figure VI-10. Comparison between the Rouse and Zimm models for the shape of ε'' curve of I-I 50-6 in PB-0.7.

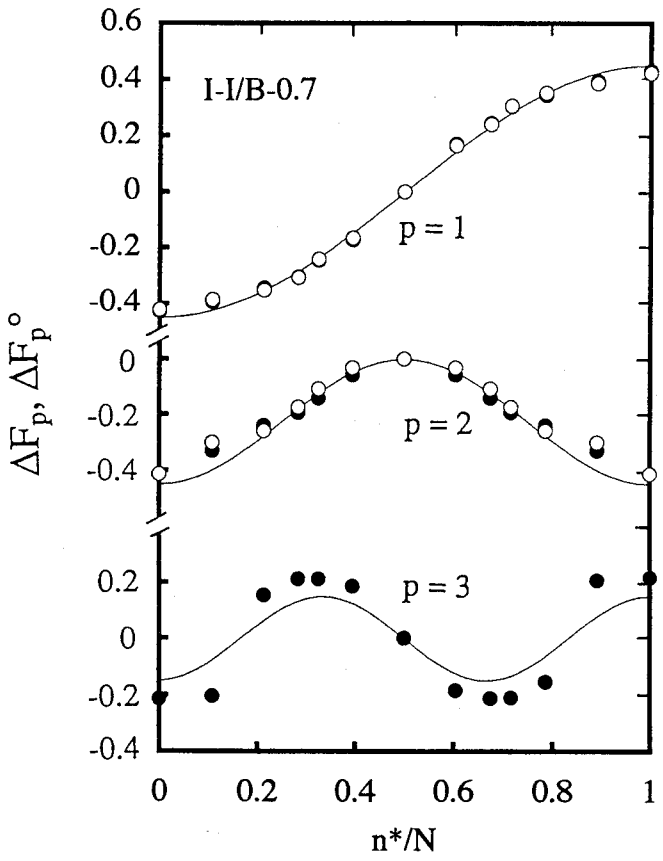

Figure VI-11. . n^* dependence of the integrals of low order eigenfunctions for the PI chains in PB-0.7. The solid lines indicate the $cos(p\pi n/N)$ (p=1 to 3) and the symbols have the same meaning as in Fig. VI-6.

experimentally determined $f_p(n)$ for bulk PI systems we observed the deviation from the sinusoidal function. We represent them by the Fourier expansion formula as

$$f_p(n) = \Sigma_q \, a_{p,q} \, sin(q\pi n/N) \qquad \text{(VI-21)}$$

It is noted that $a_{p,q}$ must satisfy the normalization condition of eq VI-9. From eqs VI-9 and VI-21, we obtain

$$\Sigma_q \, a_{p,q}^{\,2} = 1 \qquad \text{(VI-22)}$$

If the eigenfunction represented by eq VI-21 is inserted in eqs VI-10 and VI-11 with $n^* = N$, then the ε'' curve become broad, because the relaxation strength for each p mode is converted to the different q modes each other with satisfying eq VI-22. Thus the deviation of f_p from a sinusoidal function is consistent with the broadening of ε'' curves.

The deviation of $f_p(n)$ in bulk system from the sinusoidal function indicates the limit of the applicability of the eq VI-20. Thus we modify this equation as follows.

The Rouse and tube models assume the chain ends as the boundary where a memory instantly vanishes to predict the sinusoidal f_p° (cf., eq VI-20). Qualitatively, f_p° is distorted toward the experimental f_p (see Fig. VI-7) when the extra mechanism is incorporated in the model and its effect is represented by a relaxation source $U(n)$ added in eq VI-20: $U(n)$ should be large for $n \cong 0$ and N to have large effects at chain ends. The eigenfunction equation is formally identical to the Schrödinger equation with a potential term U(n),

$$\frac{1}{\tau_p} f_p(n) = -\frac{1}{\tau_1^\circ} [N/\pi]^2 \frac{d^2}{dn^2} f_p(n) + U(n) \, f_p(n) \qquad \text{(VI-23)}$$

and $[f_p(n)]^2$ is analogous to the probability density. Thus, f_p and f_p° (= f_p for U = 0) normalized by eq VI-9 would satisfy a relation, $|f_p(n)| < |f_p^\circ(n)|$ for $n^* \cong 0$, N, as noted in Figures VI-6 and VI-7 for $f_p(n) = [N/\sqrt{2}][d\Delta F_p(n)/dn]$ (in particular for those with p = 1 and 2). (A similar argument may be made also for $U(n)$ that works as a differential operator.)

The next problem is to find the origin of $U(n)$. In the previous chapter we mentioned that the viscoelastic effect of the media will be the important point to consider the chain dynamics in a dense system. Based on this idea we try to modify the bead-spring model.[10] The equational motion of Rouse is given by

$$\zeta \frac{\partial \boldsymbol{R}(n,t)}{\partial t} = \kappa \frac{\partial^2 \boldsymbol{R}(n,t)}{\partial^2 n} + f_B \qquad \text{(VI-24)}$$

where ζ is the friction coefficient, κ the spring constant, $\boldsymbol{R}(n,t)$ the position of the n-th bead at time t, and $f_B(n,t)$ the random force acting on the n-th bead at time t. We introduce in this equation a external viscoelastic force which acts between two beads through the elasticity of the media. This force must be damped by the viscosity which originates in the viscoelasticity. In addition we assume that this force acts in a certain critical spatial range characterized by the number of beads h. Then it follows that

$$\zeta \frac{\partial \boldsymbol{R}}{\partial t} = \kappa \frac{\partial^2 \boldsymbol{R}}{\partial n^2} + f_B + \beta \int_{n-h/2}^{n+h/2} dn' \int_{-\infty}^{t} \frac{\partial}{\partial t'} \left[\phi(t-t') \cdot \{ \boldsymbol{R}(n',t') - \boldsymbol{R}(n,t') \} \right] dt' \qquad \text{(VI-25)}$$

Here β represents the spring constant which originates in the elasticity of the media and ϕ is the memory function. By multiplying the operator $\{\boldsymbol{u}(m,0)\cdot(\partial/\partial n)\}$ and then taking the ensemble average, we can derive the time evolution equation for $C(n,t;m)$ (cf. eq VI-3):

$$\frac{\partial C}{\partial t}=\frac{\kappa}{\zeta}\frac{\partial^2 C}{\partial n^2}+\frac{\beta}{\zeta}\int_{n-h/2}^{n+h/2} dn' \int_{-\infty}^{t}\frac{\partial}{\partial t'}\left[\phi(t-t')\cdot\{C(n',t';m)-C(n,t';m)\}\right]dt' \qquad \text{(VI-26)}$$

If we assume $\phi(t)=exp(-t/\tau)$ where τ represents the relaxation time of media, then we can derive the eigenfunction equation:

$$\frac{1}{\tau_p} f_p(n) = -\frac{1}{\tau_1^{\circ}}[N/\pi]^2 \frac{d^2}{dn^2} f_p(n) + \frac{\beta/\zeta}{\tau_p/\tau - 1}\int_{n-h/2}^{n+h/2} dn' \left[f_p(n')-f_p(n)\right] \qquad \text{(VI-27)}$$

This equation has the same form as eq VI-23 and explains the deviation of the eigenfunction $f_p(n)$ from the sinusoidal function. Thus we can conclude that in a dense polymeric system the viscoelasticity of the media causes the relaxation spectrum to change.

APPENDIX A. Eigenfunction Expansion of C(n,t; m)

As a quantity that describes fundamental features of dielectric relaxation of type-A PI chains, a local correlation function is defined by

$$C(n,t;\, m) = (1/b^2) \langle \boldsymbol{u}(n,t) \cdot \boldsymbol{u}(m,0) \rangle \qquad \text{(A1)}$$

with $\boldsymbol{u}(n,t)$ being a bond vector for the n-th segment at time t and $b^2 = \langle \boldsymbol{u}^2 \rangle$. At short time scales, the relaxation spectrum might be continuous and an eigenfunction expansion of $C(n,t;\, m)$ might contain some ambiguities. However, this is not the case at long time scales where the PI chains actually exhibit a terminal dielectric relaxation that is decomposed into well-defined modes. These dielectric modes correspond to eigenmodes of $C(n,t;\, m)$, justifying the eigenfunction expansion at long time scales. For those cases, a time evolution of $C(n,t;\, m)$ should be generally described by an equation of a factorized form

$$\frac{\partial}{\partial t} C(n,t;\, m) = L(n)\, C(n,t;\, m) \qquad \text{(A2)}$$

where $L(n)$ represents an operator with respect to n. (Note in eq A1 that $\boldsymbol{u}(m,0)$ does not change with time, thereby no operation with respect to m is involved in eq A2.) Details of the global chain motion can be found from a functional form of the operator $L(n)$, or equivalently, from the form of the eigenfunctions $h_p(n)$ (p = 1, 2,..) associated with $L(n)$. This indicates an importance of the dielectric work on the dipole-inverted PI chains that determines $h_p(n)$.

Using $h_p(n)$ and corresponding eigenvalues $1/\tau_p$ that are determined by

$$L(n)\, h_p(n) = -(1/\tau_p)\, h_p(n) \quad (p = 1,\, 2,..,\, N) \qquad \text{(A3)}$$

we can generally solve eq A2 as

$$C(n,t;\, m) = \frac{2}{N} \sum_{p=1}^{N} h_p(n)\, A_p(m) \exp(-t/\tau_p) \quad (t > 0) \tag{A4}$$

Here, the factor $(2/N)A_p(m)$ represents the amplitude factor for the p-th eigenfunction at t = 0. At equilibrium, an origin of time (t=0) can be arbitrarily chosen and an orientation-correlation of the bond vectors should be symmetrical with respect to time. This argument leads to the relation

$$\langle \boldsymbol{u}(n,t)\cdot\boldsymbol{u}(m,0)\rangle = \langle \boldsymbol{u}(n,0)\cdot\boldsymbol{u}(m,-t)\rangle = \langle \boldsymbol{u}(n,0)\cdot\boldsymbol{u}(m,t)\rangle \quad \text{for any } t,\ n,\ m \tag{A5}$$

From eqs A1, A4, and A5, we find

$$A_p(m)\, h_p(n) = A_p(n)\, h_p(m) \quad \text{for any } n,\ m \tag{A6}$$

and thus

$$A_p(n) = \alpha_p\, h_p(n) \tag{A7}$$

Here, α_p is a numerical constant. Using normalized eigenfunctions $f_p(n) = \alpha_p^{1/2}\, h_p(n)$ in eqs A4 and A7, we finally find an expression for $C(n,t;\, m)$ on the basis of the eigenfunction expansion,

$$C(n,t;\, m) = \frac{2}{N} \sum_{p=1}^{N} f_p(n)\, f_p(m)\, exp(-t/\tau_p) \quad (t > 0) \tag{A8}.$$

APPENDIX B. Determination of g_1 and g_2

At ω below a certain characteristic ω_c, the contribution to ε'' from all higher *p-th* modes with $p \geq 3$, $\varepsilon''_{p\geq 3}$, is practically identical to its low-ω asymptote, $G_3\,\omega = [\Sigma_{p\geq 3}\, g_p\tau_p]\,\omega$, and then eq VI-16 holds. Using this equation, we made a standard linear-least-square-fit: Minimizing a sum $\Sigma[\varepsilon'' - g_1D_1 - g_2D_2 - G_3\omega]^2/\varepsilon''^2$ taken in a range of $\omega < \omega_c$, we obtained a set of linear equations that determined g_1, g_2, and G_3.

For the best fit to be made, the upper limit of the fitting range, ω_c, should be small enough so that eq VI-16 is valid. At the same time, ω_c should be large enough so that we can involve enough data points in the fit. Thus, we varied ω_c around its first estimate $1/\tau_2$ (=478 s^{-1}; cf., eq VI-14) and examined a quality of the fit. For respective PI samples, we found a range of the acceptable ω_c values: In that range, the mean square deviation of the fit, δ, was minimized and the g_1, g_2, and G_3 values were found to be insensitive to the choice of ω_c. The smallest value of the acceptable ω_c was used to finally determine the g_1, g_2, and G_3 values. That ω_c value was about $0.5/\tau_2$ for the I-I 49-0 chain ($n^* = 0$), about $2/\tau_2$ for the I-I 24-24 chain ($n^* = N/2$), and between $0.5/\tau_2$ and $1/\tau_2$ for the other PI chains. With the g_1 and g_2 values determined for these ω_c, a prerequisite of the fit, $\varepsilon'' - g_1D_1 - g_2D_2 \propto \omega$, was well satisfied at low ω, for some cases even at ω somewhat higher than ω_c (cf., Figure VI-5). This result suggests that the best fit was made.

Note here that the optimum value of ω_c should be determined in relation to the relaxation time τ_3 (=1.1 x 10^{-3} s for the best estimate; cf., Appendix C) and intensity g_3 of the third eigenmode. For large g_3, $\varepsilon''_{p\geq 3}$ at $\omega < \omega_c$ is dominated by the contribution from the third mode $g_3D_3(\omega)$. Then, ω_c should be sufficiently smaller than $1/\tau_3$ for a good fit with small δ to be made. This was the case for the I-I 49-0 chains: For $\omega_c \cong 0.5/\tau_2$ used in the fit, $D_3(\omega)$ at $\omega < \omega_c$ agrees with its low-ω asymptote $\omega\tau_3$ within a few percent. On the other hand, for smaller g_3, the third mode contribution becomes less significant and ω_c can become larger, as were the cases for the other PI's. In particular, for the I-I 24-24 chains having $g_3 = 0$, we had $\omega_c \cong 2/\tau_2$ and still found the prerequisite, $\varepsilon'' - g_2D_2 \propto \omega$, to be well satisfied up to $\omega \cong 1.3\omega_c$ (cf., Figure VI-5).

APPENDIX C. Estimation of τ_3 for the Third Eigenmode.

For the I-I 49-0 chain without dipole-inversion, only odd eigenmodes contribute to ε''. Thus, at low ω where the contribution from all higher *p-th* modes with $p \geq 5$ is practically identical to its low-ω asymptote, $G_5\,\omega = [\Sigma_{p\geq 5}\, g_p\tau_p]\,\omega$, we may re-write eq VI-10 as

$$\varepsilon'' = g_1\, D_1(\omega) + g_3\, D_3(\omega) + G_5\,\omega \qquad \text{(C1)}$$

For convenience for the estimation of τ_3, this equation is further modified as

$$\delta'' = \omega^3\,[\varepsilon'' - g_1 D_1(\omega) - G_3\,\omega\,]^{-1} = -X - \omega^2 Y \qquad \text{(C2)}$$

with

$$D_1(\omega) = \frac{\omega\tau_1}{1 + \omega^2\tau_1^{\,2}} \qquad \text{(C3)}$$

and

$$G_3 = \sum_{p\geq 3} g_p\tau_p\,,\quad X = 1\,/\,(\,g_3\tau_3^{\,3}\,)\,,\quad Y = 1\,/\,(\,g_3\tau_3\,) \qquad \text{(C4)}$$

Since τ_1 was experimentally determined (eq VI-14) and g_1 and G_3 were evaluated from the least-square-fit with eq VI-16 (cf., Figure VI-5), we made a standard linear-least-square-fit for the quantities δ'' calculated from the ε'' data: Minimizing a sum $\Sigma\,[\delta'' + X + \omega^2 Y]^2/\delta''^2$ taken for the data in a given range of ω, we obtained a set of linear equations for X and Y that determined $\tau_3 = (Y/X)^{1/2}$.

Equation C1 should be valid in a ω-range with its upper limit ω_c' being located in a vicinity of $1/\tau_3$. Thus, for the fit, we first need to know an appropriate value for τ_3. For this purpose, we used $\tau_3^\circ = \tau_1/9$ (predicted from the reptation model) as a first estimate. As did in Appendix B, we varied ω_c' around $1/\tau_3^\circ$and examined the mean-square deviation of the fit, and obtained $\tau_3 = 1.1 \times 10^{-3}$ s as the best estimate.

References And Notes

1. Yoshida, H.; Watanabe, H.; Adachi, K.; Kotaka, T. *Macromolecules* **1991**, *24*, 2981.
2. (a) Watanabe, H.; Yamazaki, M.; Yoshida, H.; Adachi, K.; Kotaka, T. *Macromolecules* **1991**, *24*, 5365. (b) Watanabe, H.; Yamazaki, M.; Yoshida, H., K.; Kotaka, T. *Macromolecules* **1991**, *24*, 5372.
3. Watanabe, H.; Kotaka, T. *Macromol. Chem.* **1991**, *2*, 139.
4. Watanabe, H.; Urakawa, O.; Kotaka, T. *Macromolecules* **1993**, *26*, 5073.
5. Cole, R. H. *J. Chem. Phys.* **1965**, *42*, 637.
6. Doi, M.; Edwards, S. F. "Theory of Polymer Dynamics", Clarendon: Oxford.
7. For integer n and m, δ_{nm} (eq VI-5) is identical to the Kronecker-delta
8. Watanabe, H.; Shimura, T.; Kotaka, T.; Tirrell, M. *Macromolecules*, submitted (**1993**).
9. PI chains exhibit dielectric relaxations due to both type-A and type-B dipoles that are parallel and perpendicular to the chain contour, respectively. However, the relaxation due to the type-B dipoles takes place at high ω and its contribution to the ε'' curves is extremely small in the ω-range examined in this study. This was confirmed from a fact that for high-M ($\geq 20 \times 10^3$) PI chains (without dipole inversion) the ε'' curves in that ω-range have an universal mode distribution being determined only by the global chain motion.
10. Rouse, P. E. *J. Chem. Phys.* **1953**, 21, 1272.
11. Klein, J. *Macromolecules* **1978**, *11*, 852.
12. Graessley, W. W. *Adv. Polym. Sci.* **1982**, *47*, 67.

VII. Summary and Conclusions

In this thesis we have studied two main subjects: One is the determination of the mean square end-to-end distance $\langle r^2 \rangle$ from the dielectric measurement on type-A chains, and the other is the chain dynamics associated with the fluctuation of the end-to-end vector of type-A chains in various surroundings. The principal results and conclusions are summarized as follows.

Dipole Moment and End-to-End Distance (Chapters II and IV)

The applicability of the dielectric method to determine $\langle r^2 \rangle$ of a type-A polymer chain was examined both theoretically and experimentally. The basic idea of this possibility is that type-A chains have a dipole moment $\boldsymbol{P}_A$ proportional to the end-to-end vector $\boldsymbol{r}$: $\boldsymbol{P}_A = \mu \boldsymbol{r}$ where μ is a constant. However, this equation contains two unsettled important problems: One is the relationship between μ and the chemical structure and the other is the dependence of μ on the surroundings such as solvent nature and polymer concentration.

First, we made theoretical considerations for the determination of μ in Chapter II, assuming that μ is given for any type-A chains by

$$\mu = \langle \boldsymbol{P} \cdot \boldsymbol{r} / r^2 \rangle = \langle (\Sigma_i \boldsymbol{m}_i) \cdot \boldsymbol{r} / r^2 \rangle \qquad \text{(VII-1)}$$

where $\boldsymbol{P}$ is the total dipole moment of a chain and $\boldsymbol{m}_i$, the monomer dipole moment. The calculation of μ was made for two polymers, *i.e.*, *cis*-polyisoprene (PI) and poly(ε-caprolactone) (PCL). We determined the monomer dipole moment $\boldsymbol{m}_i$ by the *ab-initio* MO calculation and then μ by using Flory's rotational isomeric state (RIS) model on the basis of eq VII-1. On the other hand, experimental determination of μ was made for dilute solutions of PI and PCL. We evaluated the value of μ^2 as $\langle P_A^2 \rangle / (6 \langle S^2 \rangle)$, where $\langle P_A^2 \rangle$ ($= \langle (\mu r)^2 \rangle$) was determined from the dielectric

relaxation strength $\Delta\varepsilon$ and $<S^2>$ from light scattering measurements or from the intrinsic viscosity $[\eta]$ assuming the Flory-Fox equation: $[\eta]=\Phi<r^2>^{3/2}/M_w$ with $\Phi=2.5\times10^{23}$. The experimentally determined μ agreed fairly well with the calculated one. Thus we concluded eq VII-1 to be valid.

As to the problem on the dependence of μ on the surroundings (through solvent-polymer interactions), we expected that the detailed chemical structure of the type-A chain should be reflected. Thus we classified type-A dipoles into three categories as shown in Figure II-1: (1)type-A1, *intrinsic* type-A polymer composed of only one kind of polar virtual bond, (2)type-A2, *alternating* polar-nonpolar bond type composed of one kind of polar bond and (a set of) non-polar bond(s) alternately, and (3)type-A3, *mixed* polar-and-nonpolar bond type composed of a few different polar and non-polar bonds. For type-A1 chains μ can be determined uniquely. However, for A2 and A3 polymers μ is defined as an average over all possible conformations of the bond moments. Thus there was a possibility that μ depends on the solvent quality. To investigate this problem, we compared the dielectric relaxation strengths $\Delta\varepsilon$ ($\propto<P_A^2>$) for PI in dilute dioxane (Diox) (θ solvent), heptane (marginal solvent), and cyclohexane (good solvent) solutions. We also compared these $\Delta\varepsilon$ with $<S^2>$ data obtained for the same systems. First we found that the proportionality between $\Delta\varepsilon$ and $<S^2>$ for each system holds well, and thus concluded that μ does not appreciably change in these solvents. The second finding was that the ratio of of the expansion factor for $\Delta\varepsilon$ to that for $<S^2>$, $\alpha_\varepsilon^2/\alpha_S^2$, increases with increasing solvent quality. This value corresponds to $(\alpha_r^2/\alpha_S^2)\times(\mu/\mu_\theta)^2$ where μ_θ is μ in the θ state. From the change of $\alpha_\varepsilon^2/\alpha_S^2$ found in different solvent (heptane and cyclohexane), $(\mu/\mu_\theta)^2$ for PI may be estimated to change as much as *ca.* 11% by the change in the solvent quality.

For semidilute solutions of PI and PCL, we investigated the concentration C dependence of $\Delta\varepsilon/C$ in order to check the scaling theory and also to test the C dependence of μ. The results indicated that the C dependence of $<P_A^2>$ agrees well

with the prediction of the scaling theory indicating that μ does not depend on C in the semidilute regime.

We also made dielectric measurement on a ternary system composed of a trace amount of PI and semidilute polybutadiene(PB)/heptane solutions which were dielectrically inert matrices. The dependence of $\langle P_A^2 \rangle$ ($\propto \langle r^2 \rangle$) on PB concentration C_B and on PI and PB molecular weights M_I and M_B was systematically investigated by fixing the PI concentration low enough but varying C_B over a wide range from dilute to semidilute regimes. The value of $\langle r^2 \rangle$ for the PI chains divided by that of $\langle r^2 \rangle_0$ in dilute PI/heptane solution ($C_B = 0$) are plotted against $C_B[\eta]_B$ where $[\eta]_B$ is the intrinsic viscosity of PB in heptane. In case of $M_I \geq M_B$, all the plotted points fell on a single curve. On the other hand, $\langle r^2 \rangle$ in systems of $M_I < M_B$ conformed to a universal curve when $\langle r^2 \rangle / M_I$ ($\propto \Delta\varepsilon/C_I$) values were plotted against C_B. At least, the qualitative features of these results can be favorably explained by the scaling theories developed by Joanny *et al.* and Nose.

Dynamic Properties (Chapter V)

We studied dynamic properties of three different type-A polymers, PI, PCL, and poly(δ-varerolactone) (PVL) in several different surroundings.

In dilute solutions, the normal mode relaxation times τ of PI in cyclohexane and heptane and those of PCL and PVL in benzene were expressed as a universal function of the Rouse-Zimm parameter, $\eta_s[\eta]M_w/RT$, where η_s is the solvent viscosity. In addition, the shapes of ε'' curves which represent the relaxation mode distribution conformed to the theoretical prediction by Zimm. The relaxation time τ_2 of the second mode was determined from the inverse of the peak angular frequency ω_{max} for symmetrically dipole-inverted PI chain in dilute cyclohexane solutions. The value of τ_1/τ_2 was close to that predicted by the Zimm model.

In semidilute solutions of PI/heptane and PCL/cyclohexane, τ/τ_0 was found to be well represented by the parameter $C[\eta]$ in harmony with the scaling

prediction. The mode distribution (the ε'' curve) became broader with increasing C in the regime of $C^*<C$ and tended to converge to that of the bulk systems. The shape of the ε'' curve in the crossover C range is determined by $C[\eta]$ irrespective of M_w. We compared the dielectric relaxation spectra with viscoelastic spectra of polystyrene solutions with $C[\eta] \cong 10$ reported by Ferry *et al.* who used the Rouse model to explain the shape of the complex moduli G^*. We found that the change in the shape of ε'' curve with C does *not* correspond to that of G'' curve. From this result we doubt the applicability of the Rouse model to the systems of $C > C^*$.

For the PI/PB/heptane ternary systems described above, the dynamic behavior was also investigated. The data for τ/τ_0 of probe PI were expressed by a universal function of two parameters $C_B[\eta]_B$ and $C_B[\eta]_I$. From the slope of $\log(\tau/\tau_0)$ vs. $\log(C_B[\eta]_I)$ at constant $C_B[\eta]_I$ or that of $\log(\tau/\tau_0)$ vs. $\log(C_B[\eta]_B)$ at constant $C_B[\eta]_B$, we classified the dynamical behavior of the PI chains into three regimes according to the dynamic scaling theory. The first is the *Zimm* regime in which the motion of PI probes can be explained by the non-draining Zimm model. The second regime is the *reptation* regime reflecting entanglement effects between PI and PB chains, and the third is the *transition* regime between these two regimes. The case of $C_B[\eta]_I >> C_B[\eta]_B$ belongs to the Zimm regime, and that of $C_B[\eta]_I << C_B[\eta]_B$ to the reptation regime. We found that the shape of the ε'' curve is narrow in the first regime but begins to broaden in the transition region.

In binary blends composed of dilute PI and undiluted PB matrix, we found also a broadening of the ε'' curves with increasing M_B. Even when the matrix PB chains were short enough so that they were not entangled, the broadening of ε'' with M_B was observed. This indicated that the broadening phenomenon is not a direct consequence of the entanglement effect. We propose that the elastic force of the media plays an important role in the broadening of the ε'' spectrum.

Investigation of the Polymer Chain Dynamics by Using Dipole Inverted Polyisoprene (Chapter VI)

In order to investigate the features of the chain dynamics in a greater detail, we examined dielectric normal mode relaxation of a series of asymmetrically dipole-inverted PI chains in bulk and in dilute solution. Those PI chains were specially designed so that the overall molecular weights are the same but the dipole-inversion point appears at a certain point from the chain end (no inversion) to the center of the chain. A polybutadiene oligomer with $M \cong 700$ was used as a solvent for the study of dilute solution. From the series of the ε'' data we evaluated the low-order eigenfunctions $f_p(n)$ (p up to 3) for the local correlation function $C(n,t;m) = (1/b^2)\langle \boldsymbol{u}(n,t)\cdot\boldsymbol{u}(m,o)\rangle$, where $\boldsymbol{u}(n,t)$ is the bond vector for the n-th segment at time t and $b^2 = \langle \boldsymbol{u}^2 \rangle$. The experimental $f_p(n)$ (p = 1-3) in dilute solutions was found to agree well with the sinusoidal function predicted by the Zimm model. On the other hand, $f_p(n)$'s in bulk systems exhibit a non-sinusoidal n dependence, which in turn should be related to the broad ε'' curves found in these bulk systems. We concluded that the Rouse model (and the tube model as well) should be modified by the equation of motion which can predict the non-sinusoidal eigenfunctions of the type found in this study.

List of Publications

1. Dielectric Normal Mode Relaxation of Probe Polyisoprene Chain in Semidilute Polybutadiene Solutions. 1. End-to-End Distance
   Osamu Urakawa, Keiichiro Adachi, and Tadao Kotaka
   Macromolecules **1993**, 26, 2036.

2. Dielectric Normal Mode Relaxation of Probe Polyisoprene Chain in Semidilute Polybutadiene Solutions. 2. Dynamic Behavior
   Osamu Urakawa, Keiichiro Adachi, and Tadao Kotaka
   Macromolecules **1993**, 26, 2042.

3. Slow Dielectric Relaxation of Entangled Linear *cis*-Polyisoprene with Asymmetrically Inverted Dipoles: 1.Bulk Systems.
   Hiroshi Watanabe, Osamu Urakawa, and Tadao Kotaka
   Macromolecules **1993**, 26, 5073.

4. Dielectric Normal Mode Relaxation in Dilute and Semidilute Solutions of Poly(ε-caprolactone) and Poly(δ-varerolactone).
   Osamu Urakawa, Keiichiro Adachi, and Tadao Kotaka
   in preparation

Other related papers

1. Dielectric Normal Mode Process of cis-Polyisoprene in Ternary Mixtures, Polyisoprene/Polybutadiene/Heptane.
   Osamu Urakawa, Keiichiro Adachi, and Tadao Kotaka *Rep. Prog. Polym. Phys. Japan* **1990**, 32, 85.

2. Dielectric Normal Mode Process in Semidilute Polyisoprene/Polybutadiene/Heptane Ternary solutions.
   Osamu Urakawa, Keiichiro Adachi, and Tadao Kotaka *Rep. Prog. Polym. Phys. Japan* **1991**, 36, 95.

3. Dielectric Normal Mode Process in Dilute Solutions of Poly(ε-caprolactone).
   Osamu Urakawa, Keiichiro Adachi, Tadao Kotaka, Yasunori Takemoto, and Hajime Yasuda *Rep. Prog. Polym. Phys. Japan* **1992**, 42, 161.

4. Calculation of Type-A Dipole Moments with a Rotational Isomeric State Model.
   Osamu Urakawa, Keiichiro Adachi, and Tadao Kotaka *Rep. Prog. Polym. Phys. Japan* in press.